The Canadian Journal of Chemical Engineering

THE UNIVERSITY OF MICHIGAN
OCT 16 1961
ENGINEERING LIBRARY

formerly

CANADIAN JOURNAL OF TECHNOLOGY

CONTENTS

An Analysis of Spray Evaporation in a High-Temperature Environment. I. Radiant Heat Transfer to Clouds of Droplets and Particles	*T. W. Hoffman* *W. H. Gauvin*	179
An Apparatus for the Measurement of Light Transmittance of Emulsions	*J. A. Cengel* *J. G. Knudsen* *A. Landsberg* *A. A. Faruqui*	189
Optimum Performance of Combined Flow Reactors under Adiabatic Conditions	*A. Cholette* *J. Blanchet*	192
Speed of Sound in a Non-Ideal Gas	*William Squire*	199
Kinetics of the Vapor-Phase Oxidation of Toluene Over a Vanadium Catalyst	*J. Downie* *K. A. Shelstad* *W. F. Graydon*	201
Determination of Vapor-Liquid Equilibrium Data from Total Pressure-Liquid Composition Measurements	*James C. K. Ho* *O. Boshko* *Benjamin C.-Y. Lu*	205
The Hydraulic Characteristics of Two-Phase Co-Current Flow Through Glass Fibres	*D. J. Gunn* *A. R. Aitken*	209
Pelletization and Diffusibility Studies on Silver Catalysts	*C. H. Amberg* *E. Echigoya*	215
Industrial Section		
Chemical Engineers and Computers	*Theodore J. Williams*	219
Rail Transportation of Hydrogen Chloride Anhydrous	*C. H. Drury*	227

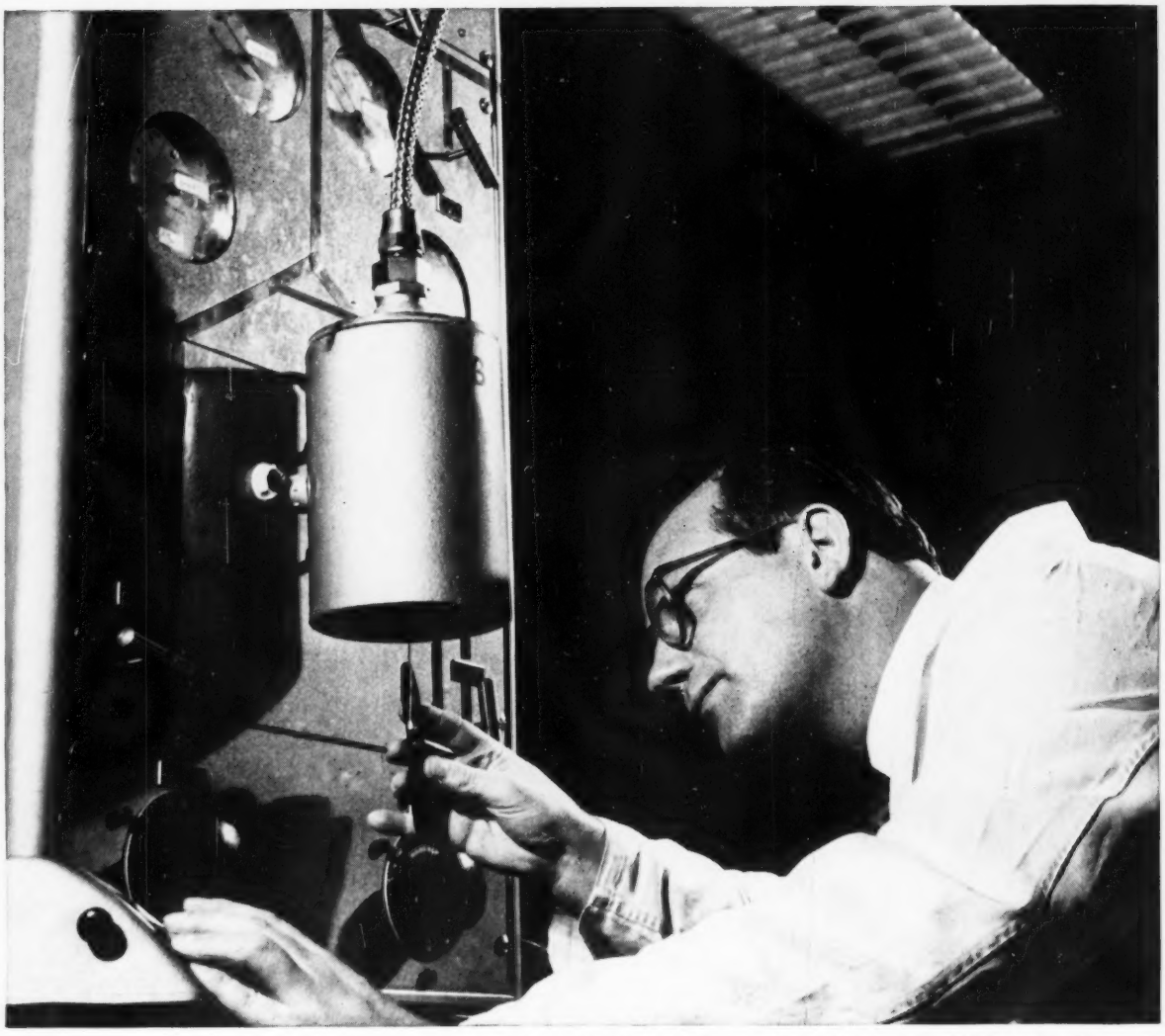

Photograph taken at C-I-L Central Research Laboratory, McMasterville, Que.

Plastics Detective

This photograph shows the High Shear Viscometer, designed and built at our Central Research Laboratory, used to investigate factors involved in complex flow behaviour of molten thermo-plastics during commercial processing.

Information on this newly developed pressure-driven capillary Viscometer has been made available to industry by C-I-L, and many industrial laboratories in the United States, England, India and Australia have built identical machines.

Such C-I-L research contributes to higher standards of performance in the plastics industry, to new and better plastics products and—through better technical service—to greater success in the application of these new materials to modern living.

C-I-L **CANADIAN INDUSTRIES LIMITED**

Serving Canadians Through Chemistry

Agricultural Chemicals • Ammunition • Coated Fabrics — Industrial Chemicals • Commercial Explosives • Paints • Plastics • Textile Fibres

The Canadian Journal of Chemical Engineering

formerly

Canadian Journal of Technology

Published by The Chemical Institute of Canada

VOLUME 39 OCTOBER, 1961 NUMBER 5

Editor
A. Cholette
Faculty of Science, Laval University
Quebec, Que.

Managing Editor
T. H. G. Michael

Publishing Editor
D. W. Emmerson

Assistant Publishing Editors
R. G. Watson
R. N. Callaghan

Circulation Manager
M. M. Lockey

EDITORIAL BOARD

Chairman
L. D. DOUGAN, Polymer Corp. Limited,
Sarnia, Ont.

P. W. BLAYLOCK, Shawinigan Chemicals Limited,
Montreal, Que.

W. M. CAMPBELL, Atomic Energy of Canada Limited,
Chalk River, Ont.

F. A. FORWARD, University of British Columbia,
Vancouver, B.C.

J. W. HODGINS, McMaster University,
Hamilton, Ont.

A. I. JOHNSON, McMaster University,
Hamilton, Ont.

R. R. McLAUGHLIN, University of Toronto,
Toronto, Ont.

G. L. OSBERG, National Research Council,
Ottawa, Ont.

A. C. PLEWES, Queen's University,
Kingston, Ont.

L. W. SHEMILT, University of New Brunswick,
Fredericton, N.B.

J. H. SHIPLEY, Canadian Industries Limited,
Montreal, Que.

H. R. L. STREIGHT, Du Pont of Canada Limited,
Montreal, Que.

EX-OFFICIO

LEO MARION, President, The Chemical Institute of Canada.

LEO YAFFE, Chairman of the Board of Directors.

J. H. SHIPLEY, Director of Publications.

Authorized as second class mail, Post Office Department, Ottawa, and for payment of postage in cash. Postage paid at Ottawa. Printed in Canada.

Manuscripts for publication should be submitted to the Editor: Dr. A. Cholette, Faculty of Science, Laval University, Boulevard de l'Entente, Quebec, Que. (Instructions to authors are on the next page).

Editorial, Production and Circulation Offices: 48 Rideau Street, Ottawa 2, Ont.

Advertising Office: C. N. McCuaig, manager of advertising sales, *The Canadian Journal of Chemical Engineering*, Room 601, 217 Bay Street, Toronto, Ont. Telephone—EMpire 3-3871.

Plates and Advertising Copy: Send to *The Canadian Journal of Chemical Engineering*, 48 Rideau Street, Ottawa 2, Ont.

Subscription Rates: In Canada—$6.00 per year and $1.25 per single copy; U.S. and U.K.—$7.00, Foreign—$7.50.

Change of Address: Advise Circulation Department in advance of change of address, providing old as well as new address. Enclose address label if possible.

The Canadian Journal of Chemical Engineering is published by The Chemical Institute of Canada every two months.

Unless it is specifically stated to the contrary, the Institute assumes no responsibility for the statements and opinions expressed in *The Canadian Journal of Chemical Engineering*. Views expressed in the editorials do not necessarily represent the official position of the Institute.

The Canadian Journal of Chemical Engineering

INSTRUCTIONS TO AUTHORS

Manuscript Requirements for Articles

1. The manuscript should be in English or French.
2. The original and two copies of the manuscript should be supplied. These are to be on 8½ x 11 inch sheets, typewritten, and double spaced. Each page should be numbered.
3. Symbols should conform to American Standards Association. An abridged set of acceptable symbols is found in the third edition of Perry's Chemical Engineers' Handbook. Greek letters and subscripts and superscripts should be carefully made.
4. Abstracts of not more than 200 words in English indicating the scope of the work and the principal findings should accompany all technical papers.
5. References should be listed in the order in which they occur in the paper, after the text, using the form shown here: "Othmer, D. F., Jacobs, Jr., J. J., and Levy, J. F., Ind. Eng. Chem. **34**, 286 (1942). Abbreviations of journal names should conform to the "List of Periodicals Abstracted by Chemical Abstracts". Abbreviations of the common journals are to be found in Perry's Handbook also. All references should be carefully checked with the original article.
6. Tables should be numbered in Arabic numerals. They should have brief descriptive titles and should be appended to the paper. Column headings should be brief. Tables should contain a minimum of descriptive material.
7. All figures should be numbered from 1 up, in Arabic numerals. Drawings should be carefully made with India ink on white drawing paper or tracing linen. All lines should be of sufficient thickness to reproduce well, especially if the figure is to be reduced. Letters and numerals should be carefully and neatly made, with a stencil. Generally speaking, originals should not be more than twice the size of the desired reproduction; final engravings being 3¼ in. or 7 in. wide depending on whether one column or two is used. For further details ask the Editor for the Guide for Drawings.
8. Photographs should be made on glossy paper with strong contrasts. Photographs or groups of photographs should not be larger than three times the size of the desired reproduction.
9. All tables and figures should be referred to in the text.

Submission of Manuscripts

1. The three copies of the manuscript, including figures and tables, should be sent directly to:
   DR. A. CHOLETTE, editor,
   The Canadian Journal of Chemical Engineering,
   Faculty of Science, Laval University,
   Boulevard de l'Entente,
   Quebec, Que.
2. The authors addresses and titles should be submitted with the manuscript.
3. The author may suggest names of reviewers for his article, but the selection of the reviewers will be the responsibility of the editor. Each paper or article is to be reviewed by two chemical engineers familiar with the topic. Reviewers will remain anonymous.
4. All correspondence regarding reviews should be directed to the editor.

Reprints

1. At least 50 free "tear sheets" of each paper will be supplied.
2. Additional reprints may be purchased at cost. An estimated cost of reprints, with an attached order form, will be sent to the author with the galley proofs.
3. Orders for reprints must be made before the paper has appeared in the Journal.

Communications, Letters and Notes to the Editor

Short papers, as described below, will be considered for publication in this Journal. Their total length should be such that they will not occupy more than one page of the Journal.

Communications

A communication is a prompt preliminary report of observations made which are judged to be sufficiently important to warrant expedited publication. It usually calls for a more expanded paper in which the original matter is republished with more details.

Letters

A letter consists of comments or remarks submitted by readers or authors in connection with previously published material. It may deal with various forms of discussion arising out of a publication or it may simply report and correct inadvertent errors.

Notes

A note is a short paper which describes a piece of work not sufficiently important or complete to make it worth a full article. It may refer to a study or piece of research which, while it is not finished and may not be finished, offers interesting aspects or facts. As in the case of an article a note is a final publication.

* * *

An Analysis of Spray Evaporation in a High-Temperature Environment

I. Radiant Heat Transfer to Clouds of Droplets and Particles[1]

T. W. HOFFMAN[2] *and W. H. GAUVIN*[3]

This series of papers presents an analysis of the rate of evaporation of a spray which is injected into a cylindrical column, the walls of which are maintained at a high temperature. The method is an extension of the Hottel-Cohen analysis of the radiant heat transfer to an absorbing gas of non-uniform temperature[1] and permits the calculation of the magnitude and distribution of the heat flux at the wall.

The present paper discusses the difficulties inherent in the calculation of the absorption of thermal radiation by clouds of particles suspended in an absorbing gas medium. Approximations to the intractable exact solution are made to permit the calculation of the absorption strength of spray from operating conditions and the properties of the atomized liquid.

The various reception factors for the cylindrical system have been accurately determined as a function of the combined absorption strength of spray and medium. The use of these factors in the present system is discussed.

Dans cette série d'articles on présente une analyse du taux d'évaporation d'un jet pulvérisé injecté dans une colonne cylindrique dont les parois sont maintenues à une température élevée. La méthode décrite est une extension de l'analyse de Hottel et Cohen pour le transport de la chaleur par rayonnement à un gaz absorbant, de température non-uniforme. Elle permet de calculer l'intensité et la distribution du taux de transport de chaleur à la paroi.

Les auteurs exposent les difficultés inhérentes au calcul de l'absorption d'énergie rayonnante par des suspensions de particules dans un milieu gazeux absorbant. Ils ont recours à des approximations des solutions exactes, difficiles à résoudre, pour calculer le pouvoir absorbant d'un jet pulvérisé à partir des conditions expérimentales et des propriétés du liquide vaporisé.

On a déterminé de façon précise les différents facteurs de réception pour le système cylindrique, en fonction du pouvoir absorbant combiné du jet et du milieu. On traite de l'utilisation de ces facteurs dans le présent système.

When a cloud of droplets flowing through a cylindrical enclosure is subjected to thermal radiation, evaporation will occur over at least part of the column. The vapors thus generated are generally athermanous, i.e., they will absorb thermal radiation in certain wave-length regions of the infra-red spectrum. As a result, an additional heat load, other than the sensible heat increase of the gas, will be maintained in the column, causing severe variations in the temperature of the gas from the top — or inlet of the column — to the bottom.

This paper deals with the problem of estimating the radiation from the heated walls of a cylindrical enclosure to a cloud of droplets of particles contained in an absorbing medium, the temperature of which varies from top to bottom. In addition, the temperature of the walls of the column may vary over the column height, depending on the process requirements. Furthermore, the cloud will be assumed to consist of droplets and/or particles which are in the size range from 10 to 200 microns. These droplets are of a size comparable to the wave lengths under consideration, since most of the infra-red spectrum is contained in the 1-to-15 micron wave length region. Moreover, these particles may be only partially opaque to the radiation striking them.

[1]*Manuscript received April 8; accepted June 29, 1961.*
[2]*Department of Chemical Engineering, McMaster University, Hamilton, Ont.*
[3]*Department of Chemical Engineering, McGill University and Pulp and Paper Research Institute of Canada, Montreal, Que.*
Contribution from the Department of Chemical Engineering, McGill University and the Pulp and Paper Research Institute of Canada, Montreal, Que.

1. *Gas Radiation*

In a recent paper[(1)], Hottel and Cohen presented a method of calculating the radiant heat exchange in an enclosure containing an absorbing medium. In this method, varying space temperatures are taken into account. The technique involves dividing the enclosure into a number of surface and gas zones, each of which can be considered isothermal. Their size and number depend upon the accuracy desired. Reception factors corresponding to F_{12} for an absorbing medium in Hottel's nomenclature[(2)] were computed for a square-cube system for surface-surface, gas-surface, gas-gas thermal radiation interchange. The determinant technique, presented earlier by Hottel[(2)] for solution of problems in a grey enclosure containing a non-absorbing medium, was extended to this system. By means of this technique, total interchange factors corresponding to $\mathscr{F}_{12}$[(2)] can be calculated from the reception factors to allow for the reflective flux from all surface zones. Heat and material balances are then made on all surface and gas zones. To perform this balance on a gas zone, for example, one must add together the net radiant heat received from all other gas zones and surface zones, the net convective/conductive heat from adjacent gas and surface

zones, and the enthalpy increase or decrease in the zone. For any such system, the unknowns in the resulting equations are the temperatures of the gas zones, and the number of unknown temperatures is equal to the number of equations. The solution of the simultaneous equations allows a prediction of the temperature of the gas zones and of the heat flux distribution in the enclosure.

The key parameter in applying this method of solution to the radiant heat interchange problem is the absorption coefficient $\underline{k}$ of the gas, which is a measure of the absorption strength of the absorbing medium. For a grey gas, $\underline{k}$ is constant over the full wave-length spectrum and the expression relating the emissivity or absorptivity of a gas to the absorption coefficient is:

$$a = \epsilon = 1 - e^{-\underline{k}l} \quad \ldots\ldots\ldots\ldots\ldots\ldots (1)$$

where l is the thickness of the gas.

However, absorption and emission of thermal radiation by a real gas occur only over several well-defined wave-length bands, i.e., only over part of the wave-length spectrum. Hottel[2] has thus proposed that the actual emissivity or absorptivity versus path length curve can be made up of the sum of a number of grey gas absorption coefficients, as in Equation (1), but each will have a specific weighting factor, namely

$$\epsilon = \sum_i a_i (1 - e^{\underline{k}_i l}) \text{ where } \sum_i a_i = 1 \quad \ldots\ldots\ldots\ldots (2)$$

Proceeding one step further, Hottel suggests that a real gas can be replaced by a grey and a clear gas. The grey gas, with absorption coefficient $\underline{k}$, can be thought of as occupying the fraction a of the spectrum and the clear gas ($\underline{k} = 0$) occupying the fraction $1 - a$. In essence, this scheme is one of fitting an emissivity versus path length curve to an exponential equation of the form:

$$\epsilon = a(1 - e^{-\underline{k}l}) \quad \ldots\ldots\ldots\ldots\ldots\ldots (3)$$

It must be remembered that a and $\underline{k}$ depend on the conditions and dimensions of the system under consideration.

Hottel and Egbert[3] have shown that, for any enclosure in which the surface emissivity is fairly high, only the first surface reflection of the radiation is of any importance, for the radiation undergoes double attenuation on each reflection — first by the gas and then by the surface. Therefore the emissivity should be keyed to Equation (3) at zero path length ($l = 0$), at one mean beam length L of the enclosure at which $\epsilon = \epsilon_L$, and at twice this length ($\epsilon = \epsilon_{2L}$). Then a and $\underline{k}L$ have been shown[2] to be given by the relations:

$$a = (\epsilon_L)^2/(2\epsilon_L - \epsilon_{2L}) \quad \ldots\ldots\ldots\ldots\ldots\ldots (4)$$

$$\underline{k}L = ln\,[\epsilon_L/(\epsilon_{2L} - \epsilon_L)] \quad \ldots\ldots\ldots\ldots\ldots\ldots (5)$$

$$\underline{k}Z = (1/\Psi)\,ln\,[\epsilon_L/(\epsilon_{2L} - \epsilon_L)] \quad \ldots\ldots\ldots\ldots\ldots\ldots (6)$$

Where Z is the characteristic length of the system and Ψ is the factor by which this characteristic length must be multiplied to give the mean beam length. Appendix C presents a method of finding Ψ for any cylindrical enclosure containing any given concentration of absorbing medium.

Hottel and Cohen[1] present a number of plots of reception factors for surface-to-surface, surface-to-gas interchange in a black enclosure, based on a square and cube system. These factors are plotted as a function of $\underline{k}b$, where b is the side of a cube or square. Total interchange factors can be built up from these plots.

When using these plots and, in fact, when employing this method, the absorption coefficient $\underline{k}$ and the weighting factor a are assumed to be constant throughout the enclosure. These authors present a detailed discussion concerning this necessary simplification. Their conclusions are that although moderate variations may occur in these parameters, the error is minimized, for one is still allowing for the major temperature variation. The factors $\underline{k}$ and a affect only the coefficients (i.e., the interchange factors); the emissive power $(\sigma T_i)^4$ is allowed to vary at will.

Thus the problem of solving for temperature and heat flux distribution in an enclosure containing a temperature-varying absorbing medium can be handled with considerable accuracy. However, if one introduces a cloud of particles into this medium, the problem becomes more complicated, for now complex surface and gas emission or absorption arises in each gas zone.

2. *Radiation to Clouds of Particles*

For the present, the following discussion is restricted to the case of radiation to a cloud of particles suspended in a non-absorbing medium.

When thermal radiation traverses a cloud of particles, part of it may be absorbed by these particles and part of it may be reflected or scattered. The magnitude and direction of the scattered portion and the amount absorbed may be found from the equations presented by Mie.* The exact Mie solution applies to electro-magnetic waves at any frequency striking a particle of any size.

Both scattering and absorption remove energy from the radiant beam in the direction of propagation of the beam.** This extinction or attenuation along the direction of travel is usually expressed by the Beer-Lambert Law:

$$I = I_o\, e^{-\gamma l} \quad \ldots\ldots\ldots\ldots\ldots\ldots (7)$$

where I is the intensity of the radiation after traversing a distance l, and I_o is the intensity at $l = 0$. The extinction coefficient γ is computed from the expression

$$\gamma = \int_o^\infty N(r)\, \pi r^2\, Q_{ext}\, dr \quad \ldots\ldots\ldots\ldots\ldots\ldots (8)$$

for the case of particles of different radii. In this expression $N(r)$ is the number of particles per unit volume with radii in the interval dr. Q_{ext} is termed the efficiency factor for extinction in the forward direction; it is the ratio of the extinction cross-section, S, to the geometric cross-section πr^2. It should be remembered that Equation (8) is valid only for a relatively thin cloud — i.e., for situations where the scattered intensity is directly proportional to the number of particles. This implies that each particle is essentially exposed to the original radiation. With large particle concentrations or relatively great thicknesses, multiple scattering may occur. Then this simple proportionality does not hold, for now particles are exposed not only to a fraction of the original beam, because of extinction, but also to the scattered radiation from other particles. This situation arises for $\gamma l > 0.1$[5], which is usually the case here. The discussion which follows is still valid for the scattering of a single particle, but the analysis of the overall picture becomes very complex, especially so in those cases where the cloud is restricted to finite dimensional limits. At still greater concentrations, i.e., when inter-particle distances are less than $3r$, phase interactions and interference phenomena result[5].

The Mie Theory predicts the extinction cross-section, S, for transparent and absorbing spheres. For non-absorbing spheres

$$S = \frac{\lambda^2}{2\pi} \sum_{n=1}^{\infty} (a_n + b_n)/(2n + 1) \quad \ldots\ldots\ldots\ldots (9)$$

where a_n and b_n are complex functions of the parameter $x = 2\pi r/\lambda$ and the refractive index m. When there is appreciable absorption within the sphere, this may be taken into account by employing

*An excellent presentation of the Mie Theory in condensed form is given by V. K. LaMer[4].

**"Scattered radiation" refers to any radiation which does not proceed along the line of original propagation. In this sense, it includes the reflected, the refracted and the diffracted part of the beam.

a complex refractive index $m = n - in'$, where n' is the absorption index and is usually a strong function of wave-length. For absorbing spheres, Equation (9) gives the scattering cross-section only, and the total radiation abstracted from the incident beam (scattered plus absorbed) is found from:

$$S_{ext} = \frac{\lambda^2}{2\pi} Re\left[\sum_{n=1}^{\infty} (-1)^n i(a_n + b_n)\right] \quad \ldots\ldots\ldots (10)$$

where Re stands for the real part of the expression in the brackets.

Thus, for the problem of thermal radiation to a cloud of droplets or particles, the difficulties in applying the Mie solution become immediately apparent. These difficulties arise because the extinction cross-section, and thus the exponent γ in Equation (7) depends on r, λ and m. Here the full spectrum of thermal radiation wave-lengths, the distribution of particle size in the cloud, and the variable refractive index must be considered. Moreover, in practice thick dense clouds are usually encountered and multiple scattering results.

Other difficulties arise when an attempt is made to apply the Mie solutions to the problem at hand. Thus, a simplification is necessary for engineering applications which is fortunately possible under certain conditions. When the parameter $x = 2\pi r/\lambda$ becomes large, the extinction efficiency Q_{ext} tends to a limiting value of two, that is, the extinction cross-section becomes $2\pi r^2$.* Geometrical optics predicts that the covering capacity of a spherical particle should be equal to the cross-sectional area of the particle, πr^2. This seeming anomaly has been explained by Sinclair[6] and Lothian and Chappel[7], who pointed out that the Mie Theory accounts for diffraction as well as absorption and reflection of the radiant beam by the particle. On the basis of Babinet's principle of diffraction of light, it is shown that a circular opaque disc diffracts an amount of light equal to that which actually strikes the disc. Furthermore, Gumprecht and Sliepcevich[8] have shown that this diffracted radiation is concentrated within a relatively small cone angle in the forward direction (ca. 2° for values of $x = 100$ and $m = 1.33$). This angle becomes larger as x decreases, but at all values of x that are of interest, and certainly for the enclosure under consideration, this part of the beam need not be considered scattered. Thus the main concern is that part of the beam which is reflected and/or absorbed.

If the average absorptivity of the particle a_p is close to one, that is, the particles behave very nearly like black bodies, then the reflected part of the radiation is inconsequential and for a cloud of particles, Equation (7) becomes:

$$I = I_o e^{-a_p N_v \pi r_s^2 l} \quad \ldots\ldots\ldots (11)$$

where r_s is the mean surface radius calculated from:

$$r_s^2 = (\sum_i n_i r_i^2)/\sum_i n_i \quad \ldots\ldots\ldots (12)$$

For this case, Equation (11) is exact; however if the particles are only partially absorbing, then this expression (with a_p removed) is restricted to the direction of propagation only. Equation (11) has been derived previously by Haslam and Hottel[9] from geometrical optics considerations and was used by Johnstone et al[10] in their studies on heat transfer to clouds of particles.

The absorptivity of a droplet depends on its material composition, the wave length of radiation striking it, and upon its size (more exactly its volume). As mentioned previously, it is possible to compute the exact absorption within the particle by employing the Mie equations. It is interesting to note that for particles approaching black conditions, a minimum size is indicated by these equations. Van de Hulst[5] points out that two conditions are necessary:

(1) that a negligible fraction is reflected;

(2) that the sphere is not transparent.

Condition (1) implies that $|m-1| \ll 1$ so that n and n' must be small. If m is not close to 1, reflection at the surface according to Fresnel's formula is:

$$R_\phi = \frac{1}{2}\left[\frac{\sin^2(\theta - \psi)}{\sin^2(\theta + \psi)} + \frac{\tan^2(\theta - \psi)}{\tan^2(\theta + \psi)}\right] \quad \ldots\ldots\ldots (13)$$

where R_ϕ is the fraction reflected and from the refractive law (see Figure 1(a)):

$$\sin\theta = m \sin\psi \quad \ldots\ldots\ldots (14)$$

Condition (2) implies that $n' x \gg 1$ and since condition (1) indicated that n' is small, then $x = 2\pi r/\lambda$ must be large (ca. 100, or the radius of the particle must be larger than about fifteen times the wave-length).

To circumvent the complex Mie solution, geometrical optical methods can be applied to this absorption problem. Nusselt[11] has shown that the absorptivity of a sphere containing an absorbing medium with an average absorption coefficient K can be calculated from:

$$a_p = 1 + [e^{-2Kr}/Kr] - [1 - e^{-2Kr}]/2(Kr)^2 \quad \ldots\ldots\ldots (15)$$

This equation is valid only for the case where the refractive index is the same as that for the medium in which it is immersed, that is, $m = 1$ for a droplet in a gas.

Simpson[12] proposed a solution for the absorptivity of a droplet when one takes into account refraction within the drop, but not external reflection. The resulting equation is:

$$a_p = m^2/K^2r^2(2)\left\{\left[(2Kr + 1)e^{-2Kr}\right] + \left[2K^2r^2/m^2 - \left\{e^{-2Kr[(m^2-1)/m^2]^{1/2}}\right\}\left\{2Kr\left(\frac{m^2-1}{m^2}\right)^{1/2} + 1\right\}\right]\right\} \quad \ldots (16)$$

If one considers reflection and refraction of the radiant beam at every liquid-gas interface, (see Figure 1(b)) then a more complicated expression results:

$$a_p = \int_o^{\pi/2} (1 - R_\phi)\sin 2\theta \left[\frac{1 - e^{-2Kr\cos\psi}}{1 - R_\phi e^{-2Kr\cos\psi}}\right] d\theta \quad \ldots\ldots\ldots (17)$$

which must be solved by graphical methods. The parameters in this equation were previously defined by Equations (13) and (14). This expression resulted from an analysis by geometrical optics or ray tracing, by Thomas[13] and Simpson[12]. It should be pointed out that the absorptivity calculated from Equation (17)

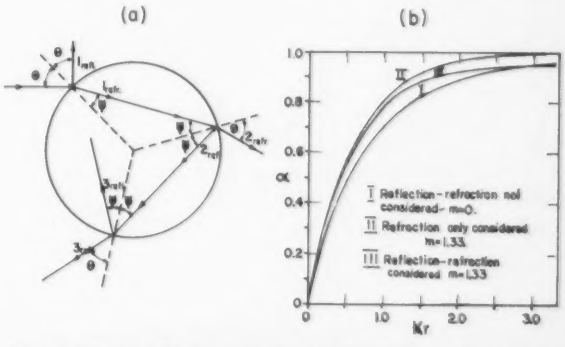

Figure 1(a) — Diagrammatic sketch of drop showing refracted and reflected radiation.

Figure 1(b)—Plot shows effect of liquid absorption coefficient and drop radius on droplet absorptivity.

*The scattering cross-section as calculated from the Mie Theory is not $2\pi r^2$ for all x. It can be more or less than $2\pi r^2$ depending upon the interference effects of the reflected, refracted and diffracted radiation. The laws of geometrical optics are asymptotic laws for electromagnetic waves. Geometrical or rayoptic methods may be used when the particles become large in comparison to the wave-length of the radiation striking the particle.

is not entirely correct. In its derivation the phase shifts and lags were not considered and thus interference effects have not been included. However the absorptivity calculated from this equation is considered to be a good approximation to the actual absorptivity, as long as the drop is fairly large.

Absorptivities calculated from these equations for a real refractive index, $m = 1.33$ (this is the average real part of the refractive index of water for wave-lengths up to 15 microns) are shown in Figure 1(b). It can be seen that the absorptivity approaches an asymptotic value at large values of the parameter Kr. Thus the absorptivity of a drop may approach that of a black body (here $a_p \approx 0.95$) if the drop radius and/or the absorption coefficient of the liquid is large.* As expected Figure 1(b) shows that reflection and refraction have a significant effect on the absorptivity of a drop. Certainly the addition of foreign solid material into the droplet will increase its absorptivity above that given by Figure 1(b).

Simpson[12] also goes on to show that refraction greatly affects the distribution of radiant energy absorption within the droplet, for all radiant beams must pass through a relative radius $r' = r/m$. Under certain conditions of absorption, this phenomenon may cause a higher absorption within the sphere at this point than at the surface, and internal boiling may result.

Returning to the cloud of droplets, consideration may be restricted for the present to the case where Kr is large enough, so that almost complete absorption does take place within the drop — at least to such an extent that reflection/refraction effects may be neglected. Then the exponent in Equation (7) would be of the form $\underline{k}_\epsilon l$, where $\underline{k}_\epsilon l = a_p \pi r_i^2 N_v$. This is convenient, for then the methods described for gas radiation would be applicable. It is unlikely that the absorptivity of the spray droplets in this process will be close to one, which would require relatively large values of K or r, unless, of course, any solute in the drop greatly affects the absorption coefficient of the drops. Thus Mie scattering or reflection/refraction effects should be considered. Since, however, the complexities arising in considering these effects are enormous (and even more so if account is taken of the absorbing medium in an enclosure of finite dimensions), it appears advisable to use Equation (7), no matter what the absorptivity of the particles may be and to ascertain experimentally the error involved in making this simplification. The deviation will arise as a result of the scattered radiation, which may be of greater importance when the particles are in an absorbing gaseous environment. At least the variables to be considered are identified; qualitative information is made available; the shortcomings of the simplification are known; and a starting point is established from this analysis.

3. *Cloud of Particles in an Absorbing Medium*

As suggested above, the attenuation of radiation during its passage through a cloud of particles can be expressed as a function of $\underline{k}_\epsilon = a_{\text{part.}} \pi r_i^2 N_v$. On the other hand, the attenuation by an absorbing gas is a function of the gas absorption coefficient, $\underline{k}_G$. Each of these factors enters as an exponent for the exponential function.

When both particles and absorbing gas are to be considered together in the same enclosure, these "resistances" operate in parallel and it can easily be shown that the exponents $\underline{k}_\epsilon$ and $\underline{k}_G$ should be added to give the attenuation of the traversing radiation. Thus over fraction 'a' of the spectrum the equation expressing this decrease in intensity is:

$$I' = I_o e^{-(\underline{k}_\epsilon + \underline{k}_G)l} \quad \ldots\ldots\ldots\ldots\ldots\ldots (18)$$

and over $(1 - a)$ of the spectrum, where only the cloud is the active absorber:*

$$I'' = I_o e^{-\underline{k}_\epsilon l} \quad \ldots\ldots\ldots\ldots\ldots\ldots (19)$$

or for the full spectrum, the intensity after traversing a distance l is given by:

$$I = I_o \left[a\, e^{-(\underline{k}_\epsilon + \underline{k}_G)l} + (1 - a) e^{-\underline{k}_\epsilon l} \right] \ldots\ldots\ldots (20)$$

Some of the problems inherent in evaluating $\underline{k}_\epsilon$ will be discussed subsequently.

4. *Choice of Zone Size*

In order to employ the Hottel-Cohen method as outlined in section 1, it is necessary to choose zones small enough that they may be considered isothermal, and such that they have substantially the same view of all other zones. This latter restriction is necessary only for the proper distribution of reflective fluxes; in industrial enclosures, where surface absorptivities are relatively high, this factor is only of minor importance. It will be realized that, for this method to be rigorous (that is, the above stipulations rigorously adhered to), the zones must necessarily be differential in size. Differential zones are mathematically impossible, however, because of the integral character of radiation, and thus zones of finite size must be considered. Maximum accuracy is possible if the zone size is kept small; this increases the number of zones in any given cylindrical enclosure, however, and makes the calculations exceedingly long and laborious.

A cylindrical zone of height equal to diameter may therefore be considered to be a satisfactory compromise. This implies immediately that radial temperature gradients are small, and that longitudinal temperature gradients within the enclosure are not excessive. The former restriction seems reasonable, at least for columns of relatively small diameter. Also, a suitable average temperature for each zone may be chosen.

Appendix A illustrates the formulation of the equations governing the reception factors for this case. The derivation of these equations is similar to that presented by Hottel and Cohen[1]. It can be seen that these equations are based on the fact that a bundle of rays leaving a radiator proceeds in a straight line. As pointed out in the previous sections, some "diffusion" of radiation from this pencil of rays takes place because of particle scatter. In computing these view factors this is not accounted for; however an exponential law will describe the decay of radiation passing through a medium such as that under consideration — the problem is to ascertain the exponent.

5. *Energy and Material Balances on Each Zone*

The Hottel-Cohen method necessitates the formulation of heat and material balances on each zone in the system. Expressing the balance on G_i:

$$\left[\begin{array}{l} \left\{\begin{array}{l}\text{Thermal radiation}\\ \text{into } G_i \text{ from } G_1, G_2 \ldots\\ \text{and } S_1, S_2 \ldots \text{ (direct}\\ \text{plus reflected)}\end{array}\right\} \\ + \left\{\begin{array}{l}\text{Enthalpy flux into } G_i\\ \text{as sensible heat in the}\\ \text{flowing material}\end{array}\right\} \\ + \left\{\begin{array}{l}\text{Convective/conduc-}\\ \text{tive heat into } G_i \text{ from}\\ \text{adjacent zones}\end{array}\right\} \\ + \left\{\begin{array}{l}\text{Heat into } G_i \text{ as a}\\ \text{result of chemical}\\ \text{reaction}\end{array}\right\} \end{array}\right] = \left[\begin{array}{l} \left\{\begin{array}{l}\text{Thermal radiation}\\ \text{from } G_i \text{ to all other}\\ \text{gas and surface zones}\end{array}\right\} \\ + \left\{\begin{array}{l}\text{Enthalpy flux out of}\\ G_i \text{ as sensible heat in}\\ \text{the flowing material}\end{array}\right\} \\ + \left\{\begin{array}{l}\text{Conductive/convec-}\\ \text{tive heat flow out of}\\ G_i \text{ to adjacent zones}\end{array}\right\} \\ + \left\{\begin{array}{l}\text{Heat load within zone}\\ G_i \text{ due to chemical}\\ \text{reaction, evaporation}\\ \text{etc.}\end{array}\right\} \end{array}\right]$$

*Simpson[12] determined a value of $K = 15.5$ cm.$^{-1}$ for heavy oil fuel droplets. Thomas[13] feels that a value greater than 100 cm.$^{-1}$ should be used for water droplets. Measurements similar to Simpson's have not been made for water, although the absorption measurements by Brown, Sato and Sage[14] on thin water films show the absorption coefficient to be quite high.

*This assumes that the droplets absorb equally over all wave lengths.

In the resulting series of equations, the wall temperatures are known but the longitudinal gas-temperature distribution is not. Furthermore, since the evaporative load in each zone depends on the temperature of the gas in that zone, this factor emerges as an unknown as well for each gas zone. The result is a very complex trial and error solution, the steps for which are briefly as follows:

(1) Assume a temperature distribution;

(2) From the drop-size distribution and drop velocity distribution at the top — or inlet — of the column and using (1), calculate the evaporation of a size interval (say, the interval from 30 to 40 microns, with $d_{ave} = 35\mu$) with distance. Repeat for all size intervals.

(3) From (2) ascertain the evaporative load in each zone;

(4) Using (3) calculate the temperature in each zone from the heat and material balance equations;

(5) Repeat steps (2), (3), (4) for this temperature distribution.

The details of these calculations will be the subject of subsequent papers.

On the basis of the balance equations, the mechanism of heat transfer in the column can be determined and this will help in estimating the temperature variation down the column.

In that part of the column where evaporation takes place, a dynamic temperature balance in the gas is maintained. The heat transfer by radiation and convection from the walls and other gas zones to the zone in question must be the same as that which is transferred by convection-conduction from the gas to the droplets to effect evaporation and to heat the generated vapours to the temperature of the gas in that zone.* The temperature of the gas will remain relatively constant** over a length of the column, as can be deduced from the following discussion. One must remember that the evaporation of a drop of diameter d_i by convection/conduction effects is given by:

$$(dm/d\theta)_i = [h_i A_{d_i} (t_G - t_{d_i})]/\lambda \quad \ldots\ldots\ldots\ldots (21)$$

where t_d is the temperature of the drop and will be very near the boiling point of the liquid. The apparent heat transfer coefficient, h_i, for a drop of diameter d_i moving at a low relative droplet Reynolds number (16, 17) can be satisfactorily approximated by the Ranz and Marshall Equation (15), corrected for the outward flow of cold vapor from the drop[18]:

$$\frac{h_i d_i}{k_d} = \frac{ln(1+B)}{B}[2 + 0.60\, Re^{1/2}\, Pr^{1/3}] \quad \ldots\ldots\ldots (22)$$

where B is Spalding's Transfer number, $c_p(t_G - t_d)/\lambda$ (18). Thus an increase in gas temperature t_G will decrease the amount of heat transferred from the walls to the gas. Since the resistance to heat transfer at the drop surface is low — that is h_i is high — relatively low temperatures will be observed in the upper zones of the tower. The governing step in this transfer process will be the heat flux from the wall to the gas. Since the gas throughput is small, it is expected that the main transfer process will be that of thermal radiation. The gas temperature in any given system and at any given wall temperature will be a function of the drop surface area available for convective heat transfer from the gas to the droplets. Thus, only when evaporation of the smaller of the size groups is completed will the temperature of the gas increase. This particular phenomenon will be discussed in greater detail in a subsequent paper.

If the feed solution does not contain any solute or suspended solid then the drops will disappear upon evaporation. If a solid residue remains suspended in the gas, Nusselt[19] and more recently Sleicher and Churchill[20] in a more rigorous mathematical development, have shown that these particles, subjected to a radiant flux, increase in temperature very rapidly and finally exceed the temperature of the gas by an amount dependent upon their size, absorptivity and position in the cloud from the radiating source. The temperature of the particle will be such that the amount of radiant heat it intercepts and absorbs, balances the amount of heat it transfers to the gas by conduction/convection. Because of the magnitude of the latter effects, however, the temperature difference between particle and gas will be relatively small[21]. The presence of particles thus should make the temperature of the gas increase at a faster rate than if they were absent.

*Radiation from the gas to the droplets will be small in comparison to that transferred by the convection/conduction mechanism.

**Otherwise some of the heat transferred from the walls will be required to increase the sensible heat content of the gas.

Conclusions

In the analysis which has just been presented, an attempt has been made to develop a method of solution capable of yielding results sufficiently accurate for engineering design purposes. Although most of the assumptions which have been made appear reasonable, it must be recognized that the proposed approach is incapable of dealing with the extremely complex effects resulting from the scattering, reflection and refraction of radiation by the particles in an absorbing medium of finite dimensions. The use of Equation (7) which is recommended in this study may prove to be an over-simplification, but appears to be a logical starting point for the present.*

Before the method of solution can be used, it is necessary to know the reception factors for a cylindrical system containing an absorbing medium. These have been calculated (see Appendix A) and the results are shown in Figures 2 to 8.

To estimate the temperature profile in the column by means of the heat balances discussed in section 5, it is necessary to calculate the magnitude and distribution of the radiant heat flux. This in turn necessitates the calculation of total interchange areas between zones, making due allowance for the multiple reflections in the system. These total interchange factors can be built up from the reception factors, as shown in Appendix B. It is interesting to note that the latter procedure also permits the estimation of the mean beam length for any cylindrical system, as discussed in Appendix C.

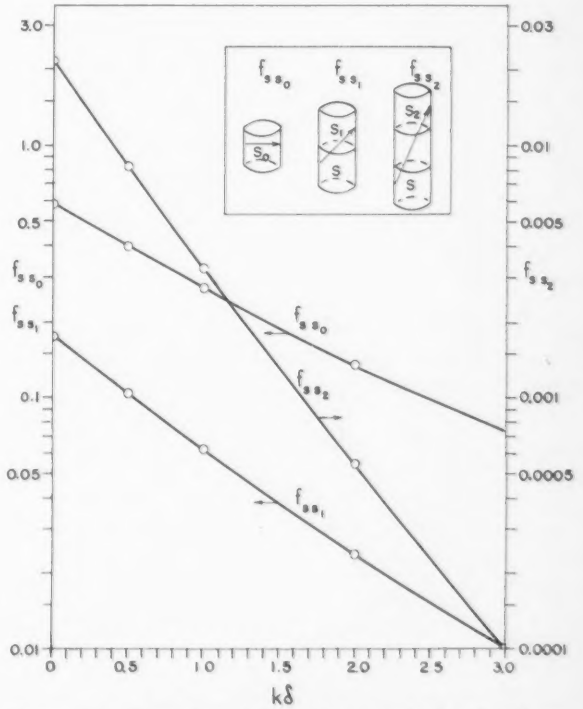

Figure 2 — Reception factors for a cylindrical column containing an absorbing medium $f_{s s_0}$, $f_{s s_1}$, $f_{s s_2}$.

*In a recent analysis, presented at the New York meeting of the A.S.M.E., Dec. 1960, Hottel and Sarofim have indicated how the zoning technique described in this paper could be modified to account, in an appropriate manner, for the scattering of radiation in particulate systems.

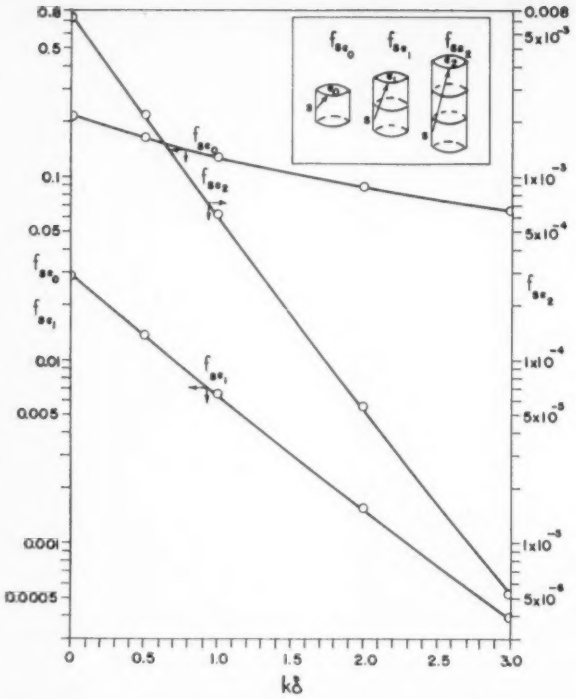

Figure 3 — Reception factors for a cylindrical column containing an absorbing medium f_{ss_0}, f_{ss_1}, f_{ss_2}.

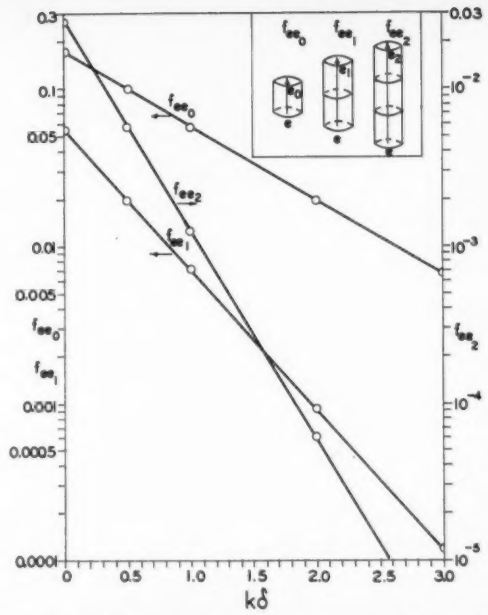

Figure 4 — Reception factors for a cylindrical column containing an absorbing medium f_{ss_0}, f_{ss_1}, f_{ss_2}.

One remaining difficulty should be mentioned. Because evaporation of the droplets in the column necessarily means a reduction in their size of their complete disappearance, the absorption coefficient k_e for the cloud is constantly decreasing with distance down the column. Approximate methods are available to deal with this problem which are discussed in Appendix D.

The details of an experimental study in which the above method of solution has been successfully applied will be presented in a subsequent paper.

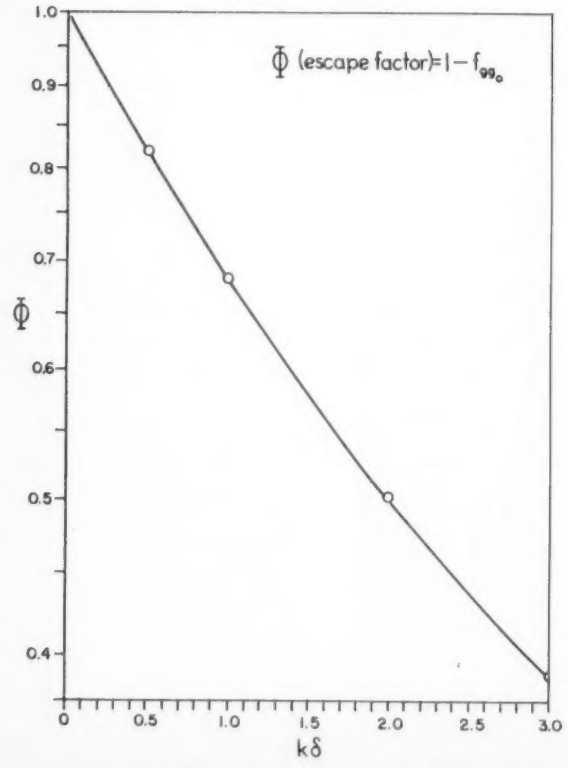

Figure 5 — Reception factors for a cylindrical column containing an absorbing medium $\Phi = 1 - f_{gg_0}$.

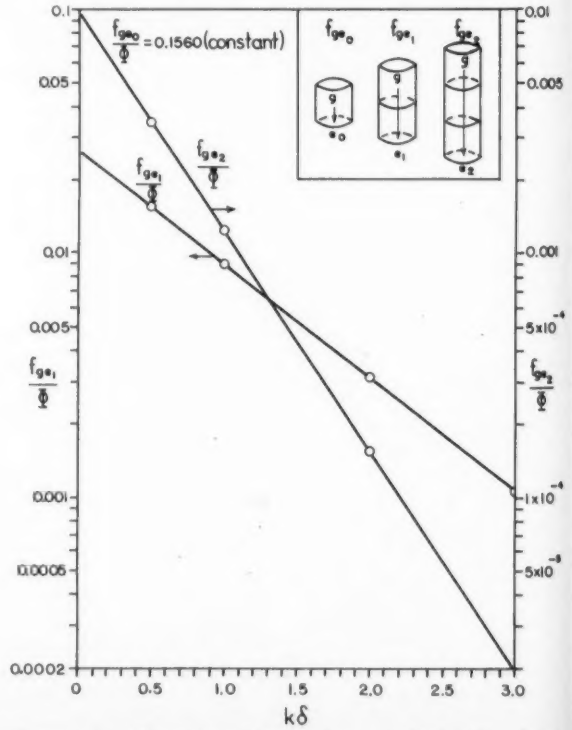

Figure 6 — Reception factors for a cylindrical column containing an absorbing medium f_{ge_0}, f_{ge_1}, f_{ge_2}.

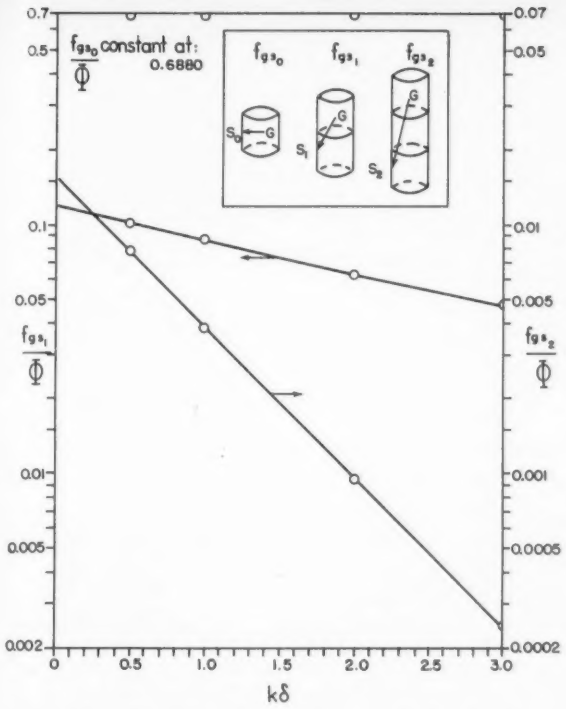

Figure 7 — Reception factors for a cylindrical column containing an absorbing medium f_{gs_0}, f_{gs_1}, f_{gs_2}.

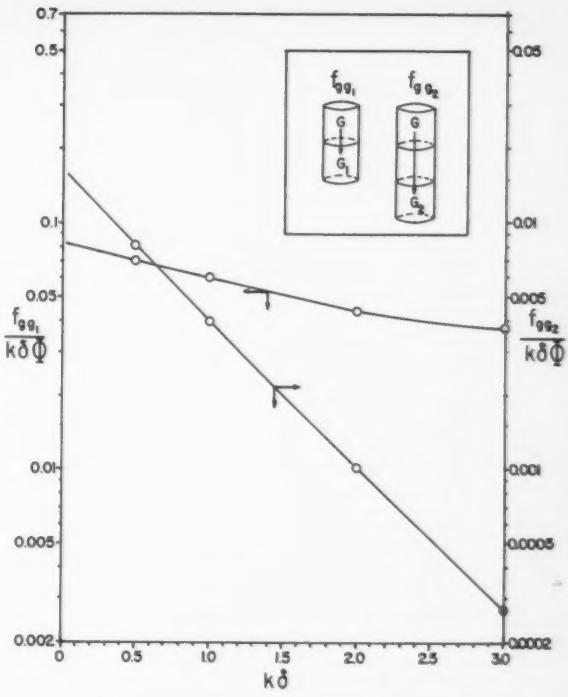

Figure 8 — Reception factors for a cylindrical column containing an absorbing medium f_{gg_1}, f_{gg_2}.

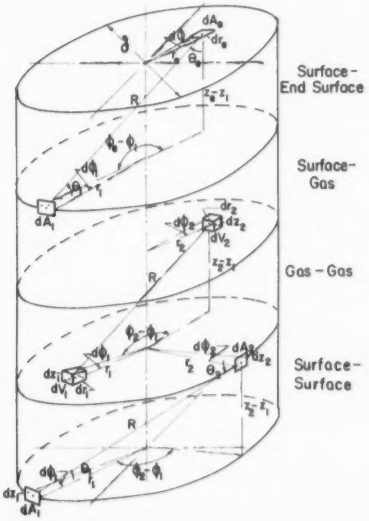

Figure 9—Differential elements upon which the formulation of the reception factors is based.

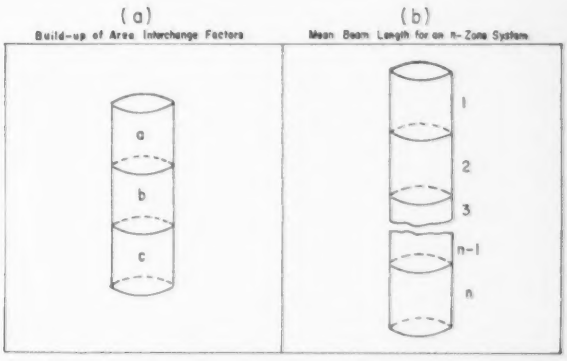

Figure 10(a)—Build-up of area interchange factors.
Figure 10(b)—Mean beam length for an n-zone system.

Acknowledgements

Financial assistance from the Pulp and Paper Research Institute of Canada and from the National Research Council is gratefully acknowledged. The authors also gratefully acknowledge the cooperation of the Computing Centre, McLennan Laboratory, University of Toronto and, in particular, W. Fraser who was responsible for some of the digital computations.

Nomenclature

Roman Symbols

A_i = surface area, ft.^{2}
a_i = weighting factors, dimensionless, (a in Equations (3) and C3)
a_n, b_n = complex functions of x, defined in Reference (4), dimensionless
b = side of cube or square
B = Transfer Number: $c_p\Delta T/\lambda$, dimensionless
c_p = heat capacity, (B.T.U.)/(lb.)(°F.)
d = diameter of droplet, ft.
$-Ei(-y)$ = exponential integral of y
f = reception factor between unit zones in a black-walled cylindrical system containing an absorbing medium — denotes the fraction of radiation leaving one zone (first letter) which reaches and is absorbed by another (second letter)
(1) f_{ss} = between two vertical surface zones
(2) f_{es} = between an end surface and a vertical surface zone.
(3) f_{ee} = between two end surface zones
(4) f_{sg} = between a vertical surface and a gas zone
(5) f_{eg} = between an end surface and a gas zone
(6) f_{gs} = between two gas zones
(subscripts defined on Figures 2 to 9), dimensionless

F_{12} = direct geometric view factor between two surfaces in a black-walled system containing a non-absorbing medium (see Reference 2), dimensionless

$\mathscr{F}_{12}$ = total interchange factor in a grey-walled system containing a non-absorbing medium (see Reference 2), dimensionless

F_{ss}, F_{ss} = . . . — elemental reception factors corresponding to f-factors, but between differential elements dh high

g, G = gas zone with numerical subscript to designate the particular zone under consideration

$\overline{gg}$ = direct interchange area between any two gas zones in a black-walled system, ft.²

$\overline{gs}$ = direct interchange area between a gas and surface zones in a black-walled system, ft.²

$\overline{GG}$ = total interchange area for a grey-walled system containing an absorbing medium which regulates the amount of radiation which reaches any one gas zone due to emission by another, including reflection at all grey surface zones, ft.²

$\overline{GS} = \overline{SG}$ = total interchange area for a grey-walled system containing an absorbing medium which regulates the total interchange between a gas and a surface zone, including reflections from other surface zones, ft.²

h = vertical separating distance, ft.

h_i = heat transfer coefficient for drop of diameter d_i

I = intensity of radiation from a surface

I_o = intensity of radiation from a surface at $l = 0$

i, j = subscripts to represent any gas or surface zone

k_g = thermal conductivity of gas, (B.t.u.)/(hr.)(ft.)(°F.)

k = absorption coefficient, ft.$^{-1}$

k_c = absorption coefficient of cloud, ft.$^{-1}$

k_G = absorption coefficient of gas, ft.$^{-1}$

K = absorption coefficient of liquid, ft.$^{-1}$

l = thickness of absorbing medium, ft.

L = mean beam-length, ft.

m = refractive index made up of a real and an imaginary part

n = integer in Equations (9) and (10)

n = real part of refractive index

n' = imaginary part of refractive index

n_i = number of particles in size group i

N = any whole number, including zero

$N(r)$ = number of particles per unit volume with radii in the interval dr

N_v = particle concentration, (number of particles)/(cu. ft.)

q = heat transfer rate, (B.t.u.)/(hr.)

Q_{ext} = efficiency factor for extinction in the forward direction, dimensionless

r = radius of droplet, ft.

r_i = radius of droplet in size group i, ft.

r_s = surface mean radius, ft. (defined in Equation (12))

R_θ = fraction reflected at surface, Equation (13)

Re = real part of expression in Equation (10)

R = subscript, refers to radiant heat

S = scattering cross-sectional area, ft.²

S_{ext} = extinction cross-sectional area (absorbed plus scattered), ft.²

S_1, S_2 = refers to surface zone, subscript number designates specific one

$\overline{ss}$ = direct interchange area between any two surface zones in a black-walled system containing an absorbing medium, ft.²

$\overline{se}$ = direct interchange area between a vertical surface and an end surface in a black-walled system containing an absorbing medium, ft.²

$\overline{sg}$ = direct interchange area between a surface and a gas zone in a black-walled system containing an absorbing medium, ft.²

$\overline{SS}, \overline{SG}$ = total interchange areas for a grey-walled system, which regulates the amount of radiation which reaches a surface or gas zone, respectively, due to emission by a surface zone, including reflections at all grey surface zones, ft.²

T = absolute temperature, °R.

t_G = gas temperature, °C.

t_d = particle temperature, °C.

V = gas volume, ft.³

V_t = total gas volume, ft.³

x = parameter: $2\pi r/\lambda$, dimensionless

Z = characteristic length of an enclosure, ft.

r, ϕ, z = cylindrical co-ordinates

Greek Symbols

a_p = particle absorptivity

γ = extinction coefficient, ft.$^{-1}$

δ = cylinder diameter, ft.

ϵ_G = gas emissivity

$\epsilon_L, \epsilon_{2L}$ = gas emissivity evaluated at one mean beam-length and at two mean beam-lengths, respectively

θ = time, hours

θ = incident angle, in Equations (13) and (14)

λ = wavelength, ft.

λ = latent heat of vaporization, in Equation (21)

ψ = refracted angle, in Equations (13) and (14)

Ψ = factor by which Z must be multiplied to yield the mean beam-length

Φ = escape factor $= 1 - f_{ss}$

References

(1) Hottel, H. C., and Cohen, E., A.I.Ch.E. Journal **4**: 3 (1958).

(2) McAdams, W. H., "Heat Transmission", Chap. IV by H. C. Hottel, 3rd edit., McGraw-Hill Book Co., Inc., New York (1954).

(3) Hottel, H. C., and Egbert, R. B., Trans. Am. Inst. Chem. Engrs. **38**: 531 (1942).

(4) LaMer, V. K., O.S.R.D. Rep. No. 1857 Washington (1953).

(5) Van de Hulst, H. C., "Light Scattering by Small Particles", 1st edit., John Wiley and Sons Inc., New York (1957).

(6) Sinclair, D. J., Optical Soc. Am., **37**: 475 (1947).

(7) Lothian, G. F., and Chappel, F. P., J. Appl. Chem. **1**: 475 (1951).

(8) Gumprecht, R. O., and Sliepcevich, C. M., J. Chem. Phys. **57**: 90, 95 (1953).

(9) Haslam, R. T., and Hottel, H. C., Trans. ASME **50**: 9, (1928).

(10) Johnstone, H. F., Pigford, R. L. and Chapin, J. H., Univ. of Ill. Eng. Expt. Sta. Bul. 33 (1941).

(11) Nusselt, W., Forsch. Gebiete. Ingenieurw. No. 264 (1923).

(12) Simpson, H. C., Sc.D. Thesis, Chem. Eng. Dept., M.I.T. (1954).

(13) Thomas, P. H., Brit. J. Appl. Phys., **3**: 385 (1952).

(14) Brown, S. L., Phys. Rev., 21 (2): 103 (1923).

(15) Ranz, W. E., and Marshall, W. R. Jr., Chem. Eng. Progr. **48**: 141, 173 (1952).

(16) Dlouhy, J., and Gauvin, W. H., A.I.Ch.E. Journal **6**: 29 (1960).

(17) Manning, W. P., and Gauvin, W. H., A.I.Ch.E. Journal **6**: 184 (1960).

(18) Spalding, D. B., Fourth Symposium (International) on Combustion, p. 847, The Williams and Wilkins Co., Baltimore (1953).

(19) Nusselt, W., Z. Ver. deut. Ing., **68**: 124 (1924).

(20) Sleicher, C. A., Jr, and Churchill, S. W., Ind. Eng. Chem., **48**: 1819 (1956).

(21) Themelis, N. J., Ph.D. Thesis, McGill University (1961).

(22) Lowan, A. N., Davids, N., and Levenson, A., Bull. Amer. Math. Soc. **48**: 739 (1942).

(23) Port, F. J., ScD. Thesis, Chem. Eng. Dept., M.I.T. (1940).

(24) Hoffman, T. W., Ph.D. Thesis, McGill University (1959).

APPENDIX A*

Derivation of Reception Factors for a Cylindrical System

This discussion is restricted to a cylindrical enclosure containing an absorbing gas of constant absorption coefficient. This enclosure is divided into a number of surface and volume zones, each of height equal to the diameter of the cylinder (hereafter referred to as unit-zones). The problem is to find the reception factors for this system, defined as the fraction of the total radiation that leaves any radiating zone (surface or gas) which is intercepted by another zone, taking into account the absorption of radiation by the intervening medium. Thus this factor corresponds to the direct-view factor, F, previously used by Hottel [2], but now for a system containing an absorbing medium.

*The complete derivations contained in Appendices A and D have been deposited as Document No. 6842 with the ADI Auxiliary Publications Project, Photoduplication Service, Library of Congress, Washington 25, D.C. A copy may be obtained by citing the Document No. and by remitting $3.75 for photoprints, or $2.00 for 35 mm. microfilm. Advance payment is required. Make cheques or money orders payable to: Chief, Photoduplication Service, Library of Congress.

1. Surface-to-Surface Interchange.

By definition, the one-way radiation exchange between any two black-walled surface zones is given by:**

$$q_{s_1 \to s_2} = A_{s_1} \cdot f_{s_1 s_2} \cdot \sigma T_{s_1}{}^4 \quad \text{.....(A1)}$$

In terms of differential areas (Figure 9), this one-way exchange is also known to be directly proportional to the area of each as viewed from the other (Lambert's Cosine Law), and inversely proportional to the square of the separating distance R. In this case the intensity at dA_2 will be further reduced, for account must be taken of the transmissivity of the gas over the distance R. Expressing this mathematically:

$$dq_{s_1 \to s_2} = (1/\pi)\,(dA_1 \cos\theta_1\, dA_2 \cos\theta_2/R^2)\,(e^{-\underline{k}R})\,(\sigma T_{s_1}{}^4) \text{ ..(A2)}$$

When this expression is integrated over the two finite areas, Equations (A1) and (A2) are equal and thus $f_{s_1 s_2}$ can be evaluated. For the general case of zone i and $j = i + N$ (where N is any whole number including zero) and when all length terms are normalized with respect to the cylinder diameter δ:

$$f_{ss_N} = \frac{1}{16\pi^2} \int_o^{2\pi} d\phi_1 \int_o^{2\pi} d\phi_2 \int_o^{1} d(z_2/\delta) \int_N^{N+1} d(z_1/\delta)$$
$$[1 - \cos(\phi_2 - \phi_1)]^2 \cdot e^{-\underline{k}\delta(R/\delta)}/(R/\delta)^4 \text{.....(A3)}$$

where

$$(R/\delta)^2 = \sin^2(\phi_2 - \phi_1)/2 + [(z_2 - z_1)/\delta]^2 \text{.....(A4)}$$

The nomenclature adopted to describe f-factors is shown on each f-plot, (see Figures 2 to 8). The final letter subscript indicates the receiving unit-zone, and its type, just as the first letter shows the primary zone. The number on the final subscript indicates the number of unit zones that the receiving zone is removed from the primary one. In each case N is this number.

2. Gas-to-Gas Interchange.

Similarly, the generalized view factor for gas zone i to gas zone $j = i + N$ becomes:

$$f_{gg_N} = \frac{\underline{k}\delta}{\pi^2} \int_o^{2\pi} d\phi_1 \int_o^{2\pi} d\phi_2 \int_o^{1/2} (r_1/\delta) d(r_1/\delta) \int_o^{1/2} (r_2/\delta) d(r_2/\delta)$$
$$\int_o^{1} d(z_1/\delta) \int_N^{N+1} d(z_2/\delta)\, e^{-\underline{k}\delta(R/\delta)}/(R/\delta)^2 \text{ ....(A14)}$$

3. Surface-to-Gas Interchange.

For the general case of surface i to gas volume $j = i + N$

$$f_{sg_N} = \frac{\underline{k}\delta}{2\pi^2} \int_o^{2\pi} d\phi_1 \int_o^{2\pi} d\phi_2 \int_o^{1} d(z_1/\delta) \int_N^{N+1} d(z_2/\delta)$$
$$\int_o^{1/2} (r_2/\delta) d(r_2/\delta)\,[1/2 - (r_2/\delta)\cos(\phi_2 - \phi_1)]$$
$$e^{-\underline{k}\delta(R/\delta)}/(R/\delta)^3 \text{.....(A17)}$$

Direct analytical integration of these integrals was not possible. They could, however, be partially solved analyticaly (the complete mathematical analysis is presented in Reference 24). The final integrations were evaluated numerically, and the f-factor working plots are shown, together with the nomenclature adopted, on Figures 2 to 8.

The numerical integrations were not carried out for zones greater than two removed, since the view-factors for these zones were very small. Approximate techniques can therefore be employed without causing serious error to the overall result. If the separating distance between unit-zones becomes large with respect to the diameter of the column, then an average transmissivity can be used for all points in either zone. It can be shown that the equations for F_{ss}, F_{sg} and F_{gg} at $\underline{k}\delta = 0$ are special cases of Equations (A25), (A26) and (A27) respectively.

$$F_{ss}(h, \underline{k}\delta = 0) = \frac{1}{2}\left[2 - \frac{h(2h^2+3)}{(h^2+1)^{3/2}}\right] \text{.....(A31)}$$

$$F_{sg}(h, \underline{k}\delta = 0) = 2\left[\frac{2h^2+1}{(1+h^2)^{1/2}} - 2h\right] \text{.....(A32)}$$

$$F_{gg}(h, \underline{k}\delta = 0) = 2\,[h^2 - h(1+h^2)^{1/2} + 1/2] \text{....(A33)}$$

These equations have been integrated with respect to h to give $f_{ss_3} = 0.004554$, $f_{ss_2} = 0.01114$, $f_{ss_4} = 0.01515$. To find the values of these factors at any $\underline{k}\delta$, it is recommended that these values by multiplied by $e^{-\underline{k}\delta(R_c/\delta)}$, where R_c is the centre-to-centre distance. Since this procedure is not possible for the surface-gas and gas-gas factors, it is recommended that they be found by proper addition and subtraction of the surface-surface factors at the required $k\delta$. For $k\delta > 1$, these factors are insignificant and can be omitted.

APPENDIX B

Calculation of Direct-Interchange Areas

So far, cylindrical surface and gas zones of a size equal to a right circular cylinder have been considered. The one-way radiation is then given by equations such as (A1).

In some cases, however, the conditions may be such that larger isothermal zones may be postulated. In these cases, it is possible to build up interchange factors from the existing plots. Using Hottel and Cohen's nomenclature, as discussed in their paper[1], one may define one-way radiant flux for surface-to-surface, surface-to-gas, gas-to-surface, and gas-to-gas respectively as:

$$q_{s_i s_j} = (\overline{s_i s_j})\,\sigma T_{s_i}{}^4 \text{.....(B1)}$$

$$q_{s_i g_j} = (\overline{s_i g_j})\,\sigma T_{s_i}{}^4 \text{.....(B2)}$$

$$q_{g_i s_j} = (\overline{g_i s_j})\,\sigma T_{g_i}{}^4 \text{.....(B3)}$$

$$q_{g_i g_j} = (\overline{g_i g_j})\,\sigma T_{g_i}{}^4 \text{.....(B4)}$$

The factors $\overline{s_i s_j}$, $\overline{s_i g_j}$, $\overline{g_i s_i}$, $\overline{g_i g_j}$ have the dimensions of area and are defined as direct-interchange areas — the first letter with its subscript indicating the sender and the second the receiver. These factors apply only in a black-walled system and are analogous to the factors $\overline{AF}$ previously used in a black system containing a non-absorbing medium. Just as in that case:

$$\sum_j \overline{s_i s_j} + \sum_j \overline{s_i g_j} = A_{s_i} \text{.....(B5)}$$

and

$$\sum_j \overline{g_i s_j} + \sum_j \overline{g_i g_j} = 4\underline{k}V_{g_i} \text{.....(B6)}$$

It also follows from the application of Kirchhoff's Law to an isothermal system that

$$\overline{g_1 s_1} = \overline{s_1 g_1} \text{.....(B7)}$$

or by definition: $4\underline{k}V_{G_1} \cdot f_{g_1 s_1} = A_{s_1} \cdot f_{s_1 s_1}$ .....(B8)

or for a right circular cylindrical zone: $\underline{k}\delta f_{g_1 s_1} = f_{s_1 s_1}$ .....(B9)

Similarly $\overline{g_1 s_2} = \overline{g_2 g_1}$ and $\overline{s_1 s_2} = \overline{s_2 s_1}$ which can also be seen from the symmetry of the defining equations for the f-factors.

The remaining problem is to find a factor such as $\overline{g_1 g_1}$ for a cylindrical-zone larger than the basic one used to formulate the f-factors. To find the direct-interchange area $\overline{g_1 g_1}$ for a gas zone comprising two right circular cylinders as shown in Figure 10(a), the following formulation is necessary:

$$\frac{q_{s_1 \to s_1}}{\sigma T_{s_1}{}^4} = \overline{g_1 s_1} = 4k\left(\frac{\pi\delta^3}{4}\right)[f_{s_a s_a} + f_{s_a s_b} + f_{s_a s_b} + f_{s_b s_a}] \text{.....(B10)}$$

where the first two f-factors are of the f_{ss_o} type, while the last two are of the f_{ss_1} type.

A similar expression results for $\overline{s_1 s_1}$.

To find $\overline{s_1 s_2}$

$$\frac{q_{s_1 \to s_2}}{\sigma T_{s_1}{}^4} = \overline{s_1 s_2} = \pi\delta^2 (f_{s_a s_c} + f_{s_b s_c}) \text{.....(B11)}$$

where the first factor is of the f_{ss_2} type, while the second is of the f_{ss_1} type.

APPENDIX C

Estimation of Mean Beam Length

By means of the foregoing procedure it is possible to determine the mean beam length for any cylindrical system.

**Simpson[12] has shown that this equation is only valid when the refractive index is one or very close to one. If it is m, then $\sigma T_1{}^4$ should be multiplied by m^2. This correction will be omitted in this discussion, only because radiation in a gaseous medium is being considered here; for other materials the refractive index must be considered.

The mean beam length of an enclosure containing an absorbing or emitting medium is defined as the radius of a hemisphere containing the same medium at the same temperature which will cause the same radiant flux density (B.t.u./ft.^{2} hr.) on a differential area at its centre as that which the walls of the enclosure experience from the total gas it contains. Thus, what is required is the flux density leaving the gas mass. Referring to Figure 10(b), the total cylindrical volume V_t is made up of n-basic right-circular cylindrical unit-zones. The flux leaving this gas mass is

$$4\underline{k} V_t \Phi_{V_t} = 4\underline{k} V_t - \overline{g_t g_t} \quad \ldots\ldots\ldots\ldots\ldots\ldots (C1)$$

It can easily be shown that

$$\overline{g_t g_t} = 4(k\delta)(\pi\delta^2/4)$$
$$[nf_{ss_0} + 2(n-1)f_{ss_1} + 2(n-2)f_{ss_2} + 2(n-3)f_{ss_3} + \ldots] \quad \ldots\ldots (C2)$$

The flux at the walls resulting from the contained gas is

$$a(4\underline{k} V_t \Phi_{V_t})\, \sigma T_{s_t}^4 \quad \ldots\ldots\ldots\ldots\ldots\ldots (C3)$$

and if this is divided by the total area of the cylinder (including the ends), the radiant flux density can be calculated. The weighting factor 'a' necessary for this equation is valid only over part 'a' of the spectrum. The emission of the gas in a hemisphere per unit of surface at the centre of a hemisphere of gas of radius L is:

$$\epsilon_{G_L}\, \sigma T_{V_t} = a(1 - e^{-\underline{k}L})\, \sigma T_{V_t}^4 \quad \ldots\ldots\ldots\ldots (C4)$$

Equating (C3) and (C4)

$$1 - e^{-\underline{k}\Psi\delta} = \frac{4\underline{k} V_t \Phi_{V_t}}{A_t} \quad \ldots\ldots\ldots\ldots\ldots\ldots (C5)$$

where Ψ is the factor by which the characteristic dimension of the system must be multiplied to give the mean beam length of the system. Since the evaluation of Φ_{V_t} involves a knowledge of $\underline{k}\delta$ and thus of L, Equation (C5) must be solved by trial and error. Ψ versus $\underline{k}\delta$ for a cylinder (length = 10δ and 15δ) is shown in Table 3. Only a small variation in Ψ is observed. The value recommended by Port (23) from his studies on rectangular parallelepipeds is included in this Table — i.e., $L = 0.85\,(4V/A)$ for average values of $P_G L$. For infinite cylinders 0.90δ is recommended[2].

APPENDIX D*

Treatment of Varying Absorption Strength

Since the temperature of the gas varies and its emission or absorption is known to depend on temperature, it follows that the absorption coefficient, as well as the weighting factor 'a', will vary as well. Moreover, a more serious variation in absorption coefficient of the cloud occurs because

(1) the size of the drops decreases as evaporation proceeds;

(2) as evaporation proceeds more vapor is evolved and thus the voidage increases or the number of particles per unit volume decreases;

(3) the voidage increases as a result of the increased temperature, increasing the volume of unit mass of gas;

(4) in some cases the droplets may disappear altogether;

(5) the particles may explode — this explosion may occur when treating some solutions where an impervious solid shell forms on the surface of the drop and the vapor generated internally causes an increased pressure inside the droplet, which finally overcomes the forces holding it in.

Theoretically it is possible to account for this changing absorption strength down the column by starting with the numerical values of F, and in the final numerical integration with respect to (z_1/δ), (z_2/δ) and/or $(z_2 - z_1)/\delta$, by using an integrated average $\underline{k}\delta$ over the separating distances in question, viz.

$$(k\delta)_{ave} = \left[\int_{z_1}^{z_2} \underline{k}\delta \, dz\right] / (z_2 - z_1) \quad \ldots\ldots\ldots\ldots (D1)$$

However the labour involved would be prohibitive and thus again a simplification is necessary. It can be shown* that the various direct-interchange areas and f-factors can be corrected for variable absorption strength approximately in the following manner:

$$(1)\quad (\overline{ss} \text{ or } f_{ss})_{var\ \underline{k}\delta} = (\overline{ss} \text{ or } f_{ss})_{ave\ \underline{k}\delta} \quad \ldots\ldots\ldots\ldots (D7)$$

$$(2)\quad (\overline{sg} \text{ or } f_{sg})_{var\ \underline{k}\delta} = \frac{(\underline{k}\delta)_{gas\ zone}}{(\underline{k}\delta)_{ave}} (\overline{sg} \text{ or } f_{sg})_{ave\ \underline{k}\delta} \quad \ldots\ldots\ldots (D8)$$

$$(3)\quad (\overline{gs} \text{ or } f_{gs})_{var\ \underline{k}\delta} = \frac{(\underline{k}\delta)_{gas\ zone}}{(k\delta)_{ave}} (\overline{gs} \text{ or } f_{gs})_{ave\ \underline{k}\delta} \quad \ldots\ldots\ldots (D9)$$

$$(4)\quad (\overline{gg})_{var\ \underline{k}\delta} = \frac{(\underline{k}\delta)_{G_1} (\underline{k}\ )_{G_2}}{(k\delta)^2_{a\ \ }} (\overline{gg})_{ave\ \underline{k}\delta} \quad \ldots\ldots\ldots\ldots (D10)$$

Sample calculations illustrating the use of these equations will be presented in subsequent papers.

---

*See footnote for Appendix A.

★ ★ ★

*See footnote for Appendix A.

An Apparatus for the Measurements of Light Transmittance of Emulsions[1]

J. A. CENGEL[2], J. G. KNUDSEN[3], A. LANDSBERG[3] and A. A. FARUQUI[3]

This paper describes an apparatus for the measurement of the light transmittance of emulsions. A photoelectric technique was employed to determine the effect of flow rate, mixing time, and dispersed phase concentration on the light transmittance of a liquid-liquid emulsion composed of a commercial petroleum solvent and water. For a given concentration, light transmittance was independent of flow rate and became constant after 10 minutes of mixing in the test apparatus. Light transmittance decreased with solvent (dispersed phase) concentration. Up to 5% solvent concentration, the light transmittance-concentration curve could be used to measure solvent concentration accurately.

The flow characteristics of liquid-liquid emulsions are of interest in many processes in which two liquid phases contact each other. The rheological properties of such emulsions depend upon such factors as the proportion of the two liquids present, the interfacial area, the type and amount of emulsion stabilizer present, and the size of the dispersed phase particles. In addition, experimental values of the rheological properties are dependent upon conditions under which measurements are made.

This paper describes a photoelectric technique for measurement of the light transmittance of liquid-liquid emulsions and demonstrates the effect of dispersed phase concentration, emulsion flow rate, and mixing time. The emulsion studied was made up of a commercial petroleum solvent as the dispersed phase with water as the continuous phase. This study is part of an over-all research program on the flow and convection heat transfer characteristics of unstable liquid-liquid dispersions. The various properties (including viscosity, the thermal conductivity, light transmittance, and interfacial area) are determined and related to dispersed phase concentration and to the momentum and heat transfer characteristics of the phase fluid.

Langloise and Gullberg[1] used a light transmittance technique to determine the interfacial area in a two-phase liquid-liquid emulsion. These workers, however, studied emulsions in which the dispersed phase droplets were relatively large and developed a relationship by which light transmittance was related to interfacial area per unit volume as follows:

$$I_o/I = BA + 1 \quad \ldots\ldots\ldots\ldots\ldots\ldots\ldots\ldots (1)$$

They considered that the constant B was independent of volume fraction of dispersed phase. In the present work, however, it was not possible to determine the interfacial area of the emulsions studied since the dispersed phase particles were very small and light scattering brought about by these particles prevents Equation (1) from being valid. As the dispersed phase particles become smaller and smaller, the light transmittance becomes independent of interfacial area for a given concentration. At small dispersed phase concentrations light transmittance is a sensitive function of concentration, however, and may be used to predict concentration.

Equipment and Procedure

The experimental system is shown in Figure 1. The photoelectric apparatus consisted simply of a constant voltage light source and a photocell. Figure 2 is a detailed drawing of the light and photocell probes.

The light-source probe (8) was mounted on the main piping system (16), perpendicular to the flow, by soldering a brass fitting (14) into a $\frac{5}{8}$-in. hole in the pipe wall. The piping system and the light-source probe were sealed from one another by the glass window (15) in the stainless steel light directing tube (9) and a packing gland (13), which was forced into the stuffing box by the fitting (12). The light-source probe (8) was soldered to a ring (10) and this combination was held to (12) by three brass screws (11). The end of the light-source probe was closed by a micarta end-piece (3) held in place by binding post (2), which also served as a ground connection. Two binding posts (1) and three adjustment screws (4) were fitted into the end piece. The aluminum lamp base (6) and the lucite holder (5) are adjustable to give the proper illumination from the lamp.

The photocell probe was soldered to the main piping system directly opposite the light source tube by means of fitting (17) in a $1\frac{1}{4}$-in. hole. This probe was sealed from the system by window (20) in the photocell supporting tube (24). The packing was held in place by gland (18) which was forced into the stuffing box by fitting (19). The photocell fitted into the socket mounted in lucite (21) and was attached to the micarta end piece (22). Binding posts (26) supplying power to the photocell were mounted on the end piece. The entire photocell mounting was held in place by set screw (25).

A Delco 6-volt lead storage battery was the voltage source of the light bulb (7). The current was first directed into an exterior electrical system so that a specified voltage (usually 4.5 volts) could be maintained at the light bulb. The voltage delivered across the light bulb was checked before each reading to insure that all data were taken under identical conditions.

The transmitted light received by the photocell tube (23) was converted into a potential which was measured by a null-

[1]*Manuscript received March 17; accepted June 28, 1961.*
[2]*Department of Chemical Engineering, Purdue University, Lafayette, Indiana, U.S.A.*
[3]*Department of Chemical Engineering, Oregon State College, Corvallis, Oregon, U.S.A.*
Contribution from the Department of Chemical Engineering, Oregon State College, Corvallis, Oregon, U.S.A.

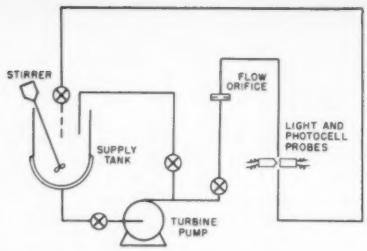

Figure 1—Experimental equipment.

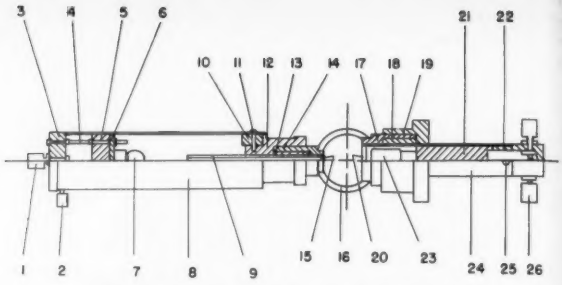

Figure 2—Light and photocell probes.

point potentiometer. A Leeds and Northrup Model 2430 galvanometer used to observe deflection was external to the potentiometer system. The face of the galvanometer was calibrated from 0 to 100 in increments of one, to allow the estimation of percent changes in light transmittance. The instrument was set to read zero with the light-source off and 100 with the light source on and with clear water flowing in the main piping system. Sensitivity of the galvanometer was $\pm 1\%$.

The electrical system is schematically shown in Figure 3. The symbols represented are as follows:

B1 90-volt battery (RCA VS090)
B2 6-volt lead storage battery (Delco dry charge)
B3 4 mercury cells (Mallory ZM-9)
C1 Two sets of contacts for phototube (RCA 1P41)
C2 Two sets of contacts for light (GE 82, 6-volt)
C3 Galvanometer connections (Leeds & Northrup 2430a)
R1 Coarse adjustment rheostat (10 turn 20,000 ohm Helipot)
R2 Fine adjustment rheostat (10 turn 20,000 ohm Helipot)
R3 Load resistor 1 megohm)
R4 Coarse adjustment rheostat (5 ohm rheostat)
R5 Fine adjustment rheostat (10 turn 25 ohm Helipot)
R6 Load resistor (50,000 ohms)
R7 Balancing voltage set potentiometer (10 turn 50,000 ohm Helipot)
R8 Voltage resistor (10 ohm)
R9 Sensitivity lowering resistor (50,000 ohms)
R10 Sensitivity lowering resistor (1000 ohms)
R11 Sensitivity lowering resistor (50 ohms)
S1 Double pole double throw circuit selector switch)
S2 Single pole double throw push button
S3 Single pole double throw cell selector switch
S4 Double pole single throw push button
S5 Single pole single throw light switch
S6 5 position sensitive selector and galvanometer switch

The emulsion, composed of a commercial petroleum solvent, (Shellsolv 360) and water was prepared in a stainless steel, jacketed tank using a variable speed stirrer for agitation. The solvent had a viscosity nearly equal to that of water in the temperature range studied. The emulsion was circulated through the piping system shown schematically in Figure 1. The system was made of $1\frac{1}{4}$-in. standard brass pipe while the section containing the probes was 2-in. standard brass pipe.

The supply tank and main piping system were flushed with solvent several times before runs were made. A calculated weight of solvent was added to previously weighed amount of water in the supply tank. To obtain thorough blending of the two liquids, mixing time was usually 2-3 hours. Agitation was continued during the test.

The mixture had a milk-white appearance characteristic of many liquid-liquid emulsions. If the agitation was stopped, a clear layer of solvent immediately appeared at the surface of the liquid in the supply tank, indicating instability of the emulsion.

Samples of the dispersion were analyzed periodically by allowing the emulsion to separate in a graduated cylinder.

Experimental Data

The light transmittance of mixtures containing 0.49, 0.97, 1.92, 2.87, 3.82, 4.75, 19.4, 34.3, and 49.2 volume percent solvent was determined at probe separations of $\frac{1}{8}$-in. and $\frac{1}{2}$-in. In addition, the effect of mixing time and mass flow rate on the light transmittance of the latter four mixtures was investigated. Details of the experimental program are available in Reference (2).

Results

Figure 4 is a plot of percent light transmitted versus length of mixing time. At zero time, the required amount of solvent is added to the mixing tank and circulation and agitation initiated. The percent transmittance decreases rapidly and becomes con-

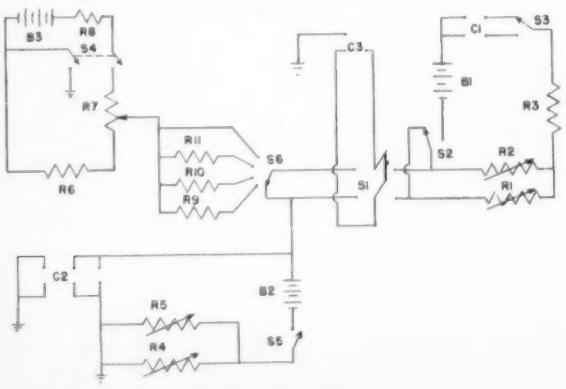

Figure 3—Wiring diagram.

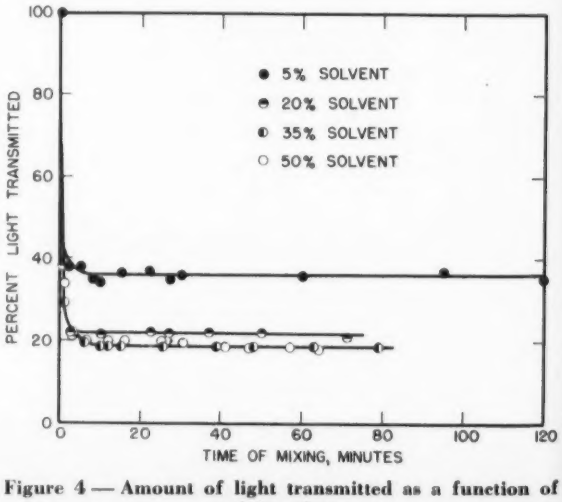

Figure 4 — Amount of light transmitted as a function of mixing time.

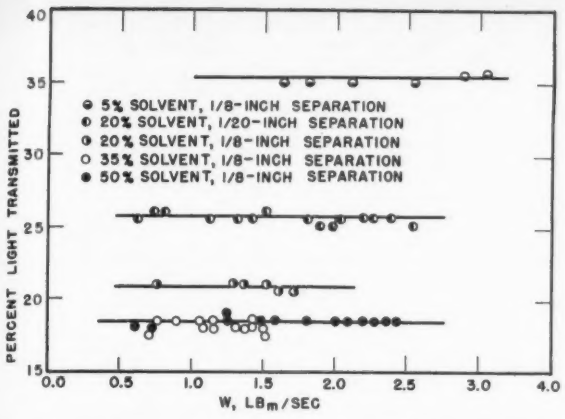

Figure 5—Effect of flow rate on amount of light transmitted.

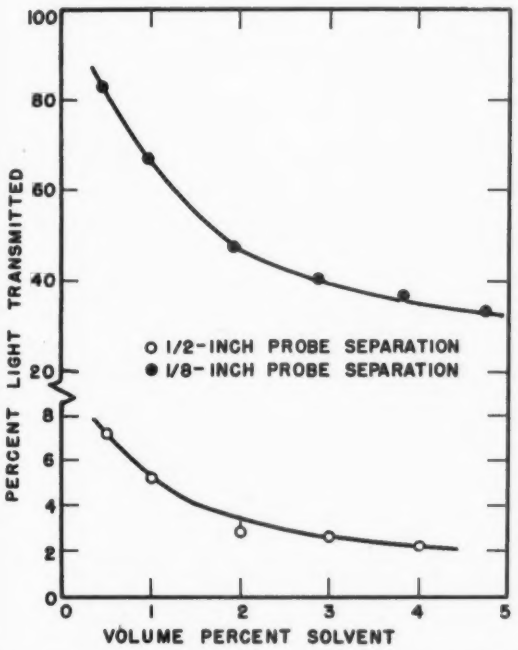

Figure 7—Relation between solvent concentration and light transmittance.

stant after about 10 minutes. It was observed by visual inspection and by measurement of friction losses that the emulsion was not yet thoroughly mixed and the dispersed phase particles were still being reduced in size. These results indicate that after about 10 minutes of mixing, the dispersed phase droplets were sufficiently small that the transmittance was independent of droplet size and was unchanged by any further size reduction.

Figure 5 is a plot of percent transmittance versus flow rate. There appears to be no effect of flow rate on percent transmittance indicating that any change in drop size or drop-size distribution could not be detected by the present apparatus.

The effect of solvent concentration is shown in Figures 6 and 7 in which percent transmittance is plotted versus volume percent of solvent in the emulsion. Figure 6 shows a rapid drop in percent transmittance with concentration in the range up to 5% solvent. Beyond this the transmittance decreases more slowly with concentration ultimately becoming constant in the range 35 to 50% solvent.

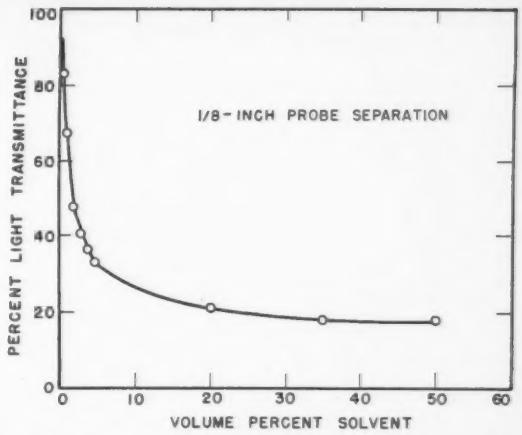

Figure 6—Relation between solvent concentration and light transmittance.

These results indicate, however, that the light transmittance technique would be useful in measuring low solvent concentrations once the light transmittance-concentration curve is established. Figure 7 shows the results obtained for two probe spacings up to 5% solvent. In this range the light transmitted is very sensitive to the concentration changes. Beyond 5% solvent, however, the light transmittance becomes sufficiently insensitive so that accurate measurements of concentration could not be made from light transmittance determinations.

In summary, an apparatus is described to measure the light transmittance of unstable liquid-liquid emulsions flowing in circular tubes. Experiments showed that for a given solvent (dispersed phase) concentration in water, light transmittance became constant after 10 minutes of mixing and was independent of mass flow rate in the pipe. Light transmittance is very sensitive to concentrations in the range up to 5% solvent. In this concentration range and for a given probe separation, the light transmittance-concentration curve may be used to measure solvent concentrations accurately. Beyond 5% solvent light transmittance becomes insensitive to concentration.

Work is presently under way to determine the droplet size of the various dispersions. At the low dispersed phase concentrations where the light transmittance is a sensitive function of concentration studies are being made on the effect of flow rate and mixing time on surface area to determine the relation if any of these factors on the light transmittance of these dilute dispersions.

Acknowledgement

The research herein reported is part of an extensive study of the flow and heat transfer characteristics of liquid-liquid emulsions. Appreciation is expressed to the National Science Foundation for a grant to support this research program.

Nomenclature

A = Interfacial area per unit volume
B = Specifying constant dependent on the ratio of refractive indices
I_o = Light intensity incident to the emulsion
I = Light intensity emergent from the emulsion

References

(1) Langloise, G. E., Gullberg, J. E., Review of Scientific Instruments, 25, 360 (1954).

(2) Cengel, J. A., "Viscosity of Liquid-Liquid Dispersions in Laminar and Turbulent Flow", M.S. Thesis, Oregon State College (1959).

★ ★ ★

Optimum Performance of Combined Flow Reactors under Adiabatic Conditions[1]

A. CHOLETTE[2] *and J. BLANCHET*[2]

Irreversible first- and second-order reactions are studied for combinations of tubular and CST reactors when endothermal or exothermal adiabatic conditions prevail.

Typical results presented for *MT* and *TM* models show the variation of either the conversion or the relative residence time as a function of the mixing level of the system.

A graphical method, applicable generally to *MT* reactors, provides a simplification over that of successive approximations required for model *TM*.

For the conditions investigated broad limits are indicated of the optimum reactor combinations.

Les auteurs étudient les réactions irréversibles du premier et du deuxième ordre pour des combinaisons de réacteurs tubulaires et bien agités, dans le cas de réactions endothermiques ou exothermiques.

Les résultats caractéristiques pour les modèles *MT* et *TM* montrent la variation de la conversion ou du temps de résidence relatif en fonction du niveau d'agitation du système.

Une méthode graphique, qui s'applique de façon générale aux réacteurs *MT*, est plus simple que celle par approximations successives que l'on utilise pour les réacteurs *TM*.

On indique, dans les grandes lignes, les combinaisons de réacteurs qui donnent un rendement maximum.

Recent studies in chemical reaction engineering indicate a growing trend toward optimization techniques and emphasize the importance of evaluating conditions leading to optimum performance[1,2,3,4].

Since flow reactor operation is highly susceptible to two important factors, temperature and the extent of mixing, each of these has been the subject of numerous investigations. Some have dealt, in particular, with temperature profiles in tubular reactors[5,6,7,8] or with temperature sequences in continuous-stirred-tank-reactors (CSTR)[9,10]. Others have been suggested by the extent of backmixing or partial mixing and resulted in such studies as on the distribution of residence times and axial mixing[11,12,13,14].

In the case of flow reactors which do not exhibit true plug flow nor CSTR behavior the use of models is being resorted to more and more as a fruitful method of approach. Thus the performance of partially mixed reactors may be analysed through models consisting of combinations of tubular and well-mixed sections[14,15,16,17,18,19]. In some instances actual results have shown good agreement with the proposed models[19].

The behavior of some model reactors, for isothermal operation, has been examined recently[15,16]. It involved the introduction of a parameter "m" defining the level of mixing as that fraction of the total volume of the reactor which was considered to be perfectly mixed. Interesting results were thus obtained and more were anticipated when considering such models in non-isothermal operation. This has triggered the present study on irreversible first- and second-order reactions carried out adiabatically in combinations of reactors.

[1]*Manuscript received December 7, 1960; accepted July 20, 1961.*
[2]*Chemical Engineering Department, Laval University, Quebec, Que.*
Based on a paper presented to the C.I.C. Chemical Engineering Conference, Quebec, Que., November 7-9, 1960.

ADIABATIC REACTORS

Since many factors affect the rate of reaction, those considered in this work have been limited to temperature and concentration, in ideal homogeneous systems. The analytical treatment of combinations of reactors requires that one consider first the overall effects of variations in temperature and concentration on the behavior of both tubular reactors and CSTR'S. This can be facilitated by expressing temperature effects in terms of variations in conversion. The latter, in first- and second-order reactions of the type:

$$A \rightarrow \text{Products}$$
$$2A \rightarrow \quad ,,$$
$$A + B \rightarrow \quad ,,$$

is, by convention, defined as the ratio of the quantity of A reacted over the original amount present.

In any adiabatic system the heat effect can be related to the conversion by the following expression[20] provided the heat of reaction ΔH_R and the specific heat of the reaction mixture remain constant:

$$T = T_o + bx \qquad (1)$$

where b, the maximum temperature variation for complete conversion, is a function of ΔH_R and $\Sigma m_i c_{pi}$.

For convenience Equation (1) may be rewritten in a dimensionless form:

$$\frac{bx}{T} = \frac{1}{1 + \dfrac{T_o}{bx}} \qquad (2)$$

Similarly, the usual Arrhenius equation can be modified from

$$k = ze^{-E/RT} \qquad (3)$$

TABLE 1
KINETIC PARAMETERS

Conditions	k_o	b/T_o	E/RT_o
Endothermal	1.0	−0.1	40
Exothermal	0.1	+0.1	40

TABLE 2
DESIGN EQUATIONS FOR ADIABATIC FLOW REACTORS

Order of Reaction	Tubular	CSTR
1.	$\theta_t = \int_o^{x_t} \frac{dx}{k(1-x)}$	$\theta_M = \frac{x_M}{k(1-x_M)}$
2.	$C_{A_F}\theta_t = \int_o^{x_t} \frac{dx}{k(1-x)(R_F-x)}$	$C_{A_F}\theta_M = \frac{x_M}{k(1-x_M)(R_F-x_M)}$

$$-\left(\frac{E}{RT_o}\right)\left(1-\frac{bx}{T}\right)$$

to:

$$k = se \qquad \text{.....(4)}$$

The latter can be further transformed after introducing Equation (2):

$$k = k_o\, e^{\left(\frac{E}{RT_o}\right)\left(\frac{1}{1+\frac{T_o}{bx}}\right)} \qquad \text{.....(5)}$$

k_o being the initial reaction rate constant, at T_o.

It can be seen from this expression that, all other conditions being equal, the reaction constant may be assumed to be a sole function of x. It then becomes easy to compare different kinds of reactions if the parameters E, b, K and T_o, or combinations of them, are properly chosen.

Although, in practice, values of the above parameters may vary over a wide range, they have been limited in the present study to those specified in Table 1. This has been done for convenience on account of the long trial and error calculations involved due to the lack of proper computing facilities. Had these been available, an investigation of much wider scope would have been possible.

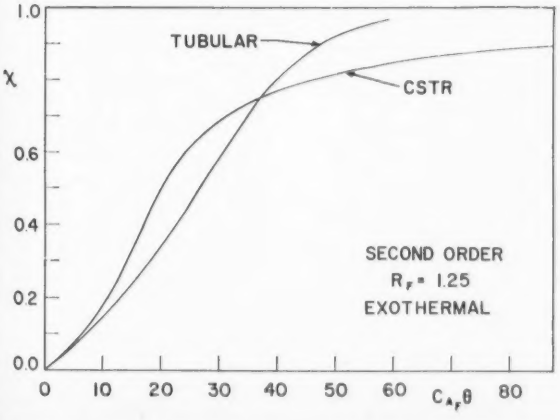

Figure 2—Variation of the conversion with residence time and initial concentration for second-order exothermal reactions.

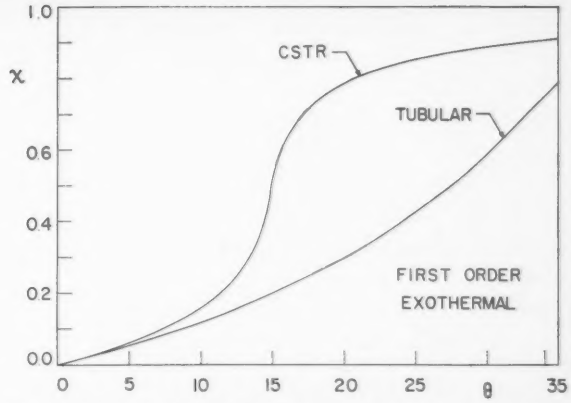

Figure 1—Variation of the conversion with residence time for first-order exothermal reactions. These "working curves" are for conditions of reaction specified in Table 1.

Some considerations may be in order at this point on tubular and CST reactors taken separately. Equations[16,20] developed for these particular cases are presented in Table 2 for first- and second-order reactions, in constant density systems.

Solution of these equations, allowing for the variation of k and using the specifications of Table 1, has resulted in 18 working graphs, three of which are shown in Figures 1, 2 and 3. The numerous curves are for first-order reactions and for second-order reactions with values of R_F equal to 1.0, 1.25, 2, 5 and 10 respectively. They were prepared, in each case, for isothermal, endothermal and exothermal conditions.

It can be observed in Figures 1 and 2 that the exothermal case exhibits curves which behave differently from those for isothermal or endothermal conditions. At small and moderate conversions the CSTR curve lies over that for the tubular reactor but at higher conversions it reverts to the relative position exhibited in isothermal[16] and endothermal reactions as in Figure 3.

While a CSTR is at a disadvantage with respect to a tubular reactor from the point of view of a lower effective concentration, it takes advantage on the other hand in exothermal reactions of the sudden increase in temperature, to the extent shown by the curves of Figures 1 and 2. This holds up to the point where the two curves meet, after which the tubular reactor again becomes more advantageous.

In the case of endothermal reactions, the CSTR is at a disadvantage from both the point of view of concentration and temperature.

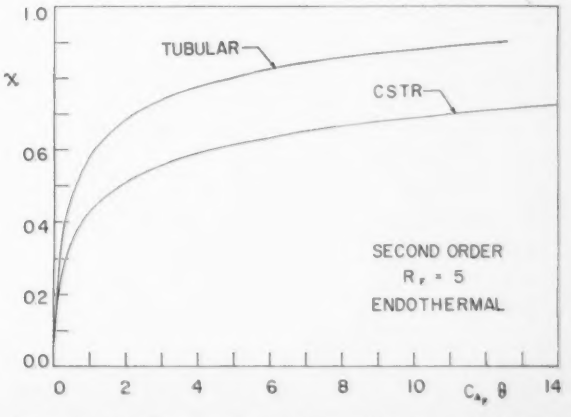

Figure 3—Working curves for second-order endothermal reactions.

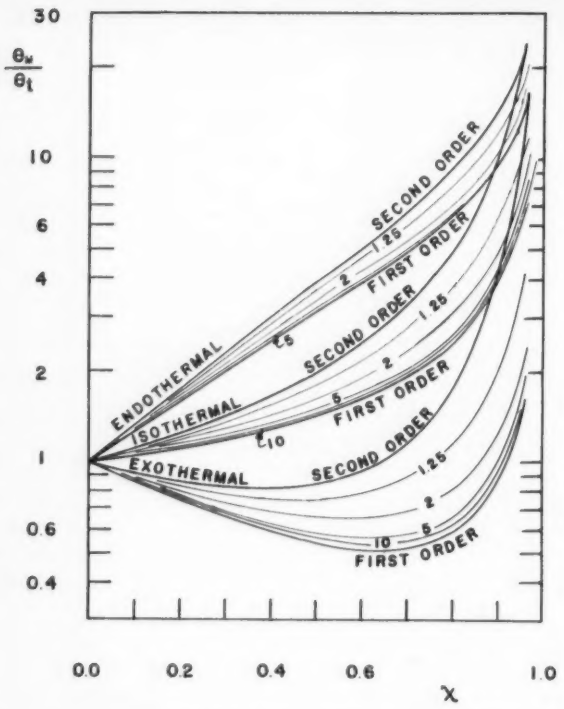

Figure 4—General comparison showing the variation of relative residence times with the conversion.

A general comparison for the 18 cases studied is presented in Figure 4, obtained directly from the eighteen sets of working curves. It shows the relative residence times required to obtain given conversions. The shape of the curves, specially of those for exothermal reactions going through a minimum, is evident from consideration of the working curves as in Figures 1, 2 and 3.

It is obvious from Figure 4 that within limitations the CSTR can be of definite advantage over the tubular reactor for exothermal reactions. In isothermal reactions, and more so in endothermal, the reverse is true as the tubular can be decidedly preferable to the CSTR.

Observation of the peculiar behavior for exothermal reactions, where the CSTR is at times superior and then inferior to the tubular, has suggested that a combination of the two might give even superior results, taking best advantage of each reactor's performance. It has led to the study of the overall effects of combined reactors as outlined hereafter.

COMBINED REACTORS

Combinations of tubular and well-mixed reactors have been studied in the case of isothermal conditions[16] for models *TM* and *MT* shown in Figure 5. Noting that the effluent of the first section becomes the feed of the second, the overall effect for combined reactors can be determined for adiabatic conditions in a way similar to that for isothermal, either with respect to the conversion obtained for a given residence time or to the relative residence time required for a given conversion.

(a) *TM Reactors*

The pertinent equations for each section are presented in Table 3, for first- and second-order reactions. Those equations cannot be resolved into simple expressions as was the case for isothermal operation[16] because of the complex nature of the integral functions. Rather, a trial and error method is involved, based on the equations of Table 3, but making use also of the working curves already mentioned.

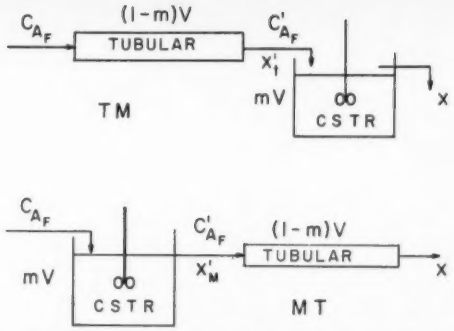

Figure 5—Illustration of model TM and MT reactors respectively.

(1) Variation of conversion with mixing level at a given residence time.

For a given residence time θ or a total reactor volume such that the conversion be x_t in a tubular reactor, the variation of conversion with the degree of mixing for any particular combination *TM* is evaluated as follows. At a given value of m, the conversion x_t' at the outlet of the tubular section, as shown in Figure 5, is read directly on the proper working curve at a residence time θ_t' corresponding to that in the tubular section and equal to $(1 - m)\theta$. Having thus taken care of the plug flow section one goes on to the particular expression of Table 3 for the CSTR section, noting that the term within brackets is obtained directly from the curve as it corresponds to θ_M if all of conversion x took place in a CSTR. Using the proper CSTR working curve the procedure consists then in finding by trial and error the value of x such that the corresponding value of θ, or $C_{A_F}\theta$ for a second-order reaction, will verify the expression for the CSTR section at the given value of m considered. An example is worked out in the Appendix.

Of the many graphs prepared from such calculations, the one presented in Figure 6 is an illustration typical of model *TM*. The degree of conversion varies slightly at low mixing levels but may, depending on conditions, vary rapidly afterward as values of m increase. As expected, when R_F increases, curves for second-order reactions approach more and more the curve for first-order.

In the particular example given all conversions at complete mixing happen to be greater than that for $m = 0$, in a tubular reactor. However, this is not the rule as lower conversions can be achieved in a CSTR; all depends, as can be seen in Figure 2, on the region where one happens to make comparisons.

TABLE 3

RELATIONS APPLICABLE TO MODEL TM

Order of Reaction	Plug Flow Section	CSTR Section
1.	$\theta_t' = (1 - m)\theta = \int_0^{x_t'} \frac{dx}{k_1(1-x)}$	$\theta_M' = m\theta = \left[\frac{x}{k_M(1-x)}\right]\left(1 - \frac{x_t'}{x}\right) = \theta_M\left(1 - \frac{x_t'}{x}\right)$
2.	$C_{A_F}\theta_t' = (1-m)C_{A_F}\theta = \int_0^{x_t'} \frac{dx}{k_1(1-x)(R_F-x)}$	$C_{A_F}\theta_M' = m\,C_{A_F}\theta = \left[\frac{x}{k_M(1-x)(R_F-x)}\right]\left(1-\frac{x_t'}{x}\right) = C_{A_F}\theta_M\left(1-\frac{x_t'}{x}\right)$

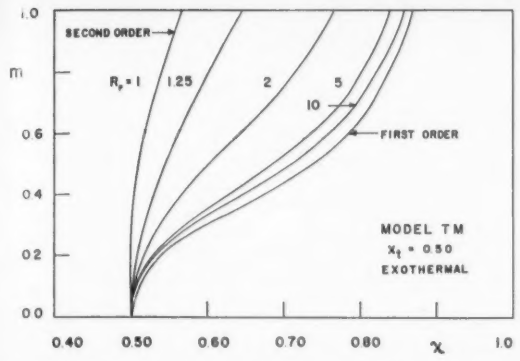

Figure 6—Variation of the conversion with the level of mixing for a TM reactor, under exothermal conditions.

(2) Variation of relative residence times with mixing level at a given conversion.

A more straightforward procedure than the one just described is available for this case.

At a given x, the values of θ_M and θ_t are read directly on the appropriate curves. A value of x_t' is then chosen determining on the tubular curve a corresponding value of θ_t'. From one of the expressions in Table 3 for the CSTR section, the value of θ_M' is then calculated from:

$$\theta_M' = \theta_M \left(1 - \frac{x_t'}{x}\right) \qquad \ldots\ldots\ldots\ldots\ldots\ldots (6)$$

The sum of θ_t' and θ_M' gives the total residence time θ and m is thus easily obtained since $m = \theta_M'/\theta$. As to the relative residence time it is simply given by the ratio θ/θ_t.

Two families of curves in Figure 7 show the variation of this ratio with the level of mixing. While very little difference exists in some cases between tubular, CSTR and combinations of reactors, there are others where it is rather pronounced. Here again, this factor depends on the region chosen for purposes of comparison.

(b) ***MT Reactors***

For such reactors, as shown in Figure 5, the design equations work out to those presented in Table 4.

Although methods similar to those used for *TM* reactors could be employed in this case, a more convenient graphical method already described for isothermal reactions[16] offers the advantage of being also applicable for exothermal and endothermal conditions. The equations of Table 4 are not even needed in this case but only the initial working curves, as shown here

(1) Variation of conversion with mixing level at a given residence time.

At a given value of m, the conversion x for a residence time θ is obtained by following first the CSTR curve, as shown in

TABLE 4

RELATIONS APPLICABLE TO MODEL MT

Order of Reaction	CSTR Section	Plug Flow Section
1.	$\theta_M' = m\theta = \dfrac{x_M'}{k_M(1-x_M')}$	$\theta_t' = (1-m)\theta = \displaystyle\int_{x_M'}^{x} \frac{dx}{k_t(1-x)}$
2.	$C_{A_F}\theta_M' = C_{A_F} m\theta = \dfrac{x_M'}{k_M(1-x_M')(R_F-x_M')}$	$C_{A_F}\theta_t' = C_{A_F}(1-m)\theta = \displaystyle\int_{x_M'}^{x} \frac{dx}{k_t(1-x)(R_F-x)}$

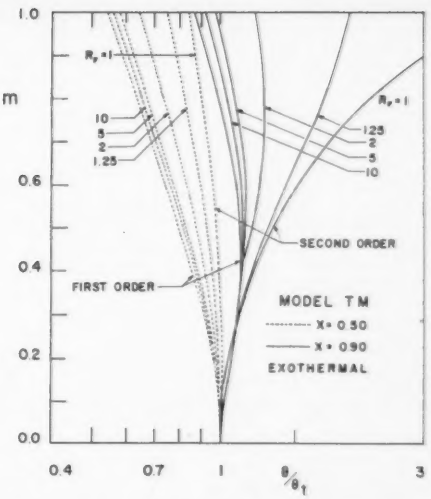

Figure 7—Variation of the relative residence time with the level of mixing in a TM reactor, for two different conversions, under exothermal conditions.

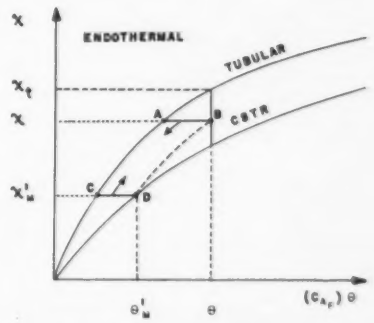

Figure 8—Graphical construction to determine directly the conversion at a given level of mixing in an MT reactor. It is applicable to endothermal, isothermal and exothermal reactions.

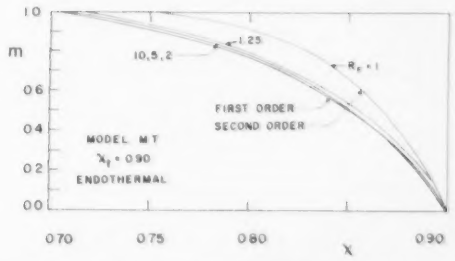

Figure 9—Variation of the conversion with the level of mixing in an MT reactor, for endothermal conditions.

Figure 8, up to point D. The latter, determined by θ_M', gives a conversion x_M' and is easily obtained since $\theta_M' = m\theta$. A path DB is then followed, parallel to the portion CA of the tubular curve, such that the abscissa of point B corresponds to the residence time θ of the system. The ordinate of point B determines the overall conversion for the particular combination considered.

In the above example the CSTR curve in Figure 8 lies below that for the tubular. It may be noted however that the same

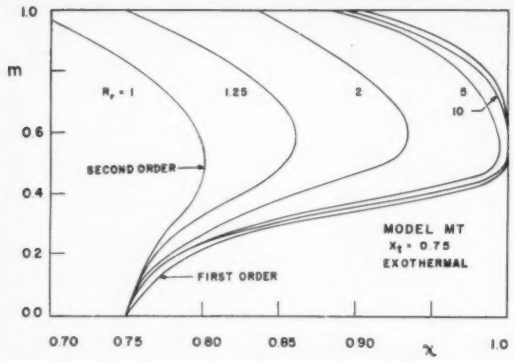

Figure 10—Variation of the conversion with the level of mixing in an MT reactor, for exothermal conditions.

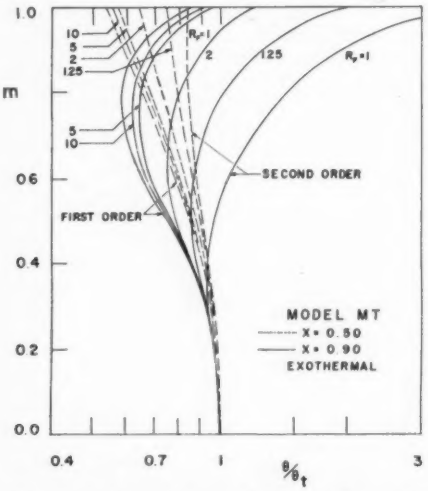

Figure 12—Variation of the relative residence time with the level of mixing at two different conversions, for exothermal reactions.

construction is also applicable even if the CSTR curve happens to lie above the tubular one as in exothermal reactions. The method always consists in following the CSTR curve up to θ_M' and then a path parallel to the tubular curve up to θ.

Curves obtained by this method and showing the variation of conversion with mixing level are presented in Figures 9 and 10 for endothermal and exothermal reactions respectively.

In the endothermal case, the degree of conversion is seen to decrease gradually as the extent of mixing increases. The tubular reactor gives the highest conversion in all cases and the CSTR the lowest.

For exothermal reactions, however, Figure 10 shows that a much higher conversion can be obtained at an intermediate mixing level than in either the tubular or CST reactors.

The particular case of a second-order reaction, for $R_F = 1.25$, is specially interesting as a conversion of 0.75 would be obtained in either a tubular or a CST reactor. Yet, a conversion approximately 15% superior can be achieved at a mixing level of 0.6.

The case of a first-order reaction is still more interesting as nearly complete conversion could be achieved at intermediate mixing levels while a tubular reactor would give one of only 0.75 and a CSTR approximately 0.9.

(2) Variation of Relative Residence times with mixing level at a given conversion.

The graphical construction in Figure 11 is used to determine directly the residence time required to reach a given conversion at different mixing levels.

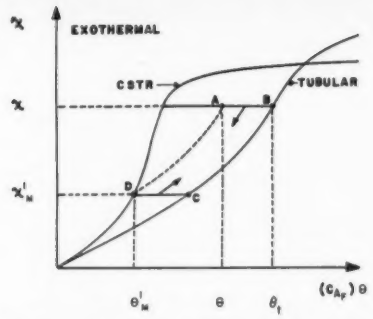

Figure 11—General graphical construction to determine the residence time required to reach a given conversion, at a certain level of mixing.

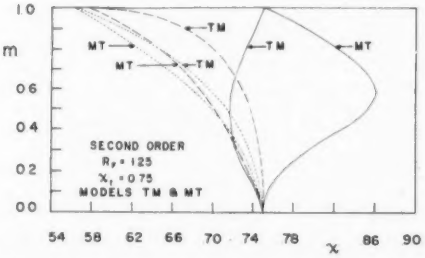

Figure 13—Comparison of the conversions obtained in MT and TM reactors at various levels of mixing. Full, dashed and dotted lines are for exothermal, endothermal and isothermal conditions respectively.

Taking a given value of θ_M' determines a point D on the CSTR curve at a conversion x_M'. Following a path DA parallel to CB on the tubular curve gives at conversion x a point A which corresponds to the overall residence time θ. The latter together with θ_M' at point D yield the particular value of m. Since point B determines θ_t for the conversion considered, one can obtain easily the values of the ratio θ/θ_t at all mixing levels.

A plot of such values is shown in Figure 12 for two different conversions, in the case of exothermal reactions.

No general conclusions can be drawn as to the best mixing level or MT combination to be used in such cases because the minima observed in the curve for the higher conversion are not found in those for the lower conversion. In this case a CSTR would be superior to any other arrangement. At higher conversion, however, a number of MT combinations would definitely provide a better utilization over a CSTR or a tubular reactor.

The graphical method outlined for use with MT reactors is applicable because of the integrated function describing the operation of the tubular section and because the values of k and x corresponding to the lower limit of the integral are also those found in the effluent of the well-mixed section.

COMPARISON OF TM AND MT REACTORS

A better picture of the relative behavior of the combinations TM and MT is perhaps obtained through a comparison of the two models for endothermal, isothermal and exothermal conditions.

For illustration purposes, Figure 13 shows such a comparison, for a second-order reaction, giving the variation of m with x. It may be seen that for endothermal and isothermal conditions, while the conversion decreases for both models with increasing level of mixing, the TM combination always gives a better performance at a given level of mixing than does the MT. Although no illustration is presented here as evidence, it may be mentioned that the horizontal spread between the TM and MT curves gets larger and larger as curves are drawn for conditions corresponding to increasing values of the conversion in a tubular reactor.

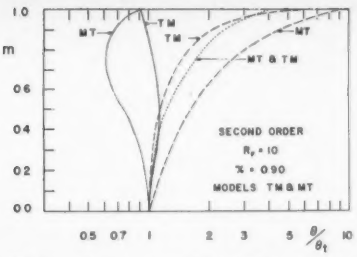

Figure 14—Comparison of models MT and TM showing, at a given conversion, the variation of relative residence times at various levels of mixing. Full, dashed and dotted lines are for exothermal, endothermal and isothermal conditions respectively.

As to the exothermal case, model *MT* stands out as giving the optimum performance. On the contrary, far from improving performance, model *TM* gives poorer results. In the particular example presented, all *MT* combinations happen to be better than either the tubular or CSTR alone, and all the *TM* poorer, because the conversions are the same at $m = 0$ and at $m = 1$. General conclusions should not be drawn on that account but the behavior of model *MT* would be worthwhile investigating in any particular case at intermediate levels of mixing.

Another basis of comparison, showing the variation of relative residence time with mixing level, is presented in Figure 14. As expected, the same advantage of the *MT* combination is again evidenced for exothermal reactions.

Since the curves of Figure 14 are for a large value of R_F, it may be noted that both curves for *MT* and *TM* combinations are identical for isothermal conditions as in the case of first-order reactions[16].

A further method of comparing results would consist in plotting the conversion as a function of residence time for various levels of mixing. This has been done in Figure 15 for an isothermal second-order reaction. At a given level of mixing the curve for the *TM* reactor lies closer to the tubular curve than does the one for the *MT* combination. It may be observed that as the conversion reaches a certain value, an increasing level of mixing would bring about a disproportionately larger residence time for isothermal conditions, and more so for endothermal. The reverse would be observed on a graph presenting the exothermal case.

Conclusions

It has been shown that in exothermal reactions an optimum performance may be obtained with combined reactors of the *MT* model. Depending on the prevailing conditions a higher conversion would be obtained, or a smaller residence time required, at intermediate mixing levels.

The usefulness of combined *MT* reactors has already been mentioned in the course of investigations dealing with combustion[21], usual chemical reactions[18], the determination of mixing patterns[19] and incomplete mixing in a single reactor[16] as would be the case for instance in a tubular reactor at low flow rates[22].

For the particular case of *MT* reactors, a graphical method is described which permits the direct and easy evaluation of the reactor performance. It constitutes in itself a valuable asset because it applies precisely to the combination of reactors which is susceptible of extensive applications.

Although the present study has been limited in scope by the particular values of the kinetic parameters chosen, the interesting behaviour of *MT* reactors should lead to a more thorough investigation of the field which, backed by experimental evidence, would contribute further to the knowledge of reactor design.

Acknowledgement

The authors wish to express their appreciation to the National Research Council of Canada for grants-in-aid of this study.

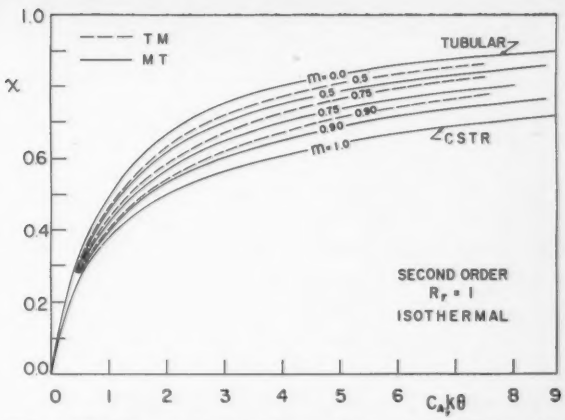

Figure 15—Curves showing the variation of conversion with residence time. They permit the comparison of MT and TM reactors at different levels of mixing.

Nomenclature

A = refers to reactant A
b = maximum temperature variation for complete conversion, °R.
B = refers to reactant B
C = volumetric concentration, lbs./ft.³
E = activation energy, B.t.u./lb. mole
k = reaction rate constant
k_M = reaction rate constant in the well-mixed section of combined reactors
k_t = reaction rate constant in the tubular section of combined reactors
m = level of mixing: fraction of the total volume of a combined *TM* or *MT* reactor which is perfectly mixed
q = volumetric rate of flow, ft.³/hr.
R = universal gas constant, B.t.u./(lb. mole) (°R.)
R_F = C_{B_F}/C_{A_F}
T = absolute temperature, °R.
V = volume, ft.³
x = conversion = $\dfrac{C_{A_F} - C_A}{C_{A_F}}$
x_M = theoretical conversion in a CSTR
x_t = theoretical conversion in a tubular reactor
$x_{M'}$ = conversion in the CSTR section of a combined *MT* or *TM* reactor
x_t' = conversion in the tubular section of a combined *MT* or *TM* reactor
z = a constant
$\theta = V/q$ = residence time, hr.
θ_M = residence time for a CSTR
θ_t = residence time for a tubular reactor
$\theta_{M'}$ = residence time for the CSTR section in a combined *MT* or *TM* reactor
θ_t' = residence time for the tubular section in a combined *MT* or *TM* reactor

Subscript

i = refers to species i
F = refers to feed conditions
M = refers to perfect mixing
o = refers to initial conditions
t = refers to plug flow operation

References

(1) Katz, S., Proceedings of the NYU-A.I.Ch.E.-ORSA Symposium, "Optimization Techniques in Chemical Engineering", New York University (1960).
(2) Aris, R., Chem. Eng. Sci., **12,** 243 (1960).
(3) Williams, Th. J., Series on: "Systems Engineering", Chem. Eng., **67** No. 3 (1960) to **68** No. 9 (1961).
(4) Aris, R., Can. J. Chem. Eng., **39,** 121 (1961).
(5) Aris, R., Chem. Eng. Sci., **13,** 18 (1960).
(6) Bilous, O., and Amundson, N. R., Chem. Eng. Sci., **5,** 81 and 115 (1956).
(7) Denbigh, K. G., Trans. Faraday Soc., **40,** 352 (1944).
(8) Calderbank, P. H., Chem. Eng. Progr., **49,** 585 (1953).
(9) Denbigh, K. G., "Chemical Reaction Engineering", Pergamon Press Inc., 1957, p. 125.

(10) Aris, R., Chem. Eng. Sci., **12,** 56 (1960).
(11) Danckwerts, P. V., Chem. Eng. Sci., **2,** 1 (1953).
(12) Tichacek, L. J., "Selectivity in Experimental Reactors", 42nd National A.I.Ch.E. Meeting, Atlanta, Georgia, Feb. 1960.
(13) Levenspiel, O., and Bischoff, K. B., Ind. Eng. Chem., **21,** 1431 (1959).
(14) Kramers, H., "Chemical Reaction Engineering", Pergamon Press, Inc., 1957, p. 45.
(15) Cholette, A., and Cloutier, Léonce, Can. J. Chem. Eng., **37,** 105 (1959).
(16) Cholette, A., Blanchet, J., and Cloutier, L., Can. J. Chem. Eng., **38,** 1 (1960).
(17) Zwietering, T. N., Chem. Eng. Sci., **11,** 1 (1959).
(18) Trambouze, P. J., and Piret, E. L., A.I.Ch.E. Journal, **5,** (3), 384 (1959).
(19) Bartock, W., Heath, C. E. and Weiss, M. A., A.I.Ch.E. Journal, **6,** 685 (1960).
(20) Smith, J. M., "Chemical Engineering Kinetics", McGraw-Hill Book Co., N.Y., 1956, p. 161.
(21) Hottel, H. C., Williams, G. C., and Bonnell, A. H., Combustion and Flame, Vol. II, No. 1, 13-34 (1958).
(22) Hovorka, R. B., and Kendall, H. B., Chem. Eng. Progr., **56,** (8), 58 (1960).

APPENDIX

The following examples are worked out to illustrate the applications of the trial and error and graphical methods described in the text. They are based on the numerical values of the kinematic parameters presented in Table 1.

(1) Find the conversion x, for a TM reactor, given: exothermal first-order reaction, $\theta = 34.0$ and $m = 0.3$.

For $m = 0.3$, $\theta_i' = 0.7 \times 34.0 = 23.8$. On the tubular curve of Figure 1, at a residence time of 23.8, the conversion $x_i' = 0.39$ is read directly. By trial and error, a value of $x = 0.79$ is finally chosen on the CSTR curve at a residence time $\theta_M = 20.1$. This latter value when multiplied by $(1 - x_i'/x)$ gives $\theta_M' = 20.1\left(1 - \frac{0.39}{0.79}\right) =$ 10.2 which checks the value of θ_M' computed by the separate values of $m\theta = 0.3\,(23.8 + 10.2) = 10.2$. For the value of $\theta = 34.0$, a single tubular reactor would give a conversion of 0.75, while in this TM reactor, one obtains a conversion of 0.79 at $m = 0.3$.

(2) Find the ratio θ/θ_i and the corresponding value of m for a conversion of 0.50 in a TM reactor given: exothermal second-order reaction, $R_F = 1.25$, and residence time in the tubular section corresponding to $C_{A_F}\theta_i' = 10$.

On the tubular curve of Figure 2 at $C_{A_F}\theta = 10$, $x_i' = 0.145$. At $x = 0.5$, on the CSTR curve, $C_{A_F}\theta_M = 19.9$. This value, when multiplied by $\left(1 - \frac{x_i'}{x}\right)$, or $\left(1 - \frac{0.145}{0.50}\right)$, gives $C_{A_F}\theta_M' = 19.9 \times 0.71 = 14.1$. The overall $C_{A_F}\theta = 14.1 + 10 = 24.1$ and the value of $m = \frac{\theta_M'}{\theta} = \frac{14.1}{24.1} = 0.58$. As for $x = 0.50$, $C_{A_F}\theta_i = 26.7$ is read directly on the tubular curve, the ratio θ/θ_i gives $\frac{24.1}{26.7} = 0.90$ for a value of $m = 0.58$.

(3) Find the conversion x for an MT Reactor, given, endothermal second-order reaction, $R_F = 5$, $C_{A_F}\theta = 12$ and $m = 0.7$.

On the CSTR curve of Figure 3, a point D at $x_M' = 0.67$ is located for $C_{A_F}\theta_M' = 0.7 \times 12 = 8.4$. Following the procedure outlined in Figure 8, the ordinate of point B gives the overall conversion $x = 0.81$. A single tubular reactor at $C_{A_F}\theta = 12$ would give a corresponding conversion of 0.90.

(4) Find the relative residence time and the level of mixing m in an MT reactor for a conversion of 0.90, given: exothermal second-order reaction, $R_F = 1.25$ and $C_{A_F}\theta_M' = 20$.

On the CSTR curve of Figure 2, a point D is located corresponding to $C_{A_F}\theta_M' = 20$ as indicated in Figure 11. A path DA parallel to segment CB of the tubular curve is then followed till the conversion of 0.90 is reached. The abscissa of point A reads $C_{A_F}\theta = 40.8$. The value of m is easily computed as it equals $20/40.8 = 0.49$. For a conversion of 0.90 a value of $C_{A_F}\theta_i = 47.5$ is read directly on the tubular curve. The ratio θ/θ_i then becomes $\frac{40.8}{47.5} =$ 0.86 at this particular value of $m = 0.49$.

★ ★ ★

Speed of Sound in a Non-Ideal Gas[1]

WILLIAM SQUIRE[2]

A method is proposed for computing the speed of sound in a non-ideal gas based on the approximation

$$\left(\frac{\partial H}{\partial E}\right)_s \simeq \frac{H}{E}$$

In conjunction with the usual generalized compressibility plot and an analogous reduced enthalpy correction plot, it can be used near the critical point of a non-dissociating gas. The method is also applicable to highly dissociated and ionized gases.

In a recent paper by Buthod and Tien[1] a method was described for computing the speed of sound in a gas which deviated appreciably from the ideal gas law because of intermolecular forces. Their method is based on the use of generalized plots of the compressibility factor, Z, and its partial derivatives with respect to temperature and pressure. In this paper, an alternate approach is described which leads to a very simple approximate expression. This approximation is applicable both to conditions where the deviation from ideal gas behavior is due to intermolecular forces and to conditions where the deviation from ideal gas behavior is due to dissociation and ionization. The second set of conditions is of importance in hypersonic flow investigations.

Thermodynamic Basis

The basis of the present approach is the thermodynamic identity

$$\left(\frac{\partial P}{\partial \rho}\right)_s = \frac{P}{\rho}\left(\frac{\partial H}{\partial E}\right)_s \quad \ldots\ldots\ldots\ldots\ldots\ldots (1)$$

This identity is easily verified by using the well-known Bridgman table[2]. It is obvious that

$$\left(\frac{\partial H}{\partial E}\right)_s = \frac{H}{E} + E\left(\frac{\partial H/E}{\partial E}\right)_s \quad \ldots\ldots\ldots\ldots\ldots\ldots (2)$$

and that the second term is a relatively small correction since the ratio of H/E is a slowly varying quantity. Therefore, the error involved in replacing $(\partial H/\partial E)_s$ by H/E is not large and the convenient approximation

$$u_e^2 \cong a^2 \frac{PH}{\rho E} = a^2 ZRT \frac{H}{H - ZRT} \quad \ldots\ldots\ldots\ldots\ldots\ldots (3)$$

can be used when adequate data along an isentrope is not available.

However, we note that while the value of $(\partial H/\partial E)_s$ is independent of the reference state, the value of H/E is dependent on the choice of a reference state.* To obtain the correct answer, it is necessary to select the reference state so that H and E will vanish simultaneously. Fortunately, many tables of thermodynamic data are based on such a reference state.

For a non-dissociating gas whose non-ideality is due to intermolecular forces, the usual corresponding state plots for Z as a function of the reduced pressure for various reduced temperatures can be used. A similar plot of a reduced enthalpy deviation, $\Delta H/T_c$, has been published by Edmister and can be used to evaluate H in Equation (3). This plot is reproduced as Figure 1 for the readers' convenience.

A gas such as air at a high temperature can be considered a mixture of ideal gases obeying the perfect gas law provided the correct molecular weight is used. The compressibility factor Z can be interpreted as the ratio of the nominal to actual molecular weight. This and the enthalpy are obtained from tables based on a solution of the equations for the equilibrium composition. Since the more recent tables[4,5,6] for air were prepared because of the growing interest in hypersonic flight, they include the speed of sound computed by a very accurate method. However, before they were available, the author found Equation (3) useful. It should also be useful for calculations involving hot combustion gases and other high temperature systems where complete tables are not available.

Application to Ethylene

Equation (3), in conjunction with the generalized plot for $\Delta H/T_c$ (Figure 1) and a conventional Z plot, was used to calculate the speed of sound in ethylene at 7.9°K. (the critical temperature) as a function of pressure. In Figure 2, these values are compared with those calculated by Buthod and Tien[1] and the experimental results cited in their paper. It is seen that the present method gives better agreement with experiment. The minimum in the vicinity of the critical point is reproduced though it is not as sharp as the experimental results indicate it should be.

Apparently the error due to the approximation involved in Equation (3) is less than the improvement resulting from the

[1]*Manuscript received October 12, 1960; accepted July 19, 1961.*
[2]*Department of Applied Mechanics, Southwest Research Institute, San Antonio, Texas, U.S.A. Present address: Department of Aero-Space Engineering, West Virginia University, Morgantown, West Virginia, U.S.A.*

*The author is indebted to Professor Agosta of Brooklyn Polytechnic Institute for an interesting correspondence on this point.

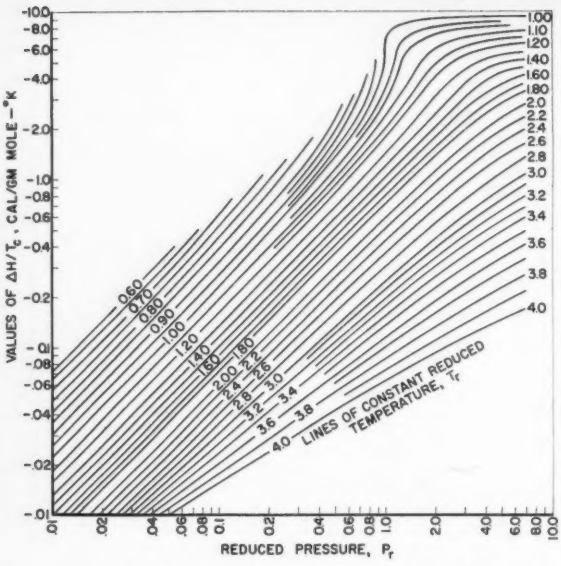

Figure 1—Generalized enthalpy correction plot.

TABLE 1

ERROR OF THE APPROXIMATE FORMULA FOR SOUND SPEED OF HIGH TEMPERATURE AIR

(T in °K. × 10^3)	$P = 10^{-3}$ atm. Exact value of Speed of Sound (meters/sec.)	% error	$P = 10^3$ atm. Exact value of Speed of Sound (meters/sec.)	% error
6	2039	+5.2	1517	− .4
7	2207	+3.9	1674	− .1
8	2352	+ .9	1816	+4.7
9	2684	+ .8	1973	− .8
10	3209	+1.7	2163	− .4
11	3700	+3.3	2389	+ .6
12	4126	+7.1	2632	+1.4

use of the generalized enthalpy correction which has an accuracy comparable to Z instead of the derivatives of Z which are subject to a larger error than Z. Also, our formulation does not require the specific heat which is difficult to evaluate in this region.

Application to Air at Very High Temperatures

Table 1 compares the approximate speed of sound obtained by applying Equation (3) to the thermodynamic data for air between 6,000 and 12,000°K. compiled by Predvoditelev[4] with the exact values. At 10^{-3} atm., the air is almost completely dissociated at 6,000°K. and highly ionized, (43% electrons at 12,000°K.). At 10^3 atm., there is an appreciable NO concentration and some oxygen dissociation at 6,000°K. and fairly complete dissociation, but only a little ionization at 12,000°K. It can be seen that over these widely varying conditions the approximate formula is frequently quite accurate, though there are regions where the error exceeds 5%. On the basis of a more extensive tabulation by Hochstim[5] and calculations by Logan and Treanor[6], it appears that the large error is associated with regions where the composition is changing rapidly rather than with a high degree of dissociation or ionization.

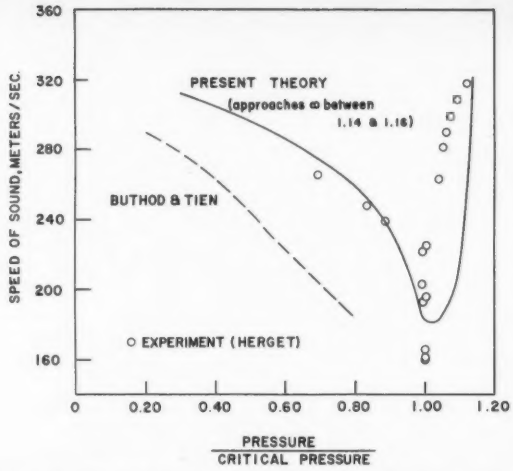

Figure 2—Variation of the speed of sound in ethylene, at the critical temperature, as a function of pressure.

Acknowledgement

Equation (3) was first suggested by Roger Weatherston as an empirical approximation for high temperature air. This led to Equation (1). Also, thanks are due to Professor Edmister for furnishing Figure 1.

Nomenclature

a = conversion factor to express u_c directly in meters/second
It is equal to $31.83 \frac{\text{meters}}{\text{second}} \left(\frac{\text{gram}}{\text{liter-atm}}\right)^{1/2}$
C_p = specific heat at constant pressure (calories/grams °K.)
C_v = specific heat at constant volume (calories/grams °K.)
E = internal energy per unit mass (calories/grams)
H = enthalpy per unit mass (calories/grams)
P = pressure (atmospheres)
R = gas constant (liter atmospheres/grams °K.)
S = enthropy per unit mass (calories/grams °K.)
T = temperature (°K.)
u_c = speed of sound (meters/second)
Z = compressibility factor (dimensionless)
$\frac{\Delta H}{T_c}$ = reduced enthalpy correction, enthalpy difference divided by critical temperature (calories/grams °K.)
ρ = density (grams/liter)

References

(1) Buthod, A. P., and Tien, C., *Can. J. Chem. Eng.*, **38,** 74 (1960).
(2) Bridgman, P. W., A Condensed Collection of Thermodynamic Formulas, Harvard University Press, Cambridge (1925).
(3) Edmister, W. C., Petrol. Refiner, **28,** 137 (February 1949).
(4) Predvoditelev, A. S., et al, Tables of Thermodynamic Functions of Air, Infosearch, London (1958).
(5) Hochstim, A. R., "Gas Properties Behind Shocks and Hypersonic Velocities", Convair Reports, Physics Section Z Ph-003, May 15, 1957, Physics Section Z Ph-004, August 1958.
(6) Logan, J. G., and Treanor, C. E., "Thermodyanamic Charts for High Temperature Air Calculations", Cornell Aeronautical Laboratory Report AD-1052-A3, July 1956.
(7) Herget, C. M., J. Chem. Phys., **8,** 537 (1940).

★ ★ ★

Kinetics of the Vapor-Phase Oxidation of Toluene over a Vanadium Catalyst[1]

J. DOWNIE[2], K. A. SHELSTAD[3] and W. F. GRAYDON[4]

Rates of oxidation of toluene were measured as a function of temperature and reactant concentration. A fixed bed reactor was operated at low conversions over the following range of conditions, 300°C. to 350°C., 1 x 10^{-3} to 15 x 10^{-3} moles oxygen per litre of gas, and 1 x 10^{-3} to 6 x 10^{-3} moles toluene per litre of gas.

The rate data for the oxidation of toluene were correlated by the following equation, which is based on a model by Hinshelwood.

$$r_t = \frac{k_a\, k_t\, C_t\, C_o}{k_a\, C_o + N\, k_t\, C_t}$$

The values of k_a obtained agree with those reported previously for naphthalene oxidation(1).

It is concluded that the Hinshelwood model is a useful one for this type of reaction, and within the limits of available data provides a satisfactory interpretation.

During the past decade interest has developed in vapor-phase catalytic oxidation which has been of a more fundamental nature than had hitherto been evident. Empirical and engineering advances had placed many processes on a sound operating basis, and, in doing so, had outdistanced the understanding which results from more fundamental approaches.

Several basic studies have now been made, especially with regard to the catalytic oxidation of naphthalene. These have been discussed in a previous paper(1). However, data have not yet been presented for the dependence of the rate of oxidation of toluene on reactant concentrations and temperature.

Experimental Work

The apparatus, shown as a flow diagram in Figure 1, consisted of independent flow systems, for oxygen and nitrogen, leading to a mixing chamber from which were drawn primary and secondary supplies. Toluene saturation of the primary supply and reunion with the secondary supply preceded the reactor. The reactor was kept at constant temperature and the gases passed through a thin catalyst bed. The products were collected in suitably designed liquid air traps. The apparatus was operated at low conversions to study the rate of oxidation directly as a function of known inlet concentrations.

One sample of the reaction products was analysed spectrophotometrically, another by potentiometric titration. From the results the moles of p-benzoquinone, benzaldehyde, benzoic acid and maleic anhydride in the reaction products were calculated. This was the information which was used to calculate the moles of toluene oxidized per run, and hence the rate of oxidation of toluene.

Carbon dioxide was measured by the weight increase of a carboxite trap. After finding negligible amounts of complete oxidation the carbon dioxide checks were only used intermittently.

From the product distribution of the low conversion runs it may be seen that of the toluene oxidized approximately 86% reacts to benzaldehyde, 7% reacts to p-benzoquinone, 3% reacts to maleic anhydride, and 4% reacts to benzoic acid. The error in the estimated rate of oxidation, due to analytical errors, is therefore approximately that of the benzaldehyde determination, i.e., 4%.

Theory

The reaction takes place at the solid surface, but our information about reactant concentrations refers to the gas phase. Therefore we require a model which permits the calculation of surface concentrations in terms of gas phase concentrations.

In the past many reactions have been explained by assuming adsorption equilibrium to be established. Then Langmuir's theory relating known concentrations to surface concentrations has been used. This approach has been most successful for high temperature reactions, e.g., incandescent metal wire catalysts, but there is another class of reactions where the reaction temperature is relatively low. For the latter Taylor found a slow rate of adsorption(2). When the rate of adsorption of reactants is of the same order of magnitude as the rate of chemical reaction the assumption of adsorption equilibrium is no longer valid, and rate relationships based on Langmuir-Hinshelwood or Rideal mechanisms are on a doubtful footing.

The present study involved using a vanadium oxide catalyst at 300° to 350°C., and it seems reasonable to assume adsorption equilibrium was not established.

It was decided to use the simplest steady state situation first and to check the resulting relationship against the experimental data.

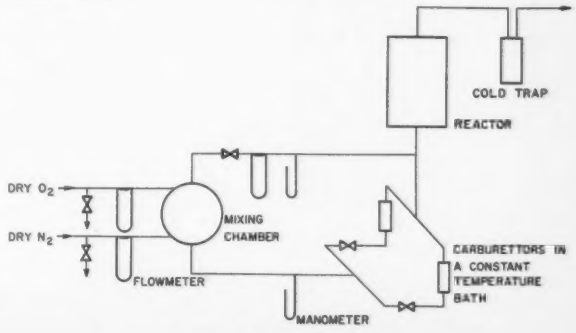

Figure 1—Flow diagram of the apparatus.

[1]*Manuscript received December 20, 1960; accepted July 14, 1961.*
[2]*Gulf Research and Development Company, Harmarville, Pa.*
[3]*Assistant Professor, Department of Chemical Engineering, McGill University, Montreal, Que.*
[4]*Professor of Chemical Engineering, Department of Chemical Engineering and Applied Science, University of Toronto, Toronto, Ont.*
Contribution from the Department of Chemical Engineering and Applied Science, University of Toronto, Toronto, Ont. Based on a paper presented to the C.I.C. Chemical Engineering Conference, Hamilton, Ont., November 9-11, 1959.

This treatment follows Hinshelwood's general treatment on page 208 of "Kinetics of Chemical Change"[3]. The introduction of N is for the general reaction of this particular study.

The following assumptions are made,

1. Only oxygen is adsorbed on the catalyst surface.
2. Reaction occurs when toluene in the gas strikes adsorbed oxygen.
3. The rate of desorption of oxygen is negligible.
4. A steady state is established in which, Rate of removal of oxygen by chemical reaction = Rate of adsorption of oxygen.

$$C_7H_8 + (N)\,O_2 \rightarrow \text{Products}$$

Therefore,

Rate of removal of oxygen by Chemical reaction

$$= N \times \text{Rate of oxidation of toluene}$$

$$= N\,k_t\,C_t\,S$$

Therefore,

$$N\,k_t\,C_t\,S = k_a\,C_o\,(1 - S)$$

$$\text{i.e.,} \quad S = \frac{k_a\,C_o}{k_a\,C_o + N\,k_t\,C_t}$$

Therefore,

$$\text{Rate of oxidation of toluene} = \frac{k_a\,k_t\,C_t\,C_o}{k_a\,C_o + N\,k_t\,C_t} \quad \ldots\ldots\ldots\ldots (1)$$

Discussion of Results

The rate of catalytic oxidation of toluene was determined as a function of toluene concentration, oxygen concentration, and catalyst bed temperature. This involved measuring the rate of oxidation both in the presence and in the absence of catalyst. Knowing the oxidation in the absence of catalyst under the conditions of the catalytic run, the oxidation due to the presence of the catalyst was found by difference. Details are given in reference 4.

The experimental results presented in Figures 2, 3, 4, 5 and 6 have been corrected for oxidation in the absence of catalyst, and have been brought to a constant concentration basis for the parameters. The solid lines were calculated from Equation (1).

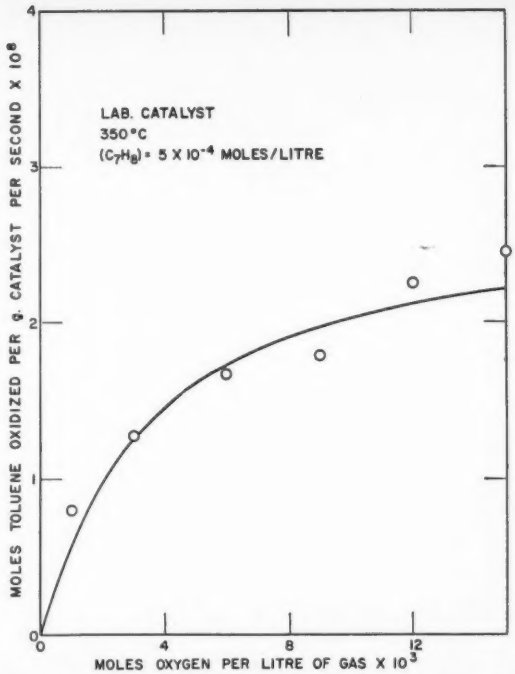

Figure 2—Rate of oxidation of toluene as a function of the concentration of oxygen, at 350°C., using the laboratory prepared catalyst.

Equation (1) becomes suitable for use in correlation when inverted.

$$\frac{1}{r_t} = \frac{1}{k_t\,C_t} + \frac{N}{k_a\,C_o} \quad \ldots\ldots\ldots\ldots\ldots\ldots (2)$$

Equation (2) was used to test the effectiveness of the Hinshelwood interpretation in the correlation of the experimental

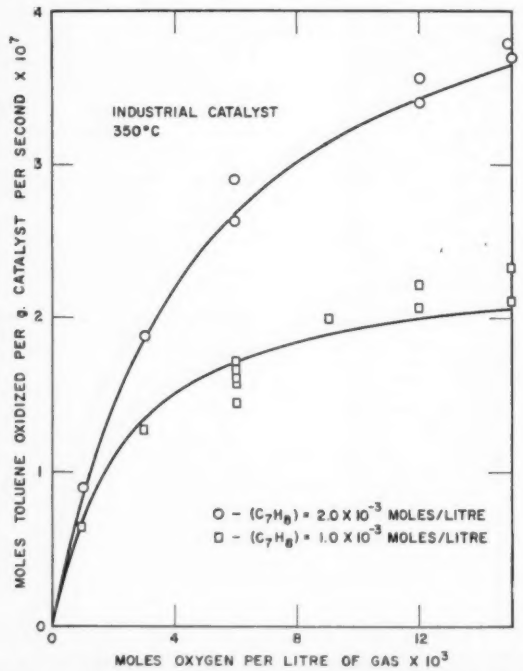

Figure 3—Rate of oxidation of toluene as a function of the concentration of oxygen, at 350°C., using the industrial catalyst.

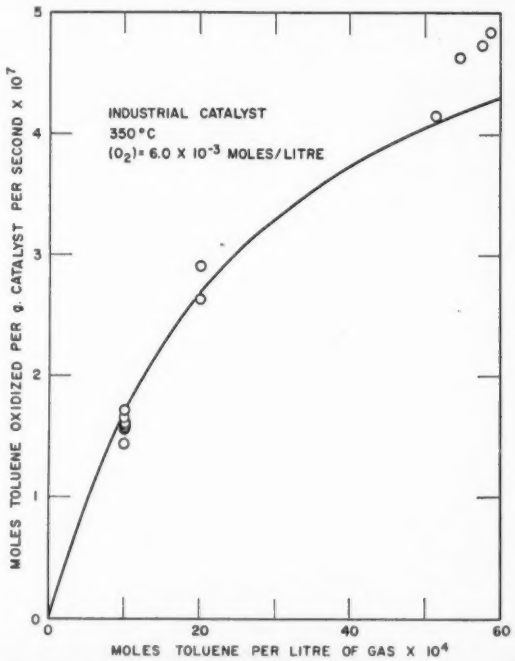

Figure 4—Rate of oxidation of toluene as a function of the concentration of toluene at 350°C., using the industrial catalyst.

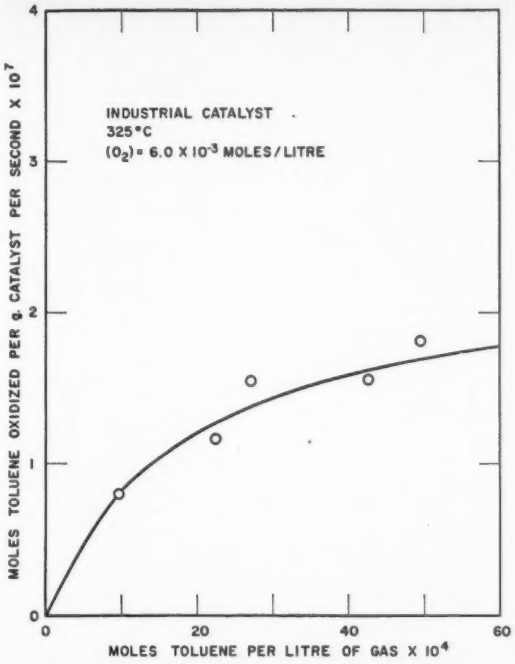

Figure 5—Rate of oxidation of toluene as a function of the concentration of toluene, at 325°C., using the industrial catalyst.

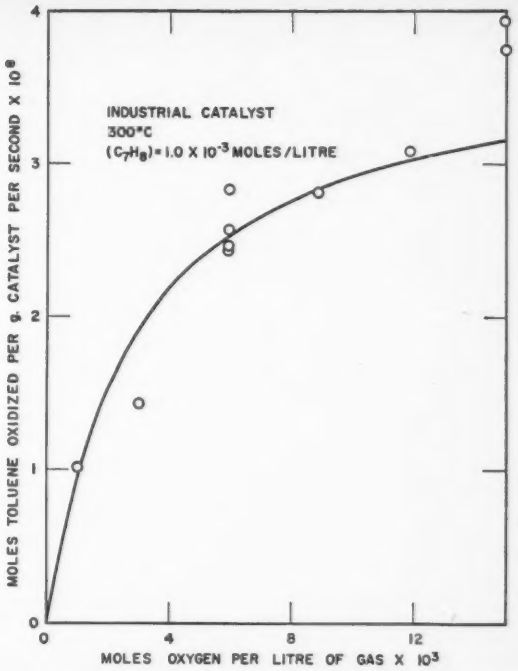

Figure 6—Rate of oxidation of toluene as a function of the concentration of oxygen, at 300°C., using the industrial catalyst.

results. The straight line relationship was a good fit of the data. k_t and k_a/N were calculated from a least squares treatment of the data and are given in Table 1.

The average values for k_t and k_a/N were used in Equation (1) to calculate the lines shown in Figures 3, 4, 5 and 6. The average relative errors of the calculated rates were estimated for each set of data and were as follows:

Set No.	1	2	3	4	5
Average % Error	7	3	7	6	10

Inspection of the curves shows a satisfactory correlation of the data, indicating the relative insensitivity to the small variations in k_a shown in Table 1. N (the moles of oxygen used per mole of toluene oxidized) was determined, from product distribution data, to be 1.35 throughout the range of conditions in Sets 1 to 5. k_a was then calculated and an Arrhenius-type plot used to obtain Arrhenius energies of activation for k_t and k_a (Figure 7).

These results can be summarized as follows:

the catalytic oxidation of toluene over industrial catalyst I in the temperature range 300° to 350°C. can be described by the following relationship:

$$r_t = \frac{k_a\, k_t\, C_o\, C_t}{k_a\, C_o + N\, k_t\, C_t}$$

where $N = 1.35$

$k_a = 1.39 \times 10^{-4}$ at 350°C.
5.22×10^{-5} at 325°C.
1.78×10^{-5} at 300°C.

Arrhenius activation energy of k_a = 29,400 cal./mole

$k_t = 2.38 \times 10^{-4}$ at 350°C.
1.27×10^{-4} at 325°C.
3.76×10^{-5} at 300°C.

Arrhenius activation energy of k_t = 26,400 cal./mole

This treatment has been applied to the rate of oxidation data for naphthalene, and we are now in a position to show that the theory not only is useful in correlating the studies independently but provides a link between them.

According to the above interpretation k_a should be independent of the organic compound oxidized when the same catalyst is used. Since the same industrial catalyst was used in both toluene and naphthalene work, a check is available.

At 350°C.

k_a from naphthalene = 0.93×10^{-4}
k_a from toluene = 1.39×10^{-4}

At 300°C.

k_a from naphthalene = 1.30×10^{-5}
k_a from toluene = 1.78×10^{-5}

Arrhenius energy of activation of k_a

from naphthalene = 28,100 cal. $mole^{-1}$
from toluene = 29,400 cal. $mole^{-1}$

The k_t values from toluene and naphthalene differed by a factor of 70. Therefore, the small difference in k_a shown above was taken as supporting the view, arrived at on the basis of the main body of results presented previously, that the Hinshelwood approach is a useful one for this type of reaction and within the limits of the available data provides a satisfactory interpretation.

Mars and van Krevelen[5] arrived at similar conclusions for their work on benzene, naphthalene, and anthracene, although they state that they could not include toluene. They did not publish results on toluene and therefore no comparison can be made.

TABLE 1

T °C.	Set No.	$k_t \times 10^4$	$(k_a/N) \times 10^4$
350	1	2.68	0.727
350	2	2.46	1.03
350	3	2.00	1.34
350	Average of 1,2,3	2.38	1.03
325	4	1.27	0.387
300	5	0.376	0.132

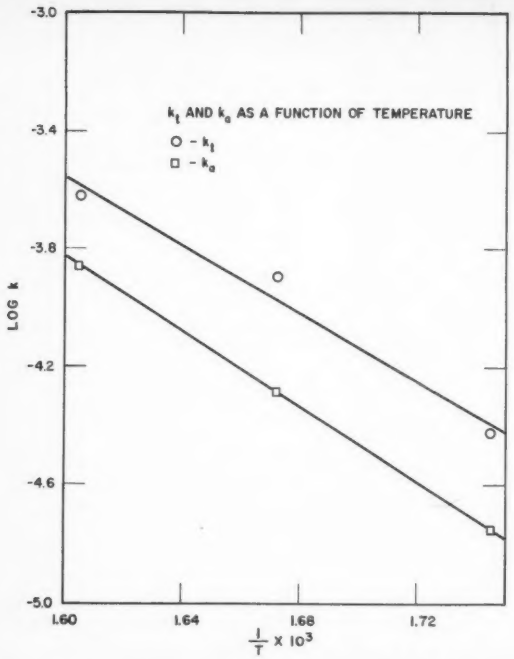

Figure 7—Arrhenius-type plot of the specific rate constants as functions of temperature.

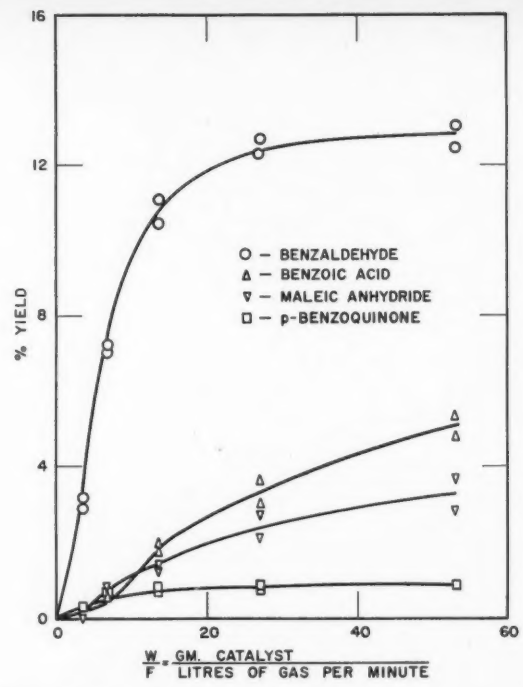

Figure 8—% yield of reaction products as a function of W/F.

The results of a series carried out using a laboratory prepared catalyst are shown in Figure 2. The results were of the same form as those using the industrial catalyst.

A series of oxidation runs was started to study the effect of contact time on product distribution. The results are shown in Figure 8.

The results show a levelling off in the yields of benzaldehyde and p-benzoquinone, and an increase in yields of benzoic acid and maleic anhydride over the entire range studied. The exit concentration of each of the above products was calculated and examined as a function of contact time.

These results were used in the following speculative calculations.

The rate of oxidation of benzaldehyde was calculated assuming that all p-benzoquinone, maleic anhydride, and benzoic acid resulted from the catalytic oxidation of benzaldehyde. These calculations were carried out for the four runs at the two lowest contact times in order to minimize the error due to CO_2 formation. The total conversion of toluene under these conditions was 4% and 9%.

The rates thus calculated were used together with benzaldehyde concentrations to determine k_a. The value found in this way was

$$k_a = 0.66 \times 10^{-4} \text{ at } 350°C.$$

i.e., about half the value previously obtained from toluene oxidation data.

This calculation was repeated for benzoic acid oxidation and resulted in a k_a value of 0.27×10^{-4} which is about one-fifth of the toluene value.

If, as is possible, there was some total oxidation during the 9% conversion runs, accounting for this will result in k_a values which approach the k_a value from toluene oxidation data.

Therefore, as a tentative conclusion, it may be possible to extend the treatment of the main body of results to cover benzaldehyde and benzoic acid oxidation.

Conclusions

The rate of oxidation of toluene over a vanadium oxide, potassium sulphate promoted, catalyst, can be described by the following relationship:

$$r_t = \frac{k_a\, k_t\, C_o\, C_t}{k_a\, C_o + N\, k_t\, C_t}$$

Values of k_a from data on the oxidation of naphthalene[1] agree to within 33% of those from the present work, and values of the temperature coefficient of k_a agree to within 4%. This interpretation therfore provides a link between toluene and naphthalene oxidation on the same catalyst.

The Hinshelwood model[3] is a useful one for this type of reaction and within the limits of available data provides a satisfactory interpretation.

Further oxidation work on toluene at varying contact time indicated that it may be possible to extend this approach to benzaldehyde and benzoic acid oxidation.

Acknowledgement

The authors are indebted to the Shell Oil Company of Canada Limited, the Ontario Research Foundation, and the Advisory Committee on Scientific Research, University of Toronto, for financial assistance.

Nomenclature

C	=	gas concentration, g. moles per liter
k_a	=	specific rate of adsorption of oxygen
k_t	=	specific rate of reaction of toluene
N	=	moles of oxygen used per mole of toluene oxidized
r	=	reaction rate, moles of toluene oxidized per g. of catalyst per second
S	=	fraction of surface covered by oxygen at steady state
T	=	temperature

Subscripts

o	=	oxygen
t	=	toluene

References

(1) Shelstad, K. A., Downie, J. and Graydon, W. F., Can. J. Chem. Eng., **38,** 102 (1960).
(2) Taylor, H. S., J. Am. Chem. Soc., **53,** 578 (1931).
(3) Hinshelwood, C. N., "The Kinetics of Chemical Change", Oxford University Press (1949).
(4) Downie, J., Ph.D. Thesis, Univ. of Toronto (1959).
(5) Mars, P. and van Krevelen, D. W., Chem. Eng. Sci., **3,** 41 (1954). Special Supplement.

★ ★ ★

Determination of Vapor-Liquid Equilibrium Data from Total Pressure-Liquid Composition Measurements[1]

JAMES C. K. HO[2], *O. BOSHKO*[2] *and*
BENJAMIN C.-Y. LU[2]

Digital computer methods are developed for evaluating equilibrium data from total pressure-liquid composition measurements of volatile binary non-electrolyte mixtures. The Redlich-Kister equation is employed for representing liquid activity coefficients. The constants B, C and D are evaluated by the method of least squares for non-linear formulas. Equilibrium vapor compositions are also evaluated by means of a step-wise integration procedure. A comparison of both methods is presented.

Total pressure-liquid composition measurements are in general easier than the equilibrium vapor composition measurements, especially for solutions of high relative volatilities and for solutions which are difficult to analyze. Several methods have been proposed in the literature for evaluating liquid activity coefficients, partial pressures and equilibrium vapor compositions from the total pressure-liquid composition measurements[1,2,3,4,5,6,7]. In general, these methods involve evaluations of either constants of equations representing the liquid activity coefficients or equilibrium vapor compositions directly by means of a step-wise integration procedure. All methods involve, however, the Gibbs-Duhem equation.

In the course of investigation of various thermodynamic properties of non-electrolyte solutions in this laboratory, it appeared desirable to develop a method for evaluating excess thermodynamic functions which are represented by a power series with respect to liquid compositions. The use of a digital computer (IBM 650) was intended. In this paper, application of this method is illustrated for evaluating activity coefficients from total pressure-liquid composition measurements. It is also of interest to this laboratory to evaluate equilibrium vapor compositions directly from the total pressure measurements without involving any conversion to liquid activity coefficients. The advantages of these two approaches are compared and discussed in this paper.

Evaluation of Activity Coefficients

Total pressure-liquid composition measurements are usually made at constant temperature conditions. The Gibbs-Duhem equation of the form

$$x_1\left(\frac{\partial \log \gamma_1}{\partial x_1}\right)_{T,P} + x_2\left(\frac{\partial \log \gamma_2}{\partial x_1}\right)_{T,P} = 0 \quad \ldots\ldots\ldots (1)$$

is generally employed for developing equations for representing liquid activity coefficients. It is obvious that Equation (1) is applicable only at constant temperature and pressure and all the equations developed from it are applicable only at these conditions. However, it is due to the fact that the pressure effect on liquid activity coefficient is expressed by

$$\frac{\partial \log \gamma_i}{\partial P} = \frac{\bar{V}_i - v_i}{2.303RT} \quad \ldots\ldots\ldots (2)$$

which is small and can be neglected over a moderate range of pressure, that integrated forms of the Gibbs-Duhem equation can be employed at isothermal conditions.

The expression for representing the excess free energy function, Q, as proposed by Redlich and Kister[8] is employed in this investigation

$$Q = x_1(1 - x_1)[B + C(2x_1 - 1) + D(2x_1 - 1)^2 + \ldots] \ldots (3)$$

It may be readily seen that from Equations (3) and (1) the liquid activity coefficients may be represented by the following expressions:

$$\log \gamma_1 = (1-x_1)^2[B + C(4x_1-1) + D(2x_1-1)(6x_1-1)+\ldots)] \ldots (4a)$$

and

$$\log \gamma_2 = x_1^2[B + C(4x_1-3) + D(2x_1-1)(6x_1-5) + \ldots] \ldots (4b)$$

If the vapor phase is considered ideal, then

$$P = x_1 \gamma_1 p_1^\circ + x_2 \gamma_2 p_2^\circ \quad \ldots\ldots\ldots (5)$$

Simultaneous solution of Equations (4) and (5) would provide the required information. The problem is therefore to determine the constants involved in Equations (4a) and (4b) so that the total pressure values calculated from Equation (5) agree with the experimentally observed values.

Christian[6] employed expressions similar to Equations (3) and (4) for representing liquid activity coefficients and determined the constants (restricted to three) using three experimental points. The three points were chosen either from the smoothed curve or from three actual data points without any preference in the choice of liquid compositions. Should only three constants be considered in the equations representing activity coefficients and only three points be employed, it was observed in this laboratory[9] that the best three points would be at $x_1 = 0.25$, $x_1 = 0.5$, and $x_1 = 0.75$. The evaluation of the constants could be very much simplified. Such a computing program was developed in this laboratory[10].

In the present investigation, the method developed uses all the experimental points in the evaluation of the constants. The principles involved could be employed for any number of constants involved in Equations (4a) and (4b). The IBM program developed for this paper is limited however to three constants, B, C and D. The mathematical approach is similar to that of Baker[4] and outlined below.

As the Equations (4a) and (4b) are not linear, the constants B, C and D cannot be determined directly by means of the method of least squares. A set of initial values of B, C and D may be

[1]*Manuscript received November 4, 1960; accepted March 20, 1961.*
[2]*University of Ottawa, Ottawa, Ont.*

assigned, using constants of a similar system as a guide or approximated by assuming that the solution behaves as a regular solution[4] so that C and D are zero. Using the first approximation, the pressure residuals, ΔP, and the derivatives $\partial P/\partial B$, $\partial P/\partial C$ and $\partial P/\partial D$ are determined by means of the following equations.

$$\Delta P = P_{obsvd.} - P_{calcd.} = \Delta B \frac{\partial P}{\partial B} + \Delta C \frac{\partial P}{\partial C} + \Delta D \frac{\partial P}{\partial D} \quad \ldots\ldots(6)$$

$$\frac{\partial P}{\partial B} = 2.303\,[x_1(1 - x_1)^2\, p_1^\circ\, \gamma_1 + x_1^2\,(1 - x_1)\, p_2^\circ\, \gamma_2] \quad \ldots\ldots(7)$$

$$\frac{\partial P}{\partial C} = 2.303\,[x_1(1 - x_1)^2\,(4x_1 - 1)\, p_1^\circ\, \gamma_1 + x_1^2\,(1 - x_1)\,(4x_1 - 3)\, p_2^\circ\, \gamma_2] \quad \ldots\ldots(8)$$

and

$$\frac{\partial P}{\partial D} = 2.303\,[x_1\,(1 - x_1)^2\,(2x_1 - 1)\,(6x_1 - 1)\, p_1^\circ\, \gamma_1 + x_1^2\,(1 - x_1)\,(2x_1 - 1)\,(6x_1 - 5)\, p_2^\circ\, \gamma_2] \quad \ldots\ldots(9)$$

The activity coefficients γ_1 and γ_2 in these expressions are represented by Equations (4a) and (4b). The procedure of calculation is to determine the changes ΔB, ΔC and ΔD in B, C and D, so that the pressure residuals be reduced to a minimum by means of the least square method, which is described below. These increments are added to the initial values of B, C and D for improved approximations. Thus, the quantities B, C and D are determined by successive approximations. The process is repeated until the increments ΔB, ΔC and ΔD are equal to or less than the tolerance desired in the values of B, C and D.

For n number of observations, we have n residual equations:

$$\Delta B \frac{\partial P_1}{\partial B} + \Delta C \frac{\partial P_1}{\partial C} + \Delta D \frac{\partial P_1}{\partial D} = \Delta P_1$$

$$\Delta B \frac{\partial P_2}{\partial B} + \Delta C \frac{\partial P_2}{\partial C} + \Delta D \frac{\partial P_2}{\partial D} = \Delta P_2$$

$$\Delta B \frac{\partial P_n}{\partial B} + \Delta C \frac{\partial P_n}{\partial C} + \Delta D \frac{\partial P_n}{\partial D} = \Delta P_n$$

Therefore, the "normal" Equations[11] are

$$\Delta B \sum\left(\frac{\partial P}{\partial B}\right)^2 + \Delta C \sum\left(\frac{\partial P}{\partial B}\right)\left(\frac{\partial P}{\partial C}\right) + \Delta D \sum\left(\frac{\partial P}{\partial B}\right)\left(\frac{\partial P}{\partial D}\right) = \sum \Delta P\left(\frac{\partial P}{\partial B}\right) \quad \ldots\ldots(10)$$

$$\Delta B \sum\left(\frac{\partial P}{\partial B}\right)\left(\frac{\partial P}{\partial C}\right) + \Delta C \sum\left(\frac{\partial P}{\partial C}\right)^2 + \Delta D \sum\left(\frac{\partial P}{\partial C}\right)\left(\frac{\partial P}{\partial D}\right) = \sum \Delta P\left(\frac{\partial P}{\partial C}\right) \quad \ldots\ldots(11)$$

and

$$\Delta B \sum\left(\frac{\partial P}{\partial B}\right)\left(\frac{\partial P}{\partial D}\right) + \Delta C \sum\left(\frac{\partial P}{\partial C}\right)\left(\frac{\partial P}{\partial D}\right) + \Delta D \sum\left(\frac{\partial P}{\partial D}\right)^2 = \sum \Delta P\left(\frac{\partial P}{\partial D}\right) \quad \ldots\ldots(12)$$

where the summations $\sum$ are taken over all n observations. There are three normal equations as there are three quantities B, C and D to be determined. Multiplying the 1st, 2nd, ... and nth residual equation by ΔP_1, ΔP_2, ... and ΔP_n respectively, and adding all the corresponding factors together, Equation (13) is obtained,

$$\Delta B \sum(\Delta P)\left(\frac{\partial P}{\partial B}\right) + \Delta C \sum(\Delta P)\left(\frac{\partial P}{\partial C}\right) + \Delta D \sum(\Delta P)\left(\frac{\partial P}{\partial D}\right) = \sum(\Delta P)^2 \quad \ldots\ldots(13)$$

from which one may judge the quality of the fittings.

In the calculations, it is observed that the values of first approximation do not affect much the computing time required. For the system ethanol-water at 25°C.[12] two sets of initial values of B, C and D were assumed. In the first set, $B = 0.200$, $C = 0.040$ and $D = 0.020$ were employed and in the second set $B = 0.830$, $C = 0.000$ and $D = 0.000$ were employed. The difference in the required machine time is less than half a minute.

There are two modes of output in the program. In the condensed output, the following items are printed:

(1) Initial estimates of the constants, B_o, C_o and D_o and the tolerance desired.

(2) Final values of B, C and D and number of iterations performed.

(3) The quantities, x, $P_{obsvd.}$, ΔP, p_1, p_2, γ_1 and γ_2.

In the optimum output, the quantities ΔB, ΔC, ΔD and ΔP are printed for each iteration. The course of the computation may be easily followed step by step. The program was originally written in FORTRAN symbolic language. The machine time required per set of data depends, in general, on the number of experimental data, initial estimates of B, C and D, and the desired tolerance. As an average, four iterations are adequate for a tolerance of the order of 10^{-5} and approximately four minutes are required per set with condensed output. The program occupies 1,005 locations.

The calculated B, C and D values for 13 systems at 20 temperature conditions are listed in Table 1. A typical output is shown in Table 2 for the system ethanol-water at 25°C.[12]. The computed equilibrium vapor compositions of this system are compared with the experimental values in Table 3.

It is of interest to note that in Table 1, with the exceptions of the data for the extremely imperfect systems ethanol-isooctane[13] and ethanol-methylcyclohexane[14], the $|\Delta P|_{av.}$ values are generally small, indicating that the three constant Redlich-Kister equations are adequate for representing liquid activity coefficients. This is significant in testing data consistency[9]. It may be mentioned that for the system ethanol-water at 74.79°C., the computed B, C and D values from the total pressure measurements (Table 1) are in good agreement with the values calculated[15] from the experimentally determined vapor-liquid equilibrium compositions[16]. However, in the case when experimental data were used, the values $B = 0.5311$, $C = -0.1650$ and $D = 0.0441$ were obtained after the data were adjusted for consistency. The advantage of evaluating activity coefficients using total pressure measurements is obvious.

Evaluation of Equilibrium Vapor Compositions

In the above section, the evaluations of the constants B, C and D of the Redlich-Kister equation, the activity coefficients and the partial pressures have been described. The equilibrium vapor compositions may be determined by using Equation (5). Thus

$$y_1 = x_1\,\gamma_1\,p_1^\circ/P = p_1/P \quad \ldots\ldots(14a)$$

and

$$y_2 = x_2\,\gamma_2\,p_2^\circ/P = p_2/P = 1 - y_1 \quad \ldots\ldots(14b)$$

However, it is also of interest to develop a computing method for evaluating equilibrium vapor compositions directly from the total pressure measurements without involving any conversion to liquid activity coefficients.

The relationship between the total pressure measurements and the compositions of liquid and vapor phases may be expressed by

$$\frac{dP}{P} = \frac{y_1 - x_1}{y_1(1 - y_1)}\, dy_1 \quad \ldots\ldots(15)$$

TABLE 1

CALCULATED CONSTANTS AND DEVIATIONS

System	Temp. °C.	B	C	D	$\lvert\Delta P\rvert$ av. mm. Hg.
1. Acetone-Chloroform[19]	25	−0.4276	0.1105	0.0571	0.71
	35	−0.3343	0.0701	0.0357	0.47
	50	−0.3877	0.0941	0.0436	0.33
2. Benzene-n-Heptane[20]	80	0.1578	0.0455	0.0142	0.28
3. Carbon Disulfide-Benzene[21]	20	0.1623	0.0594	−0.0406	0.24
4. Carbon Tetrachloride-Benzene[22]	40	0.0538	0.0000	−0.0024	0.03
	70	0.0469	−0.0002	0.0010	0.05
5. Chloroform-Ethanol[23]	44.98	0.4540	0.2295	0.0214	1.47
6. Ethanol-Isooctane[13]	25	0.9838	−0.0740	0.2270	1.12
	50	0.9458	−0.0839	0.2610	5.75
7. Ethanol-Methylcyclohexane[14]	35	0.9498	−0.1074	0.2358	1.87
	55	0.9185	−0.0867	0.2260	4.78
8. Ethanol-Toluene[24]	35	0.7946	−0.1149	0.1962	1.27
	55	0.7596	−0.0897	0.1188	1.53
9. Ethanol-Water[12]	25	0.5251	−0.1270	−0.0258	0.25
,, [16]	74.79	0.5246	−0.1595	0.0476	1.80
10. n-Hexane-Chloroform[20]	65	0.2500	−0.0150	−0.0101	0.67
11. n-Hexane-Ethanol[25]	−10	1.0007	0.1194	0.1947	0.18
12. Methanol-Water[17]	25	0.2134	−0.0218	−0.0603	0.37
13. Methylcyclohexane-Ethanol[26]	0	1.0149	−0.1376	0.1291	0.33

in which the vapor phase is assumed to be ideal. Equation (15) may be obtained by substituting the following expressions

$$p_1 = y_1 P, \qquad dp_1 = P dy_1 + y_1 dP$$

and

$$p_2 = y_2 P, \qquad dp_2 = P dy_2 + y_2 dP$$

in the Gibbs-Duhem equation of the following form

$$x_1 \left(\frac{\partial \log p_1}{\partial x_1}\right)_{T,P} + x_2 \left(\frac{\partial \log p_2}{\partial x_1}\right)_{T,P} = 0 \ldots\ldots\ldots (16)$$

Equilibrium vapor compositions may be evaluated from Equation (15) by means of a step-wise integration procedure as illustrated by Othmer et al[2]. In the integration, the smaller the increment of Δx used, the better are the integrated results. For a small increment of Δx, for example, 0.01, it would be a quite time-consuming task to do the calculation using a desk calculator. An attempt has been made in this laboratory to develop a satisfactory digital computing program for doing such a calculation.

Without a computer, the step-wise integration procedure may be carried out by using Equation (15) in the rearranged form of

$$\Delta \ln P = \frac{y_1 - x_1}{y_1(1 - y_1)} \Delta y_1 \ldots\ldots\ldots\ldots\ldots (17)$$

TABLE 2

COMPUTED VALUES FOR SYSTEM ETHANOL-WATER AT 25°C.[12]

B	C	D	No. of Iterations			
0.5251	−0.1270	−0.0258	4			
x_1	P mm.Hg.	$P_{obsvd} - P_{calcd}$	p_1	p_2	γ_1	γ_2
0.0523	33.17	−0.34	10.89	22.62	3.528	1.005
0.0917	38.44	−0.24	16.79	21.89	3.103	1.015
0.1402	43.42	0.16	22.13	21.13	2.675	1.035
0.1670	45.69	0.54	24.39	20.76	2.475	1.050
0.2027	47.21	0.04	26.85	20.32	2.245	1.073
0.2849	50.33	0.04	30.84	19.45	1.834	1.145
0.3368	51.17	−0.42	32.63	18.96	1.642	1.204
0.4902	53.95	−0.30	36.84	17.41	1.274	1.438
0.5820	55.71	0.18	39.47	16.06	1.149	1.618
0.7810	58.08	0.24	47.13	10.71	1.023	2.058

and a plot of $\ln P$ vs. x_1. The integration starts at $x_1 = 0$, where $y_1 = 0$ and $P = p_2°$. In order to carry out the same procedure by means of a computer, it is necessary to represent the $\ln P$ vs. x_1 plot analytically. However, as the representation of the function $\ln P$ by means of a polynominal expressed in terms of x_1 was found to be not sensitive enough to the variations of x_1, it was decided to represent the total pressure P by means of a polynominal expressed in terms of x_1. Thus,

$$P = a + bx_1 + cx_1^2 + dx_1^3 + ex^4 \ldots\ldots\ldots\ldots (18)$$

in which $a = p_2°$ and $a + b + c + d + e = p_1°$. In other words, for total pressure measurements obtained at isothermal conditions, Equation (18) involves three unknown constants. Should more constants be employed in Equation (18) the computing time required for performing the step-wise integration procedure would be more than the time required for evaluating the activity coefficients and partial pressures. It was observed also that for azeotropic systems having rather flat total pressure readings in the vicinity of the azeotropes, Equation (18) was not adequate for representing the data. The equilibrium composition curves obtained by starting the integration from $x_1 = 0$ and $x_1 = 1$ respectively would not meet at the azeotrope. Although the integration procedure could be carried out initially at the azeotrope, the time required for locating the azeotropic composition by solving $dP/dx = 0$ was considerable and the result obtained was misleading due to the poor fitting. It is because of these difficulties that the computing program developed is limited to non-azeotropic systems. For azeotropic systems, it is recommended that the method presented in the first section of this article be followed.

TABLE 3

COMPUTED AND EXPERIMENTAL EQUILIBRIUM VAPOR COMPOSITIONS FOR THE SYSTEM ETHANOL-WATER AT 25°C.[12]

x_1	$y_{expt.}$	$y_{calcd.}$
0.0523	0.3166	0.3283
0.0917	0.4334	0.4367
0.1402	0.5129	0.5097
0.1670	0.5450	0.5338
0.2027	0.5687	0.5687
0.2849	0.6106	0.6128
0.3368	0.6287	0.6377
0.4902	0.6791	0.6829
0.5820	0.7096	0.7085
0.7810	0.8161	0.8115

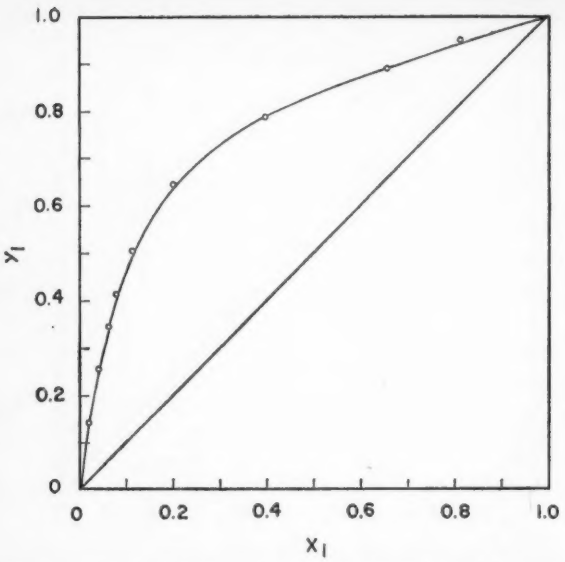

Figure 1—The calculated and experimental equilibrium composition values for the system methanol-water at 25°C. O Experimental; — Calculated.

In the computing program, Equation (15) is rearranged in the following manner:

$$\frac{\Delta P}{P} = \frac{y_1 - x_1}{y_1(1 - y_1)} \Delta y_1 \quad \ldots\ldots\ldots\ldots\ldots\ldots (19)$$

An increment of $x_1 = 0.01$ is employed in the step-wise calculations. It should be mentioned, however, that the computing program developed is not limited to this increment. Between $x_1 = 0$, $y_1 = 0$ and at the end of the first increment,

$$\Delta P = P_{x_1 = 0.01} - P_{x_1 = 0}$$
$$\Delta y_1 = y_1$$

and

$$y_1 = \frac{\Delta P/P + x_1}{1 + \Delta P/P} \quad \ldots\ldots\ldots\ldots\ldots\ldots (20)$$

The equilibrium vapor composition at the end of the first increment is thus obtained. At the end of the second increment, the equilibrium vapor composition may be obtained by solving the quadratic equation for y_1 resulting from Equation (19). The larger value of the two roots is taken to be the answer. This is necessary as y_1 is always greater than x_1 for non-azeotropic systems. Subsequent integrations are carried out in the same manner. As an average, the machine time required per set of data is approximately four minutes, which is about the same as the time required for evaluating the values of B, C and D. The integrated values of the equilibrium vapor compositions from the total pressure measurements for the system methanol-water at 25°C.[17] are compared with the experimental values in Figure 1 as an illustration.

Conclusions

Two digital computer methods are developed for evaluating vapor-liquid equilibrium data from total pressure-liquid composition measurements of volatile binary non-electrolyte mixtures. One of which calculates the constants B, C, D of the Redlich-Kister equation, hence the values of activity coefficients, partial pressures and equilibrium vapor compositions (Method 1). The other evaluates the equilibrium vapor compositions directly by means of an integration procedure (Method 2). Although Method 2 does not involve any conversion to liquid activity coefficients and offers the equilibrium vapor compositions directly, the machine time required per set of data is about the same as that required by Method 1, should an increment of 0.01 of x is chosen. Also, Method 2 developed is limited to non-azeotropic system. Method 1 offers, on the other hand, complete equilibrium values.

The calculated results using Method 1 provide further support of the suggestion[18] that three-constant Redlich-Kister equation is adequate for representing liquid activity coefficients for most systems.

Acknowledgment

The authors (J. C. K. Ho and B. C.-Y. Lu) are indebted to the National Research Council of Canada for financial support. The authors are also grateful to the Computing Centre of the University of Ottawa for making the computer time available and for its assistance in developing the computing program.

Nomenclature

B,C,D	=	constants
a,b,c,d,e	=	constants
P	=	total pressure
p	=	partial pressure
p°	=	vapor pressure of pure component
Q	=	excess free energy function
R	=	gas constant
T	=	absolute temperature
$\overline{V}$	=	partial molal volume
v	=	molal volume
x	=	liquid composition, mole fraction
y	=	vapor composition, mole fraction
γ	=	liquid activity coefficient

Subscript

$1,2,i$	=	components
$1,2,\ldots n$	=	no. of observations

References

(1) Carlson, H. C., and Colburn, A. P., Ind. Eng. Chem. **34,** 581 (1942).
(2) Othmer, D. F., Ricciardi, L. G., and Thakar, M. S., Ind. Eng. Chem. **45,** 1815 (1953).
(3) Redlich, O., and Kister, A. T., J. Am. Chem. Soc. **71,** 505 (1949).
(4) Baker, J. A., Australian J. Chem. **6,** 207 (1953).
(5) Scatchard, G., Ann. Rev. Phys. Chem. **3,** 269 (1953).
(6) Christian, S. D., J. Phys. Chem. **64,** 764 (1960).
(7) Prengle, H. W., and Palm, G. T., Ind. Eng. Chem. **49,** 1769 (1957).
(8) Redlich, O., and Kister, A. T., Ind. Eng. Chem. **40,** 341 (1948).
(9) Lu, B.C.-Y., Chem. Eng. p. 105, Oct. 3 (1960).
(10) Ho, J. C. K., Thesis (1959).
(11) Scarborough, J. B., Numerical Mathematical Analysis, Chapter 16, 3rd ed., Johns Hopkins Press, Baltimore (1955).
(12) Dobson, H. J. E., J. Chem. Soc. **127,** 2866 (1925).
(13) Kretschmer, C. B., Nowakowska and Wiebe, R., J. Am. Chem. Soc. **70,** 1785 (1948).
(14) Kretschmer, C. B., and Wiebe, R., J. Am. Chem. Soc. **71,** 3176 (1949).
(15) Lu, B.C.-Y., Can. J. Chem. Eng. **37,** 193 (1959).
(16) Wrewsky, M. S., J. Russ. Phys. Chem. Soc. **42,** 1, (1910).
(17) Butler, J. A. V., Thomson, D. W., and Maclennan, W. H., J. Chem. Soc. (London) 674 (1933).
(18) Redlich, O., Kister, A. T., and Turnquist, C. E., Chem. Eng. Progr., Symposium Ser. **48,** No. 2, 49 (1952).
(19) Mueller, C. R., and Kearns, E. R., J. Phys. Chem., **62,** 1441 (1958).
(20) Brown, J., Australian J. Sci. Research, Ser. A, Phys. Sci., **5,** 534 (1952).
(21) Sameshima, J., J. Am. Chem. Soc. **40,** 1503 (1918).
(22) Scatchard, G., Wood, S. E., and Mochel, J. M., J. Am. Chem. Soc. **62,** 712 (1940).
(23) Scatchard, G., and Raymond, C. L., J. Am. Chem. Soc., **60,** 1279 (1938).
(24) Kretschmer, C. B., and Wiebe, R., J. Am. Chem. Soc. **71,** 1793 (1949).
(25) Isii, N., J. Soc. Chem. Ind. (Japan) **38,** Supplemental Binding, 661 B (1935).
(26) Isii, N., J. Soc. Chem. Ind. (Japan) **38,** Supplemental Binding, 659 B (1935).

★ ★ ★

The Hydraulic Characteristics of Two-Phase Co-Current Flow through Glass Fibres[1]

D. J. GUNN[2] and A. R. AITKEN[3]

The mechanism of flow of air and water through packed glass fibres has been studied. Pressure drops and liquid hold ups were measured as a function of gas and liquid flow rates and the packing characteristics. It has been found that the pressure difference measured is dependent upon the history of previous gas and liquid flow rates in the bed. The liquid hold up is defined entirely by the gas and liquid flow rates. An analysis of the flow mechanism shows that the capillary forces interact with the fluid pressures in the bed. For example an increase in gas flow rate followed by a reduction to the same flow rate has been shown to reduce the resistance of the bed to gas flow even though the liquid flow rate is unchanged. A measure of the irreversibility of the flow operation is suggested.

The subject of gas and liquid flow through solid porous bodies has been extensively studied. Flow of this type occurs in units designed for diffusional separations. Experimentalists interested in collecting design information for these units have presented a familiar correlation for countercurrent flow of gas and liquid through packings in which the pressure gradient in the gas phase is plotted as a function of gas mass velocity with liquid mass velocity as a parameter[(1)]. A number of approaches to single phase flow through porous bodies have been applied to two phase flow[(2)].

This work is a continuation of an earlier investigation[(3)] into the nature of co-current and countercurrent flow of gas and liquid through glass fibre beds. The effects of variables such as bulk density of the glass fibres, and the type of fibre are also investigated. The extremely fine nature of the bodies forming the solid bed strongly influences the hydraulic behavior and the results are significantly different from other reported studies, even though one or two have been concerned with the flow of two phases through glass fibres[(4)]. The conclusion from previous work is that the pressure drop across a given bed is defined by the liquid and gas flow rates. The work reported here shows that for some porous bodies at least, the pressure drop may be *different* for the same gas and liquid rates.

[1]*Manuscript received March 7; accepted July 25, 1961.*
[2]*Department of Chemical Engineering, University College, Swansea, Wales.*
[3]*Department of Mines, Ottawa, Ont.*
Based on a paper presented to the Joint C.I.C.-A.I.Ch.E. Chemical Engineering Conference, Cleveland, Ohio, May 7-10, 1961.
Contribution from the Department of Chemical Engineering, Queen's University, Kingston, Ont.

Apparatus and Procedure

The arrangement of the apparatus is shown in the flow diagram Figure 1. The glass fibre bed was held in a 2-in. I.D. glass column. Clean compressed air was delivered through a rotameter system to the top level of the fibre bed. The air pressure was controlled by a pressure reducing valve and a fine needle valve, so that the pressure of the gas entering the rotameter was close to atmospheric. Distilled water was drawn from a thermostatically controlled circulation system, measured by a series of rotameters and delivered to the top of the fibre bed through a liquid distributor. Pressure tappings at either end of the bed were connected to a differential vertical manometer. The guaranteed accuracy of the rotameters was $\pm 2\%$ of the indicated flow rates; the manometer was fitted with a vernier scale which allowed pressure differences as large as thirty inches of fluid to be read to 1/100-in.

One of the most important operations was the preparation of the fibre bed. The arrangement of the glass fibres was standardized; each fibre lay within a plane normal to the main axis of the fibre bed and the fibres were randomly orientated within this plane. Discs of fibre matting of diameter equal to the internal diameter of the column were cut from a principal fibre mat, adjusted to a pre-determined weight and loaded into the glass column with each disc normal to the main axis of the column. The finished length of the fibre packing was constant for most of the experiments. The bulk density of the fibres was controlled for each bed. This was adjusted by increasing or decreasing the weight of the fibre mats in the standard length of column. Thus a change in bulk density was achieved by increasing or decreasing the fibre density along the main axis of the column. The fibre density normal to the main column axis was not adjusted and remained constant. Variations in the bulk density of the fibres along the main axis of the column could arise if the packing was not carefully done and this distorted the hydraulic results.

To assist in the definition of bed preparation, the variation of bed length with applied mechanical load was studied. It was found that the volume — load relation for the bed after proper consolidation was given by an expression of the form

$$P_2 - P_1 = \frac{1}{K} ln \frac{V_1 - V_e}{V_2 - V_e} \quad \ldots\ldots\ldots\ldots\ldots\ldots (1)$$

where P_2 and P_1 are applied loads and V_1 and V_2 are the bed volumes at conditions 1 and 2, K is a compressibility coefficient and V_e is the volume of the bed as $P \rightarrow \infty$ (an extrapolated value). It was essential that the method of bed preparation gave a (P, V) value which followed this relation for this indicated a constant bulk density of fibre in the bed. If the mechanical load

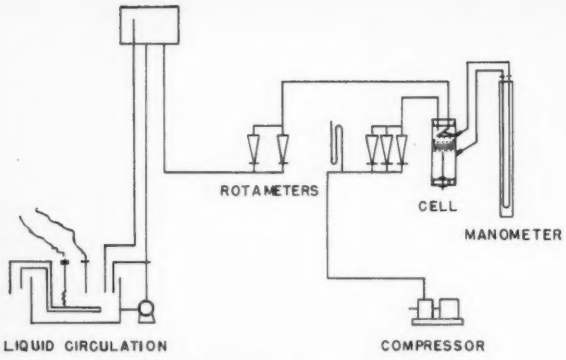

Figure 1—Arrangement of apparatus.

applied to the fibre bed was increased without attempting bed consolidation, unbalanced frictional forces acting at the ends of the fibre and the column wall produced a variation in the fibre bulk density which destroyed reproducibility of the hydraulic results. In this case the (P, V) values did not follow relation 1, but a marked hysteresis effect was found as the load was increased and then decreased. An even bulk density was assured if the bed was consolidated by alternately increasing and reducing the applied mechanical load, so that the (P, V) values were given by Equation (1). At other (P, V) conditions the value of $\partial V/\partial P$ depended upon the direction of the pressure change. This is a result of unbalanced frictional forces within the column.

The bed when prepared was held in the column between two perforated plastic discs. The discs were supported between the pressure taps. The equipment was designed so that the fibre bed length could be adjusted and the whole column could be easily detached from its supports. The success of the method of bed preparation was accepted when the two phase pressure drops were reproducible for different beds of the same fibre packed in the same manner.

The degree of reproducibility depended upon the nature of the fibre mat. If the mat showed little fibre aggregation, a representative sample of the fibre was easily obtained and the hydraulic results were reproducible within $\pm 2\%$. If fibre aggregation was prominent a small number of fibre mats did not constitute a representative sample of the bulk fibre. Consequently the reproducibility limits were somewhat wider but in all cases better than $\pm 5\%$.

Before making any pressure drop determinations, the fibre bed was treated with an aqueous solution of detergent to remove adsorbed impurities and to make sure that the fibre was properly wetted by the liquid. The detergent was removed by flushing the bed with water.

The pressure drop across the bed at any set of flow conditions has been found to be dependent upon the previous flow history of the bed[3]. Consequently the starting condition was standardized and two principal starting conditions were used; liquid is allowed to flow through the bed for 15 minutes before the gas flow was directed through the bed (starting procedure 1) and the gas is allowed to flow through the water saturated bed for 15 minutes before liquid flow is directed through the bed (starting procedure 2). Most of the determinations were made with starting procedure 1.

The liquid hold up in the bed was measured by removing the glass column from its supports and weighing. Because the liquid and gas flows are co-current, the liquid weight measured was the dynamic hold up. There was no drainage of liquid from the bed when the liquid and gas flows were shut off.

Results

The experimental results are shown in the series of graphs Figures 2-15. The numerical results are given more fully in Reference 5. Figure 2 shows the change of pressure difference across the bed with gas flow rate at a fixed liquid rate. The

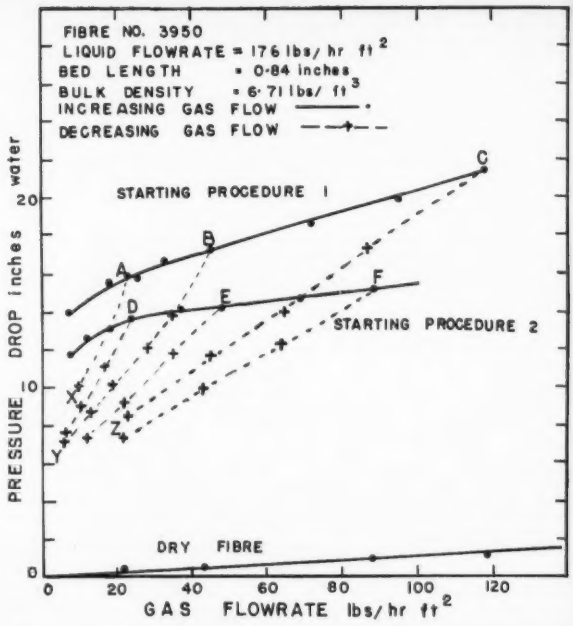

Figure 2—The effect of gas flow rate upon pressure drop at fixed liquid rate.

line *ABC* is obtained when gas flow is increased from starting condition 1 i.e., the gas flow is started when the liquid has been flowing for some time. The points *A*, *B* and *C* mark the maximum gas velocities in these experiments. From these points the gas velocity was reduced and the pressure difference — gas flow relation follows the lines *AX*, *BY* and *CZ*. Thus the operation of increasing the gas flow is not reversible. The graph also shows that the lowest pressure differences at fixed gas and liquid rates, are obtained if there has previously been a very high rate of gas flow. The lowest line on Figure 2 is the pressure difference — gas flow relation for the dry bed.

Curves for this type were reproducible for the same bed and for other identically prepared beds. Thus there was no rearrangement of the fibres and, in fact, the fibre packing density was so high, that the fluctuations in gas pressure during an experiment did not affect the packing density.

Points *D*, *E* and *F* record the pressure differences at the corresponding gas flows for starting procedure 2. The relevant liquid hold up measurements are shown in Figure 3. This graph shows that liquid hold up falls off as gas flow is increased, but Figure 5 shows that the irreversible fall in pressure difference is not matched by a comparable change in liquid hold up. In fact the change in liquid hold up was reversible with gas flow. The hold up values were independent of the previous gas flow rates, and the hold up — gas flow rate relation was single valued.

Figure 4 shows the change in pressure differences at different gas rates for starting condition 1 with liquid rate shown as a parameter. Both liquid hold up and pressure difference increase with liquid rate.

The effect of a change in bulk density is shown in Figures 6 and 7 for starting condition 1. Both pressure difference and hold up are increased by an increase in fibre bulk density.

Figure 8 shows the experimental results for three types of fibre.

Table 1 shows the character of each type of fibre under test.

The dispersion of the fibre bed refers to the manner in which the fibres are arranged relative to each other in a plane normal to the main axis of the bed. A well dispersed bed shows fibres which are randomly arranged without aggregation. Figure 9 shows a photograph of a well dispersed bed. This may be compared with Figure 10, which clearly indicates fibre aggrega-

TABLE 1

Fibre	Mean Fibre Diameter	Standard Deviation	Fibre Dispersion
3950	3.83×10^{-4} in.	1.97×10^{-5} in.	Good
11-391	7.43×10^{-4} in.	11.0×10^{-5} in.	Poor
11-390	8.53×10^{-4} in.	9.0×10^{-5} in.	Poor

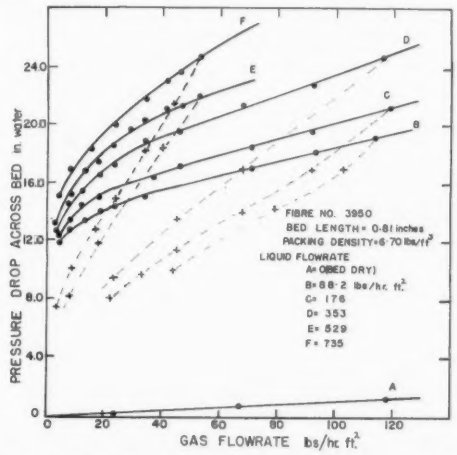

Figure 4—The effect of liquid rate upon pressure drop.

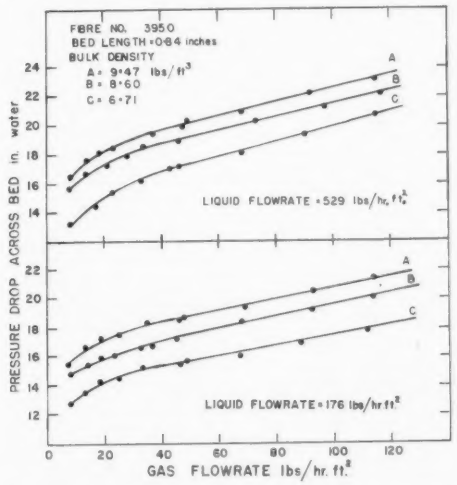
FIBRE NO. 3950
BED LENGTH = 0·84 inches
BULK DENSITY
A = 9·47 lbs/ft³
B = 8·60
C = 6·71
LIQUID FLOWRATE = 529 lbs/hr. ft.²
LIQUID FLOWRATE = 176 lbs/hr ft.²
PRESSURE DROP ACROSS BED in. water
GAS FLOWRATE lbs/hr. ft.²

Figure 6—The effect of packing density upon pressure drop.

tion and preferred orientation. Such a bed is poorly dispersed. Evidently the diameter and dispersion of the fibre greatly affect the hydraulic characteristics. All of the fibres, however, showed the type of behavior illustrated in Figure 2. The general effects of bulk density and liquid rate shown in Figures 4 and 6 were confirmed for all types.

Discussion

The pore structure of the dry fibre bed is a continuous, twisting complex of interconnected channels bounded by the cylindrical walls of the individual fibres. Because of the method of bed preparation, the size distribution and arrangement of fibres in a small (but not differential) volume of the bed is the same as any other small volume provided the bed dispersion is good. In two phase flow of air and water, the fibre is preferentially wetted by the liquid and the flow path of the liquid embraces the fibre and forms the continuous phase. The gas

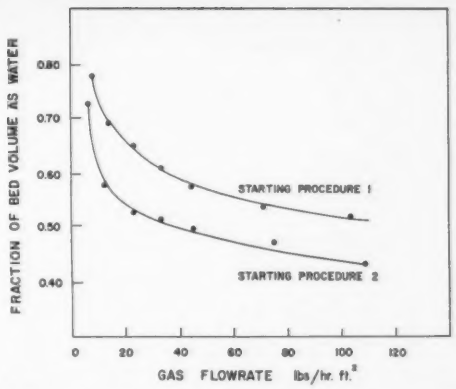

Figure 3—The effect of a change in starting procedure upon liquid holdup.

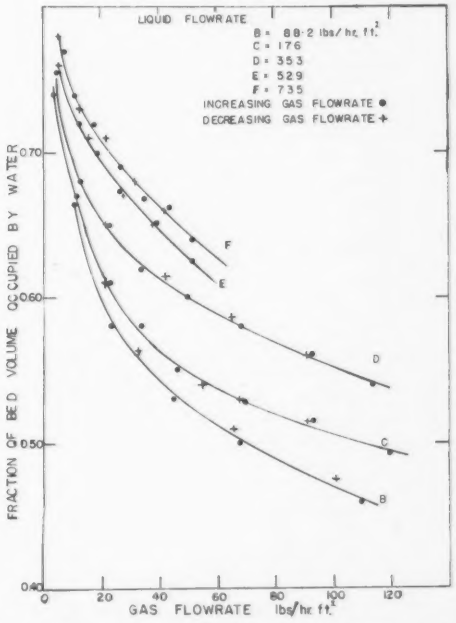

Figure 5—The effect of liquid rate upon liquid hold up.

flows through segregated channels in the bed and is the dispersed phase, bounded by liquid and solid fibres. The channels bounded by solid in the bed are small, hence capillary forces are important at an interface, and as the fibre is wetted by the liquid, there is an excess of pressure in the gas phase over the liquid phase.

The governing relation is

$$p = T\left(\frac{1}{r_1} + \frac{1}{r_2}\right) \quad \ldots\ldots\ldots\ldots\ldots\ldots (2)$$

where p is the pressure excess, T is the surface tension, and r_1 and r_2 are the principal radii of curvature at the elementary section of the interface considered. In this study, the gas phase pressure only was measured and we have no direct knowledge of static pressures in the liquid phase because of the capillary effect. The balance between the capillary forces and the fluid pressures determines the flow volume occupied by the gas and liquid phases. If the pore size is small, gas may be locked out of sections of the bed and can only advance into these sections if the gas phase static pressure is increased.

For a small length of bed we can assume that the static pressure difference between the two phases is constant. Also as we have arranged geometrical similarity along the length of the bed, the distributions of flow for each phase are similar and

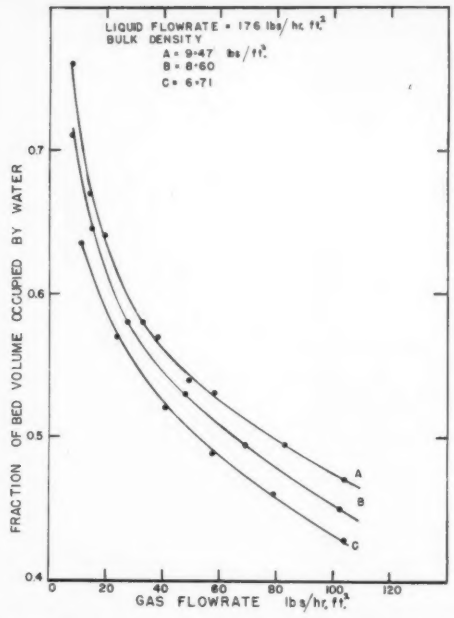

Figure 7—The effect of packing density upon liquid hold up.

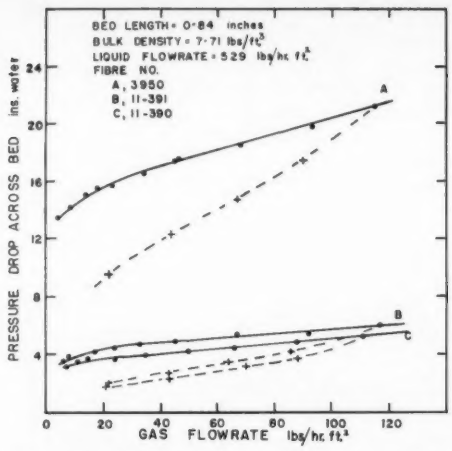

Figure 8—The effect of fibre type upon pressure drop.

random. The total volumetric flow rates are the same for each plane normal to the main axis of the bed. This suggests that the hydraulic characteristics may be studied through a model of continuous, irregular, interconnected channels whose walls are parallel to the main axis of the bed. The walls of the channel are formed from the supporting structures of the fibres and the interconnections are filled with liquid. The position of the liquid — gas interfaces are maintained by a balance between the capillary and pressure forces.

Initially the fibres are wetted and a number of starting conditions are possible. We have defined two starting conditions and condition 1 probably corresponds to the bed voids filled with liquid. For the bed as a whole, gas flow can only be established in flow channels if the pressure difference across the bed exceeds the surface tension forces in the channel.

If we use our model and apply it to the whole bed, the condition for this is:

$$\Delta P.A > T.R \text{ or } \Delta P > T.\frac{R}{A} \quad \ldots\ldots\ldots\ldots\ldots\ldots (3)$$

where ΔP is the gas phase pressure difference, T is the surface tension, A is the cross-sectional area of the channel and R is the perimeter of the channel. The quantity A/R has the dimensions of a length and may be thought of as an 'effective' or 'hydraulic' radius. From this relation it can be seen that the larger channels will admit gas flow at lower pressure differences than the smaller channels. As the pressure difference across the bed is increased, a greater number of channels will admit gas flow and consequently the resistance of the bed to gas flow will decrease.

We have assumed that the pressure excess of the gas over the liquid phase is constant, independent of length, for a small length of bed. Suppose that the constant value is increased — for example by increasing the static pressure of the gas phase and the flow of gas. The position of the gas — liquid interface at each point is adjusted until a new position of balance between the capillary and pressure forces is reached. Figure 11 illustrates a possible situation.

The line AB marks the initial position of the gas — solid interface before the gas flow is increased. As the gas phase pressure grows larger, the interface position is adjusted so that the curvature $(1/r_1 + 1/r_2)$ is increased. This means that the interface retreats to a position where the interfacial area is smaller. From the diagram it can be seen that this is not accomplished until a portion of wider section has been traversed and a balance is reached at the new position, CD. If the gas phase static pressure now is reduced to its former value, the interface will move back to EF and not to AB. Clearly to return to position AB the gas pressure would have to be lowered to a value sufficient to move the interface past the widest part of the flow section. Thus the increase in gas flow rate has led to an irreversible change in the flow distribution of the two phases.

The Navier-Stokes equations describe the flow of gas through the bed and for the simplified case of the model the gas flow may be assumed to take place in one direction and two dimensions. When the flow is constant at steady state these equations reduce to:

$$\frac{\partial^2 u}{\partial x^2} + \frac{\partial^2 u}{\partial y^2} - \frac{1}{\mu}\frac{\partial P}{\partial z} = 0 \quad \ldots\ldots\ldots\ldots\ldots\ldots (4)$$

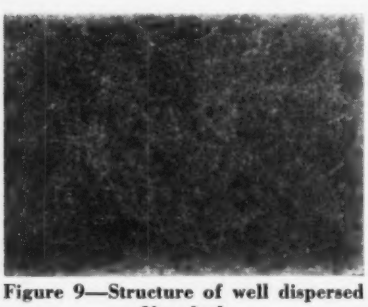

Figure 9—Structure of well dispersed fibre bed.

Figure 10 — Structure of poorly dispersed fibre bed.

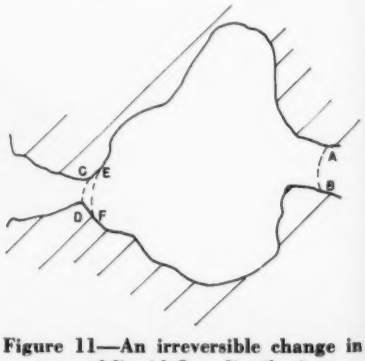

Figure 11—An irreversible change in gas and liquid flow distribution.

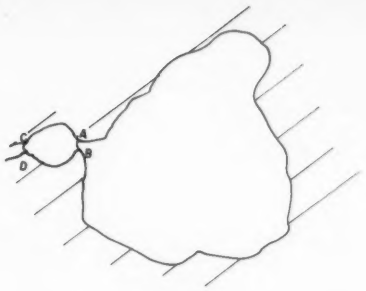

Figure 12.

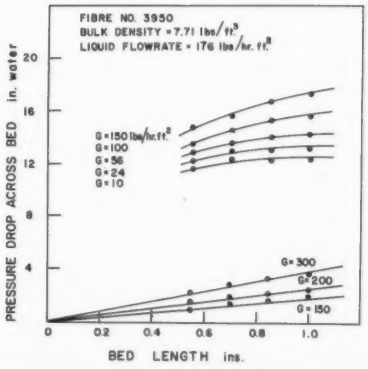

Figure 14—The effect of bed length upon pressure drop.

where u is the gas velocity, μ is the gas viscosity, P is the gas phase pressure and x, y and z are space co-ordinates.

Throughout the experimental work, the rate of gas volumetric flow was much greater than the rate of liquid volumetric flow, and as the liquid hold up determination showed that the volume of the bed occupied by liquid was greater than that occupied by gas, it follows that the gas phase velocities in the bed were generally much higher than the liquid phase velocities. The boundary conditions for each flow channel are $u_s = u_1$ at the liquid gas interfaces and $u_s = 0$ at the solid boundary. As the liquid phase velocities are much lower than the gas, we can assume that a general boundary condition is given by $u_s = 0$ at the solid or liquid boundary of the gas phase.

The differential equation is a form of Poisson's equation if $\partial P/\partial z$ is constant. With the condition of zero velocity at the boundary, the solution to this equation which gives u as a function of x and y may be studied by analogy with Prandtl's loaded membrane. Thus the displacement of a membrane secured at the boundary and subjected to a pressure difference will give the form of the relation.

The solution gives $u_s = 0$ at the boundary and a maximum at points most distant from the boundary. The gradient of velocity is a maximum at the boundary and falls to zero at the points of velocity maxima. The general nature of the solution may be used to illustrate an important relation concerning the resistance to flow of the model.

An arbitrary gas flow section is shown in Figure 12. The shear stress τ at the boundary of the flow section is

$$\tau = \mu \text{ grad } u \quad \ldots\ldots\ldots\ldots\ldots\ldots\ldots\ldots (5)$$

where μ is the fluid viscosity and grad u is the derivative of velocity measured normal to a line of equal velocity on the flow surface. This is positive if measured in a direction of increasing velocity. If we equate pressure and viscous forces over the flow channel during gas flow

$$\Delta P.A = H\int_B^A \mu \text{ grad } u dR + H\int_A^B \mu \text{ grad } u dR \quad \ldots\ldots (6)$$

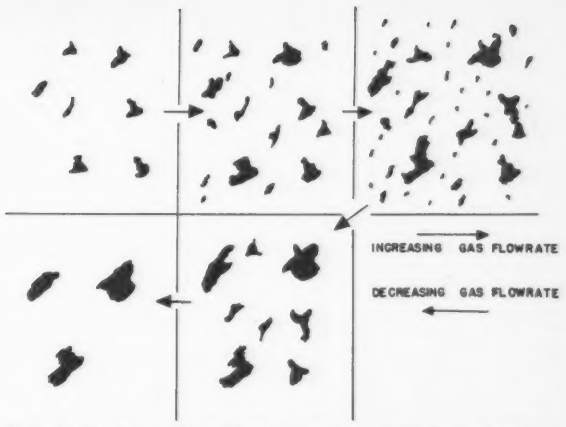

Figure 13—The effect of gas flow rate upon flow structure.

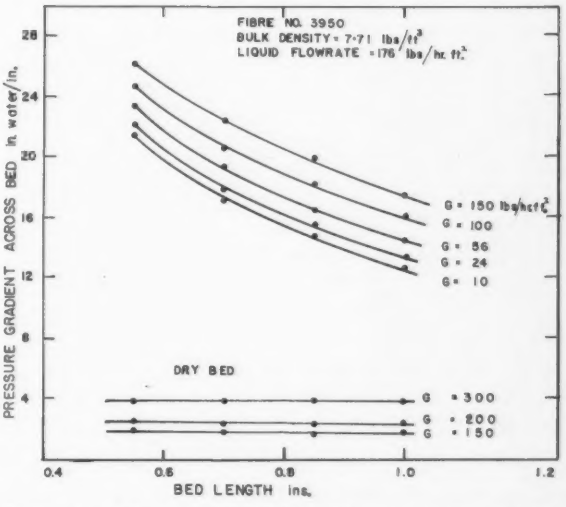

Figure 15—The effect of bed length upon mean pressure gradient.

where A is the cross-sectional area of the flow channel, ΔP is the pressure difference for a length of channel H and R is the perimeter of the boundary. $H\int_A^B \mu \text{ grad } u dR$ is the shear force acting at the short portion of the boundary marked AB. Suppose that the gas phase static pressure is increased and reduced to its former value in the manner we have described. As a result of this the interface position AB is now moved to CD. If we again equate pressure and viscous forces over the *original* channel:

$$\Delta P.A = H\int_B^A \mu \text{ grad } u dR + H\int_A^B \mu\left(\frac{\partial u}{\partial \phi}\right) dR \quad \ldots\ldots\ldots\ldots (7)$$

where $\mu(\partial u/\partial \phi)$ is the shear stress normal to the boundary AB. The left hand side of Equations (6) and (7) remains unchanged. The last term on the right hand side is the shear force acting over the section AB. This is reduced when the boundary is extended since the velocity along AB is increased from zero and hence $\partial u/\partial \phi$ along the boundary is reduced. Thus the shear force represented by the last term in Equation (7) is smaller than the last term in Equation (6). The shear force represented by the first term in the *RHS* of Equation (7) is larger than the first term on the *RHS* of Equation (6). This shows that the velocities in the region of the solid section of the boundary have increased. The total gas flow in the original

section is increased at the same pressure gradient by extending the boundary in this arbitrary manner.

This may be expressed: If the boundary of a viscous fluid flowing in a channel of constant cross-sectional area is extended in any way, the resistance to flow of the *original* channel is decreased. For a single gas flow channel an increase in gas flow rate followed by a decrease to the same value will lower the resistance of the *original* channel to gas flow as some of the extension of the flow channel is retained. It follows that the gas flow resistance for unit gas flow area in the fibre bed is reduced by an increase in the gas flow rate followed by a decrease.

The extension of the gas flow channels reduces the liquid hold up. There is however, a counteracting effect; the reduction in pressure drop across the bed corresponding to the reduced flow resistance will close off some of the gas flow channels according to Equation (3). These channels, active before the increase in flow rate are filled with liquid and this will increase the liquid hold up. Under the experimental conditions of this investigation these effects were found to be counterbalancing and the liquid hold up — gas flow relation was reversible.

From the study of the flow equation and the flow behavior in the bed, it follows that an increase from, followed by a decrease to the same gas flow rate will extend some of the larger gas flow channels. As a result the resistance of the fibre bed to gas flow will fall even though the porosity (liquid hold up) is unchanged.

Figure 13 shows the change in flow structure of the bed as the gas rate is first increased and then decreased at a fixed liquid rate. As the gas rate is increased, more channels become open to gas flow in accordance with Equation (3) and existing flow channels are extended. As gas flow is reduced, the extended channels retain some of their extension, thus the resistance of the bed to gas flow is lowered and the pressure difference across the bed is reduced. Consequently, fewer channels are open to gas flow. The aggregation of gas flow channels is shown in the marked reduction of resistance to gas flow illustrated in Figure 2.

In the development we assumed that the static pressure difference between the gas and liquid phases is constant for a short length of bed. It is of interest to see if this is true for the total length of bed. Figure 14 shows the pressure difference across the bed plotted as a function of bed length. Figure 15 shows the mean pressure gradient plotted as a function of bed length. The gas phase mean pressure gradient falls off at equal gas and liquid rates as the bed length is increased. Thus the fall in gas phase static pressure across the bed reduces the static pressure difference between the two phases. Consequently the liquid hold up is larger at the lower levels of the column and as a result the relation between gas phase static pressure and bed length is non linear. The effect is more marked at lower gas rates. Figures 3 and 5 show that the change in liquid hold up is most pronounced at the lower gas rates. The effects are evidently the same.

Irreversibility of the Change in Flow Structure

The study of this flow system has shown that an increase in the gas flow rate at a fixed liquid rate, causes an irreversible change in the flow structure of the bed. Consider a cycle of flow changes: the gas flow rate is increased at a fixed liquid flow rate, the liquid rate is then decreased to a lower value maintaining the gas flow rate constant, the gas flow rate is reduced to its first value, and finally the liquid rate is increased until the original pressure difference across the bed is attained. If the flow changes do not cause an irreversible change in the flow structure of the bed, the liquid rate at this point is the same as the initial value:

$$\phi_{PG}\, dL = 0 \qquad (8)$$

where ϕ_{PG} indicates that the integration is carried round a complete cycle of pressure difference-gas flow conditions. If, however, there is an irreversible change in the flow structure of the bed:

$$\phi_{PG}\, dL > 0 \qquad (9)$$

Combining these two expressions, for any cycle of changes on the $P - G$ diagram

$$\phi_{PG}\, dL \geqslant 0 \qquad (10)$$

where the equality sign applies to reversible changes, and the inequality sign applies to irreversible changes. This integral is thus a measure of the irreversibility of the operation.

Acknowledgements

The authors wish to acknowledge a grant in aid of purchase of apparatus obtained from the Ontario Research Foundation. ARA wishes to acknowledge a scholarship received from the National Research Council of Canada.

Nomenclature

A	=	area of cross-section
G	=	gas phase mass velocity
H	=	length
K	=	compressibility coefficient
L	=	liquid phase mass velocity
ln	=	natural logarithm
p	=	static pressure excess of gas phase over liquid
P	=	load, pressure
R	=	perimeter
r	=	radius of curvature
T	=	surface tension
u	=	velocity
V	=	volume
x	=	space co-ordinates
y	=	" "
z	=	" "
Δ	=	difference quantity
μ	=	viscosity
τ	=	shear stress

Subscripts

g	=	gas
l	=	liquid

References

(1) Perry, J. H., Chemical Engineer's Handbook, 3rd Ed., McGraw Hill (1950).

(2) Brown, G. G., Unit Operations, John Wiley (1950).

(3) Gunn, D. J., Unpublished Research (1955).

(4) Winning, M. D., Ph.D. Thesis, University of Toronto (1952).

(5) Aitken, A. R., M.Sc. Thesis, Queen's University (1960).

★ ★ ★

Pelletization and Diffusibility Studies on Silver Catalysts[1]

C. H. AMBERG[2] and E. ECHIGOYA[3]

Powders of silver catalyst of low calcium content and an 8.5% calcium in silver alloy were pelletized at different compacting stresses. The diffusibility of each pellet was measured, using hydrogen, and correlated with internal void volume. The surface area of the powders and of some representative pellets was obtained by nitrogen adsorption. All these parameters were used in an attempt to interpret the changes taking place with decreasing porosity. With the help of two plausible assumptions it was concluded that the tortuosity remained constant over the range examined. The figures obtained have limited usefulness for the prediction of approximate pellet diffusibilities from a knowledge of the compacting stresses applied to similar metal powders.

In heterogeneous catalysis a knowledge of the internal structure of a catalyst is frequently desirable in order to evaluate the contribution of diffusion to the rates of transport of different chemical species to and from the active surface[1]. In this laboratory porous sprayed silver films have been employed in the catalytic oxidation of ethylene. In the hope of approximating their structure in a controlled fashion, several series of pellets of varying porosity were prepared from a powdered Ag-Ca alloy and from silver catalysts originating from this and similar alloys. The diffusibility of each pellet was measured using hydrogen; this was correlated with the internal void volume in an attempt to gain some insight into the highly complex geometry of the compact. In some instances the available surface area was determined by nitrogen adsorption. We have also compared compacting pressures with the void volumes so that one might be able to prepare pellets of predictable diffusibility. However, as will be seen this relationship lacks generality; only very approximate diffusibilities can be predicted unless extensive experimental information about a given catalyst powder is available to begin with.

Experimental

The apparatus used was essentially the same as that described by Weisz and Prater[2] which, in turn, is a simplified version of an earlier one devised by Wicke and Kallenbach[3]. It contains a sample pellet exposed on one side to a stream of hydrogen, on the other to one of nitrogen. Flow rates were such that there was zero hydrostatic pressure difference across the pellet, while maintaining a partial pressure drop of one atmosphere.

The concentration of hydrogen diffusing through the sample into the nitrogen stream was measured by a thermal conductivity cell (Gow-Mac Co., Model 9285) immersed in a bath thermoregulated at 30.0°C. Flow rates, including those used for calibrating the conductivity cell, were read from differential manometers. Pure nitrogen was employed as the reference gas in the thermal conductivity cell before being passed into the diffusion cell.

Pellets were prepared in a simple right cylindrical punch-and-die assembly. Pressure was applied from opposite directions to the two punches (diameter approximately 1 cm.) for one-half minute, no attempt being made to study time effects with the continued application of pressure. The pellets, usually 2-4 mm. thick, were mounted in Tygon tubing as described by Weisz and Prater[2].

Diffusion measurements were carried out at room temperature and corrected to 25°C. Each figure quoted comprises the average of about five determinations over a wide range of nitrogen flow rates. When the product of nitrogen flow rate and hydrogen concentration remained constant within 1%, this quantity was used to calculate the effective diffusion coefficient D_{eff} and hence the diffusibility $\delta = D_{eff}/D$. Failure to attain constant values was taken to mean that the pellet was defective or imperfectly mounted.

The main materials employed were an Ag-Ca alloy containing 8.5% Ca, a silver catalyst prepared from this alloy by steam and acid treatment[4] and a similarly prepared catalyst. The latter is designated as No. 1 (Figures 1 and 2), while the alloy-derived catalyst and its parent alloy are Nos. 2 and 3, respectively. The two catalysts differed somewhat in their residual Ca content, which amounted to 0.10% Ca for No. 1 and 0.06% Ca for No. 2. Spectrographic analyses of trace elements were similar, except that No. 1 showed slightly higher Al and slightly lower Fe content than did No. 2. B.E.T. nitrogen surface areas were 0.43 m.²/g. for No. 1 and 0.22 m.²/g. for No. 2, while the alloy gave a value of 1.50 m.²/g. A variety of mesh sizes (Tyler) and size ranges were used; these will be found indicated in the Figures.

Additional materials used in a few separate experiments will be described along with the pertinent results.

Results

In Figure 1 are shown the correlations between the axial stress exerted on the pellets during compacting, plotted logarithmically, and the void fraction. It is customary to report compacting stresses as pressures $p = F/A$; we have followed Duffield and Grootenhuis[5] in employing what is probably a more realistic quantity, namely the axial stress $s = FT\rho/W$.

[1]*Manuscript received May 16; accepted July 3, 1961.*
[2]*Division of Applied Chemistry, National Research Council, Ottawa, Ont.*
[3]*N.R.C. Postdoctorate Fellow. Present address: Tokyo Institute of Technology, Ookayama, Meguro-ku, Tokyo, Japan.*
Contribution from the Division of Applied Chemistry, National Research Council, Ottawa, Ont. Issued as N.R.C. No. 6499.

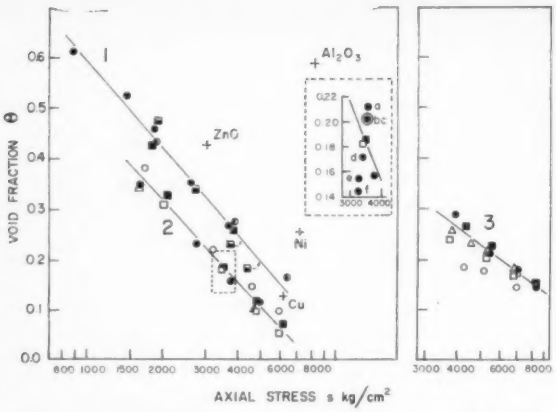

Figure 1—Void fraction vs. axial stress. 1 and 2, silver catalysts; 3, Ag-Ca alloy. Mesh size ranges: 35-80, ○; 48-100, ▬; 80-100, □; 100-150, △; 100-200, ◐ ; 150-200, ●; 200-250, ■. Insert: see text.

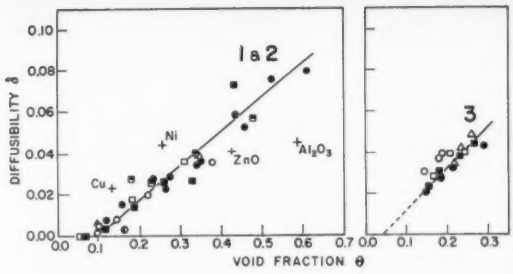

Figure 2—Diffusibility vs. void fraction. Numbering and points as in Figure 1.

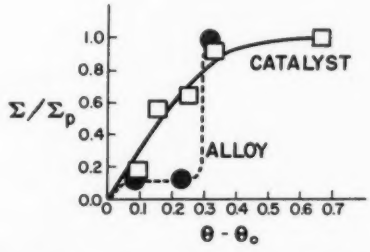

Figure 3—B.E.T. surface area relative to that of loose powder vs. accessible void fraction, for catalyst No. 2 and alloy.

In contrast to p, which does not differentiate between solid and void, s represents an average stress on the solid matter only. In calculating s, the "dry friction" which causes a decrease in axial stress (and thus pellet density) as one proceeds axially from the faces to the interior of a pellet was neglected. The error thus introduced was probably not larger than 3%[5]. Possibly similar errors were introduced by changes in packing density in a radial direction. Thus a photomicrograph taken near the rim of a lightly compressed silver pellet, sectioned parallel to its faces, showed a 2% area of somewhat higher porosity. This is never evident from the outside appearance of a pellet as the rims look always particularly smooth. The void fraction θ was calculated from the external pellet dimensions and the density of the solid. It thus includes both open and totally enclosed, i.e., inaccessible, void spaces.

All three types of metal powders gave different compacting curves, which were linear over the regions examined. Curves 1 and 2 appear to be separated by an approximately constant void fraction increment of 0.1. The alloy powder, curve 3, was less easily compressible; moreover it was not possible to form coherent compacts with void fractions in excess of $\theta = 0.3$. As indicated in the figures, each type of powder was used over a fairly wide range of particle sizes. Void space formation for the two catalysts appeared to show no evidence of dependence on particle size or, within the very limited number of tests, extent of size range. In the case of the alloy it was particularly difficult to form good pellets from coarse particles, which may have given rise to errors as reflected by the spread in points. On the other hand it is possible that the effect was real. Since the alloy powders had been prepared by crushing and several stages of grinding, the largest particles had experienced the least amount of shear. Thus different size ranges may well have exhibited variations in surface structure which, in turn, became less prominent after the leaching process.

The framed area about curve 2 is redrawn in the insert to Figure 1 with the ordinate enlarged 2½ times. All points save the lowest were obtained with catalysts similar to No. 2 and serve to illustrate the possible effect of composition and pretreatment on pellet formation at a constant compacting pressure of 2830 kg./cm.². Points *a* and *b* are duplicates for a catalyst somewhat higher in residual Ca(0.33%) and presumed to have a surface area higher than No. 2. Point *c* represents a catalyst prepared from alloy No. 3, but by a method resulting in more than double the surface area (0.48 m.²/g.) at the same residual Ca content (0.06%). Catalyst No. 2 was rechecked (*d*) and subjected to heat treatments (*e*). Identical values were obtained after 6 minutes at 425° or 10 hours at 350°C. This is of interest in view of the equal activities in ethylene oxidation achieved in this laboratory after comparable pretreatments of a similar catalyst[6]. Finally, point *f* was determined with a pure commercial silver powder.

For purposes of orientation commercial powders of Cu, Ni, ZnO and Al_2O_3 were pelletized and the results indicated in the diagrams. The Cu, particularly, consisted of smooth, nearly spherical particles and the Ni particles, while not quite so regular in shape, still presented a far smoother appearance under the microscope than the silver catalyst.

The diffusibility values as a function of void fraction are shown in Figure 2, the straight lines having been computed by the method of least squares. Curves No. 1 and 2 were similar enough so that they were treated as arising from one and the same catalyst. In the case of the alloy the three values for the 35-80 mesh powder were omitted in the calculation. In both cases the extrapolated lines intersect the abscissa at finite values of $\theta = \theta_o$ which are, respectively, 0.095 and 0.040 for the catalysts and the alloy.

Following the method of Weisz and Prater[2] we have conducted a number of forced flow experiments with air and have found no evidence for Knudsen flow. This is to be expected also on the basis of pore sizes (estimated from our photomicrographs as well as from initial particle diameters), which lie well within the region of Poiseuille flow at atmospheric pressure[1]. In this connection it should be mentioned that the extrapolations to zero diffusibility are likely to be fictitious, although for the catalysts departures from the straight line occur only within a small region. A forced flow experiment with the pellet characterized by the lowest point was unfortunately inconclusive because of the extremely low rate of flow involved.

B.E.T. nitrogen surface areas, Σ, were determined for catalyst No. 2 and for the alloy at several stages of compression. In Figure 3 these are plotted as fractions of the value of the uncompacted powder, Σ_p, against $\theta - \theta_o$. The void fraction of the powder bed was obtained from the dimensions of the bed after tapping to constant height.

Discussion

The relationship between pelletizing pressure and total void space of the compact formed has been extensively examined by Duffield and Grootenhuis for spherical copper particles[6], where equations proposed by other workers were also critically discussed. In view of their findings no general significance should be attached to the approximate linearity exhibited by our curves in Figure 1. However, for the purpose of preparing pellets of a given void volume and diffusibility it should prove useful in an empirical fashion once initial data have been determined for a given powder.

Duffield and Grootenhuis noted that the behavior under compression was independent of particle size except through its influence on the initial packing which, in turn, governed the absolute position of their pressure-volume curves. Within the limits of accuracy of the present investigation there was again no dependence on particle size. Moreover, it may be presumed that initial packing, in this case strongly determined by particle shapes and, at least for the catalysts, by easy agglomeration under low stress[7], again played a decisive part in fixing the absolute value of the void space at a given axial stress. Indeed, the greater roughness of catalyst No. 1, also observed visually when compared to No. 2 under a low-power microscope would, if this picture is correct, provide the basis for the observed higher void volume when the particles become "locked" in position upon the initial application of pressure. It is unlikely that the greater volume can have been caused by significant differences in sack pores or totally enclosed voids, since these would have given rise to differences in diffusibility between Nos. 1 and 2 at a given total void fraction. This was clearly not observed (Figure 2).

The inset to Figure 1 shows the influence of Ca content and surface structure on void formation for a constant compacting pressure, with particle geometry being the predominant factor at least in the range $0 - 0.3\%$ Ca. It might be added that owing to the method of computing θ, reproducibility is only about $\pm 3\%$ in these cases. The total pellet volume per gram on the other hand was reproducible to within $\pm 1\%$ and might well be used to good advantage for a rapid characterization of the macrostructure of catalyst powders.

At the higher Ca content of the alloy (curve 3) conditions were markedly different. The material is more brittle and, although we have worked with freshly prepared samples, there is always the possibility of CaO formation. This would provide a barrier to surface diffusion and the growth of inter-particle necks, all necessary elements of the sintering process (see, e.g., [8,9]). Both factors would be reflected in the smaller slope of curve 3. The spread in points with particle size has already been referred to; the curve as drawn is biassed towards the smaller size ranges.

It is interesting to note that the microscopically fairly smooth particles of pure Ni, Cu and Ag compressed at 5230 kg./cm.^{2} (Ag not shown in Figure 1) form pellets with void fractions correlating approximately linearly with T_m, the melting point of the pure metals in °K., and very roughly in line with their respective shear moduli (see Table 1). The value of $0.5\ T_m$ is often taken to signify the approximate temperature at which two like metal surfaces form adhesive bonds under normal load. Rowe[10] has measured the T_m factors to be 0.45 and 0.40, respectively, for clean Ni and Ag cylinders in a high vacuum. Our correlation could be interpreted in terms of the significance of surface mobility and malleability in the processes under discussion, but data on further metals are obviously required to raise this out of the realm of speculation.

The values for ZnO and Al_2O_3 shown in Figure 1 may be explained on the basis of much higher resistance to sintering and deformation, as well as microporosity in the case of Al_2O_3. Thus, Taylor and Amberg found relatively little loss in surface area[11] on pressing high-area ZnO powders under loads up to ten times those employed in the present investigation[12].

TABLE 1

COMPARISON OF VOID FRACTION WITH MELTING POINT AND SHEAR MODULUS. COMPACTING PRESSURE: 5230 kg/cm^2.

	$0.5\ T_m$°K.	Shear Mod. dyne/cm.^{2}	θ
Ag	617	2.9×10^{11}	0.112
Cu	678	4.6×10^{11}	0.130
Ni	864	7.7×10^{11}	0.256

The meaning of the diffusibility δ in terms of idealized pore structures has been discussed fully by Zimens[13] and Wheeler[1]. Discrepancies between δ and θ are customarily ascribed to tortuosity, expressed as $\chi = \delta/\theta$. Hoogschagen[14] has quoted values of χ for various pelletized catalyst powders, which were of a magnitude similar to ours (Figure 2). Apart from the contribution of the true tortuosity of the path of the diffusing fluid, χ when computed in the above manner must also include contributions from void spaces not participating in fluid transfer. These could be either totally enclosed voids or "stagnant" volumes across which the partial pressure gradient of the diffusing species is zero.

If we accept the evidence for Poiseuille flow in our compacts, it would follow from the work of Wheeler[1] and others that the approximate linear relationship exhibited for the curves shown in Figure 2 indicates an essentially uniform decrease in pore sizes without change in pore number or geometry over the linear region. This assumes that there is no fortuitous occurrence of counteracting effects (e.g., an increase in the size of large pores at the expense of smaller ones and decrease in pore number) which is considered unlikely because of the similar behavior of the physically different systems 1 + 2 and 3. It is also compatible with the measurements of the internal surface area discussed below. We shall now assume as a first approximation that the "stagnant" void volume is negligible and that the blocked void fraction θ_o is a constant throughout the linear region. It is difficult to assess the validity of these assumptions. No experimental method is available to us for measuring the first quantity and helium density determinations have failed, for lack of the required precision with the available samples, to define the second. For the blocked void *fraction* to be constant with decreasing pellet volume per unit weight, the blocked void *volume* must decrease, which seems reasonable, especially since one may expect the immediate creation of blocked spaces on first forming a coherent compact of "open" structure. If this were not so, one should have expected marked curvature in the diffusibility curve, or even a kink at the onset of blocked pore formation. However, approximate linear behavior of θ_o with δ other than constancy cannot be discounted.

In the light of the foregoing arbitrary assumptions we may express the graphs in Figure 2 by the relation

$$\delta = \chi(\theta - \theta_o),$$

where χ is now a representation of the actual tortuosity. In previous studies[14] it had always been caluclated from separate pairs of values, which in the present case would have resulted in a tortuosity increase (decreasing value of χ) with increasing compression; the above expression indicates maintenance of essentially constant tortuosity over the whole range. The least square values of χ so obtained were $0.17 \pm 0.01_8$ and $0.20 \pm 0.01_4$ for the catalyst and the alloy respectively.

We have already commented on the relative lack of dependence of the pressure-volume curves on particle size for a given type of powder. Figure 2 lends support to the idea that particles initially interlock forming agglomerates which are of similar geometry for different particle sizes because individual particles have lost their identity. Indeed, the similarity of curves 1 and 2 would suggest that the geometry of the two catalysts is essen-

tially the same, even though, for reasons mentioned earlier, different loads had to be applied to create pellets of the same total void fraction.

With the additional assistance of Figure 3 we shall attempt to describe the processes involved in pellet formation. Perhaps the simplest case to interpret is that of the alloy. From measurements of the available surface area it appears that there was a tenfold decrease in area on first compressing the powder into a coherent compact of the maximum possible void volume. The comparatively small value of θ_o can only mean that this decrease was caused either by removal of roughness through shear forces[8] and the formation of large interparticle contact areas (i.e., flattening of particles), or possibly the closure of internal fissures, rather than by entrapping large voids. One might expect the shearing process to be predominant at this stage, since one could expect particle flattening to be accompanied by substantial densification of the pellet, whereas there was in fact little change in void fraction between the loose powder and the first compact. On further compression the available surface area remained constant while the void fraction decreased. At the same time the diffusibility decreased linearly with void fraction. These facts rule out any effective destruction of pores, either by closing their outlets or by complete densification, and again point to maintenance of the original geometry. One may visualize this, for instance, as a narrowing down of flat-walled pores.

The situation is somewhat more complicated with the catalyst. For reasons referred to above it is understandable that coherent compacts could be formed at pressures five times as low as for the alloy, resulting in a total void fraction as high as 0.6. The surface area did not materially decrease on reducing the void fraction to ~ 0.4, after which it decreased rapidly. Thus the initially wide open structure was first condensed by increasing the number of inter-particle weld-necks or the contact area of the existing ones, without however changing the pore geometry to any significant extent, as evidenced by the approximately constant surface area and the linear decrease in diffusibility. Further compression occurred with a concomitant decrease in surface area, probably involving surface or bulk diffusion processes and plastic deformation[9], but still did not involve a change in flow pattern. Possibly also a surface "smoothing" by shear as described for the alloy may have been involved, although it should be noted that Σ_ρ for this catalyst was only 0.2 m.²/g., whereas it amounted to 1.5 m.²/g. for the alloy. This meant that the catalyst presented a much smoother surface to begin with and probably contained far fewer mechanically weak protuberances than did the alloy.

Acknowledgements

The authors wish to thank G. L. Osberg for his constant and helpful interest in this work and D. Kulawic for technical assistance.

Nomenclature

A = area of pellet face, cm.²
D = diffusion coefficient of H_2 in N_2, at 25°C., cm.²/sec.
D_{eff} = effective diffusion coefficient in pellet, at 25°C., cm.²/sec.
F = applied load, kg.
p = compacting pressure, kg./cm.²
s = axial stress, kg./cm.²
T = pellet thickness, cm.
T_m = melting point, °K.
W = pellet weight, g.
δ = diffusibility, dimensionless
θ = total void fraction of pellet, dimensionless
θ_o = extrapolated void fraction of pellet at $\delta = 0$, dimensionless
ρ = density of solid, g./cm.³
Σ = B.E.T. nitrogen surface area of pellet, m.²/g.
Σ_ρ = B.E.T. nitrogen surface area of uncompacted powder, m.²/g.
χ = tortuosity, dimensionless

References

(1) Wheeler, A., Advances in Catalysis **3,** 249 (1951).
(2) Weisz, P. B., and Prater, C. D., Advances in Catalysis **6,** 143 (1954).
(3) Wicke, E., and Kallenbach, R., Kolloid-Z. **97,** 135 (1941).
(4) McKim, F., and Cambron, A., U.S. Pat. 2,562,857 (1951); Can. Pat. 457,366 (1951).
(5) Duffield, A., and Grootenhuis, P., in "Symposium on Powder Metallurgy 1954", Special Report No. 58, The Iron and Steel Institute, London, 1956, p. 96.
(6) Echigoya, E., Amberg, C. H., and Osberg, G. L., Can. J. Chem. **37,** 2101 (1959).
(7) Echigoya, E., and Osberg, G. L., Can. J. Chem. Eng. **38,** 43 (1960).
(8) Goetzel, C. G., "Treatise on Powder Metallurgy", Interscience Publishers, New York, 1949, V.I. p. 259 ff.
(9) Rhines, F. N., in "Plansee Proceedings 1958", Pergamon Press and Metallwerk Plansee AG., Reutte/Tyrol, 1959, p. 38.
(10) Rowe, G. W., in Ref. (5), p. 343.
(11) Taylor, J. H., and Amberg, C. H., unpublished results.
(12) Taylor, J. H., and Amberg, C. H., Can. J. Chem. **39,** 535 (1961).
(13) Zimens, K.-E., in "Handbuch der Katalyse", Springer, Vienna, 1943, V. 4, p. 151.
(14) Hoogschagen, J., Ind. Eng. Chem. **47,** 906 (1955).

★ ★ ★

Chemical Engineers and Computers[1]

THEODORE J. WILLIAMS[2]

Computers as tools for the chemical engineer have begun to revolutionize his concepts of reaction kinetic analysis, of plant design methods, and of plant control systems. The new field known as systems engineering has arisen to fulfill and exploit the promises which computers offer in these areas. This paper outlines the applications of analog and digital computers to chemical engineering problems, points out the specific advantages of each, and details the numbers and backgrounds of the operating personnel required. The newer field of application of computers to process control is reviewed in the light of progress to date and of present and future trends.

Computers are now revolutionizing chemical engineering. As tools of the design engineer they can release him from the hours of drudgery formerly associated with the trial and error aspects of design. They permit him to try many, many more different and vastly more complex design concepts. As tools of the research engineer they can mechanize the data collection and data reduction aspects of his experiments. They permit him to try out very complex mathematical models of his system prior to experimentation so that only the minimum number of the most crucial experiments need be made. As tools of the plant production engineer they can remove the necessity for close monitoring of plant operation by human operators; they can smooth out plant operations; and they can assure that the plant is always operating at its economic production level.

In fact, the impact of the computer on chemical engineering has been so great that a new branch of chemical engineering, known variously as systems engineering, or dynamic analysis, or applied mathematics, or by many other terms depending upon the group involved, has come into being. To implement the uses of computers listed above, systems engineering has taken the charter given in Table 1[1]. As a result of this and allied work many important changes have already taken place in chemical engineering studies. Some of these are:

(1) The most striking changes have come in chemical reaction kinetics. Where older methods required the development of overall orders of reaction and overall rate constants, the newer methods along with computers permit the specification of each of the reaction steps and their individual rate constants. While the resulting systems of equations are very large and the determination of the correspondingly large numbers of reaction coefficients can be quite difficult, computing machines make such work now practicable.

(2) Methods are now being devised which promise to enable the determination of the physical properties of gaseous and liquid systems from readily made measurements of only a few of the physical properties of the components of the system[2]. Such methods will be of immeasurable aid to plant design studies when finally perfected.

(3) Current experimental research along with the application of servomechanism techniques is rapidly establishing the dynamic behavior of process equipment when under transient conditions as when subject to upsets or during start up.

Analog and digital computers each have specific advantages and disadvantages in relation to a particular problem which must be kept in mind in applying them. Table 2 summarizes this information.

The short but spectacular history of computers, their exponential increase in numbers, and capacity, and the fact that they have only been applied to chemical and petroleum industry problems to a high degree within the last five or six years means that most of the major discoveries concerning their use in our industry are still ahead of us.

TABLE 1

THE AIMS OF SYSTEMS ENGINEERING IN APPLYING COMPUTERS TO THE CHEMICAL ENGINEERING FIELD

(1) In Plant Design
- (a) To optimize the process while in the design stage, so as to obtain the best possible combination of processing conditions and plant design to assure the maximum return on investment.
- (b) To use computer techniques in plant unit designs, especially where trial and error procedures are necessary, to obtain the best possible designs for the plant units involved.
- (c) To correlate process dynamics and process control studies directly with process unit design studies.

(2) In Research and Process Development
- (a) To render as much service as possible to the research chemist in developing the nature and characteristics of the chemical reactions involved in a process.
- (b) To make the fullest possible use of computer simulation in the process development stage in order to reduce the experimentation necessary in proving the process and establishing the most desirable operating conditions and the data necessary for the design phase.

(3) In Plant Optimizations and Plant Control
- (a) To study the operation of each existing plant to determine what, if any, changes in their control systems or methods of operation would improve their return on investment.
- (b) Study each of the newer techniques of plant control to determine their applicability to existing processes.

[1]*Manuscript received November 15, 1960; accepted May 27, 1961.*
[2]*Monsanto Chemical Company, St. Louis, Mo., U.S.A.*
Based on a paper presented to the C.I.C. Chemical Engineering Conference, Quebec City, Que., Nov. 7-9, 1960.

TABLE 2

A COMPARISON OF THE APPLICATION OF ANALOG AND DIGITAL COMPUTERS TO CHEMICAL ENGINEERING PROBLEMS

(1) The Advantages of Analogs in Comparison to Digital Computers.

Analog Computer	Digital Computer
Simulates behavior of any system by action of easily manipulated and measured variables.	Performs arithmetic operations with numbers.
Simulation is continuous, permits inclusion of concepts such as distance, velocity, acceleration.	Operates discontinuously; can only approximate higher order effects.
Results presented as family of graphs of variation of dependent variable (same data obtained with recorder connected to process).	Results presented as tables of numbers; must be plotted.
Speed of problem solving is direct function of actual speed of physical system, is independent of size or complexity of system.	Speed is direct function of problem complexity and size, relatively independent of operating speed of process.
Programmed so that parameter magnitudes are entered as settings on variable potentiometers; parameter values can be changed at will.	Flexibility not present without special programming precautions.

(2) The Advantages of Digital Computers in Relation to Analog Computers

Digital Computer	Analog Computer
Problem size reflected in computing time; no limit to size of problem if time is available.	Size of computer (number of computing components) determines size of problem which can be solved; simplifying assumptions often made to reduce complexity.
Useful in nearly all types of problems. Complex partial differential equations more amenable to solution by digital equipment.	Specifically designed for solution of ordinary differential equations; other problems — e.g., solution of simultaneous algebraic equations — made by trial and error. Less complex partial differential equations solved if converted to ordinary differential equations and one variable assumed constant; family of solutions for different values of variable results.

(3) The Relative Applicability of Each Type to Specific Problem Areas.

Application	Analog	Digital
Equipment and Plant Design	Show great promise for working out relative sizes of plant equipment by solving dynamic equations of plant performance.	Superior for details of mechanical design — e.g., stresses, sizing of members, costs — which are trial and error arithmetical problems.
Instrumentation and Data Reduction	Small, special purpose analogs important in converting and plotting single variable and directly correlated multiple variable data in form of graphs.	
Process Control Simulations (Research)	Best tool in existence for studying resulting phenomenon; limitation on system complexity imposed by computer size.	
Chemical Plant Applications	Definite promise as final control elements for units of highly automated chemical plants.	Flexibility and accuracy of digital computers better for control of whole plants.
Research in Basic Processes	Well suited to simulation of chemical reaction kinetics involved in chemical process development.	Better for determination of kinetic parameters by statistical data reduction where necessary.
Research in Unit	Well suited for study of transient state such as heat transfer, distillation.	Better suited for steady-state studies which are usually arithmetical or statistical.
Plant Operations and Management Technique Studies		Better here because statistics and arithmetical operations predominate.

However, this in no way implies that the difficulties and research necessary to apply computers is at an end. As an example of the status of one branch of chemical engineering the field of reactor dynamics and reaction kinetics will be discussed.

Reactor Dynamic Analysis and Process Kinetics

The most important class of chemical processing units from a dynamic behavior viewpoint and because of its ultimate importance to the chemical process involved is the chemical reactor. Therefore, the most important research task of the process control or systems engineer is to determine the mixing characteristics of these devices and the kinetic mechanisms of the chemical reactions taking place therein[1].

Mixing studies are important in order to define the degree of complexity to which analog or digital computer simulations of the reactor must be carried out. If a stirred tank reactor can be considered completely mixed only one stage needs to be simulated On the other hand, inadequate mixing may require the simulation of 2 or 4 or even more stages per reactor. Thus if a very complex kinetic model is required this may automatically make the simulation impossible to carry out on available computing machines.

As previously stated, the development of kinetic mechanisms should be considered from the differential reaction rate viewpoint rather than from the steady-state equilibrium ratio viewpoint so prevalent in the standard chemical engineering texts on the subject. Only in this way may the true relationships of some of the transitory species such as radicals be properly considered. The previous reference[1] has described more completely the procedure which should be followed in determining the various steps in a kinetic mechanism by analog simulation.

Even with the help of the analog computer this is still a very tedious task since a complex trial and error procedure must be used to determine the best values of the reaction rate constants. Therefore, the recent work by the International Business Machines Corporation[3] on digital computers and by Computer Systems Incorporated[4] on analog computers promises to eventually make possible the determination of the proper values of kinetic constants automatically, by a machine controlled and operated trial and error procedure. The investigator can then try a very large number of possible mechanisms in a short period of time. Since the machine also determines the value of the minimum root mean square error function for each separate mechanism, it is a simple matter to then choose the most probable mechanism from the available choices presented to the computer.

Batch reactors and stirred tank continuous reactors along with their kinetics are readily simulated on large scale analog computers including their control relationships provided only that reactor mixing is reasonably complete. However tubular reactors are another matter if their control functions must be considered. Because of the multiple sectioning necessary for a finite difference type approximation in real time, most computers are quickly overtaxed.

The only solution is then to use a repeated multi-step procedure. The steps required are:

(1) Determine the steady-state composition distribution in the reactor by converting the length variable to time and solving on analog or digital computers.

(2) From the resulting composition history determine the regions of possible heat exchange and the heating or cooling load required.

(3) Solve the reactor dynamically (i.e., time-wise) for the heat transfer-control relationships only. If the control system cannot regulate the required heat transfer from step 2 as an input function at the proper point determine the resulting temperature excursions in the reactor.

(4) Repeat step 1 for the limits of the temperature excursions found in step 3. Determine whether or not this causes the outlet composition to deviate outside the allowed limits.

(5) If the composition deviation is too great determine the new heat load requirements for the temperature control system.

(6) Revise the control system as necessary and then repeat step 3 to determine new temperature excursions.

(7) Repeat as necessary until the temperature control system can properly regulate the outlet composition for the reactor.

While this is a difficult, long-term procedure it is the only one known which can be used at present to check the suitability of a tubular reactor control scheme by theoretical means.

Other Chemical Engineering Computations

Just as was the case with reaction kinetics and reactor dynamic investigations, most other types of chemical engineering calculations are still in a state of flux. For example, despite years of effort and unnumerable papers on the subject[5], the design of distillation columns by trial and error algebraic solution of the steady-state equations of the column is still unsuccessful in a large proportion of the important cases. This is particularly true for those cases where multiple feeds or sidestreams are present, where very close separations are necessary, or small impurities are present, or where non-ideal equilibrium relations are present. Unfortunately these are the cases of greatest interest and at the same time the most difficult to carry out by hand methods.

There is however a method of machine computation, which, though tedious, can be used for such computations. This is an integration of the dynamic equations of the column, a set of ordinary differential equations[6]. The steady-state condition is, of course, a special case of the solution of the dynamic behavior of the column.

Computation of the design of absorption and extraction columns is an even more difficult task than that of distillation columns since the equilibrium relations involved are still more non-ideal than in distillation. Again, though, the integration scheme will work if the equilibrium relations involved are known.

THE TOOLS AND THE PEOPLE REQUIRED

With some knowledge of the places where computers can and are being applied one may discuss the required computer sizes for specific tasks and the numbers and types of personnel required to operate them effectively.

Some Notes Concerning the Required Size of an Analog Computer Installation

There is a fact of life about all computers, particularly analog computers, which should be kept in mind by everyone concerned with their procurement and use. This is the fact that no computer (at least to date) has even been big enough to handle all of the problems which would eventually be applied to it in the future. As a result, computer facilities have continued to grow and grow in size, flexibility, and speed in almost a geometrical progression.

Therefore, the first caution one can give to the organization contemplating a computer installation is to be sure that the resulting machine and installation are readily expandable when the need arises.

There are four main uses to which a chemical industry analog computer could be placed. These are:

(a) Instruction in computer usage, process dynamics, and control system operation.

(b) Investigations of control system (i.e., instrumentation only) response and design.

(c) Simulation of control system response and design (including rudimentary process dynamics and chemical kinetics).

(d) Complete simulations of chemical kinetic systems, process development investigations, and overall processing system designs with control included.

Each of these in turn requires a larger and much more versatile computer as shown in Table 3. Of course, the larger machines can readily carry out the tasks of the smaller machines and separate installations are not required, unless the workload of the larger machine should necessitate such action.

The first thing the reader will note concerning the computers recommended in Table 3, particularly if his experience has been with computers in the defense industries, will be the extremely high proportion of non-linear gear, especially in the larger

TABLE 3

DISTRIBUTION OF COMPONENTS FOR TYPICAL ANALOG COMPUTER APPLICATIONS IN THE CHEMICAL INDUSTRY

Type of Usage to Which Computer Will Be Applied / Type of Component	Instructional Only	Control System Instrumentation Response and Design	Simulation of Control System Response with Some Process Dynamics	Complete Simulation of Chemical Kinetics, Process Development and Processing System Design with Control
Operational Amplifiers	10–20	15–50	40–100	80–200+
Multiplication Channels	1–2	2–5	10–30	50–100+
Function Generation Channels	1–2	2–6	5–10	25–50+
Operational Relays	1–2	6	12	25–50+
Function Switches	3	6	12	25–50+
Separate Control Consoles	1	1	1–2	2–3+
Plotting Channels x, y	1	1	3	3–4+
Plotting Channels x, t	2–4	6	12	18
Repetitive Operation	Yes	If Desired	If Desired	If Desired

machines. These recommendations are made because of the nature of chemical problems, particularly those involving chemical kinetics. Here a very large number of multiplications and function generations, particularly exponential functions, are required. In addition, the large selection of operational relays and function switches permits the direct simulation of multi-step processes — such as batch drying and crystallizations as a continuous operation — thus avoiding the necessity of breaking the problem into a number of separate steps with the attendant possibilities of error and difficulties of correlation of results.

Other points which should be particularly emphasized concerning Table 3 are as follows: First, repetitive operation is extremely useful for instructional purposes, since its use with an oscilloscope display permits the most extensive display of the dynamics of a process or control system in the shortest possible time. In addition, this "continuous display" demonstrates most vividly to the student the effect of changes in the system parameters and thus gives him by far the best intuitive "feel" for process behavior. However, there are severe limitations on plotting accuracy with such displays. Thus, they may be used for research and design problems only as rough "ball-park" approximations. The solution should be repeated at normal speeds to get the final most accurate answer. Thus, repetitive operation is not specifically recommended for the larger installations but is left a matter of personal preference of those involved.

Second, the extreme flexibility of the x, y plotter as a function generator should be brought to the readers' attention. It is particularly useful for presenting such functions as temperature variable heat transfer coefficients which cannot readily be presented by standard function generation equipment.

Organization and Numbers of Personnel Required

Just as each of the different contemplated applications of the analog computer requires a somewhat different size of computer and a different distribution of components, a somewhat different organization is necessary for their proper utilization. Table 4 outlines recommendations in this regard.

Several points concerning Table 4 are worth reiteration or further explanation. First, since electrical and mechanical engineers at present have a better background in automatic control theory and the associated mathematics, they are recommended almost exclusively for the smaller organizations. However, as the group delves more and more into the intricacies of the chemical processes themselves, the chemical engineer's knowledge becomes more and more important until they outnumber the others. Note that a certain number of electrical engineers are still recommended because of their familiarity with the operation and capability of the computer.

Second, full-time maintenance personnel are recommended only when the computer becomes large enough to demand such

TABLE 4

NUMBERS AND BACKGROUND OF PERSONNEL REQUIRED TO OPERATE ANALOG COMPUTER FACILITIES OF VARIOUS SIZES AND USAGES

Type of Usage to Which Computer Will Be Applied / Type of Personnel Involved	Instructional Only	Control System Instrumentation Response and Design	Simulation of Control System Response with Some Process Dynamics	Complete Simulation of Chemical Kinetics, Process Development and Processing System Design with Control
Electrical or Mechanical Engineers (M.S. or Equivalent)	1	1–2	2–3	3–6+
Chemical Engineers (M.S. or Ph.D.)	—	1	2–3	6–8+
Analog Computer Technicians (Repairmen)	—	—	1–2	2–3+
Open Shop	Yes	Yes	As Desired	No

attention (50-100 amplifiers). For smaller machines, the attendant engineers should be capable of performing the necessary preventive maintenance checks and repairs.

Third, the staff for the larger computer continues to increase even though the contemplated problem size has also increased. This is due to the fact that the economics of the utilization of large-scale computers almost demands their use on a multi-shift basis because of the very high depreciation charges involved. Thus, the staff recommended here is for two shift operation of the largest machine recommended.

Fourth, because of the difficulty of training the necessary personnel and the extreme complexity of the problems involved, it is the majority opinion of those concerned that a very large computer facility should be operated on a closed-shop basis. However, every effort should be made to obtain the complete cooperation of the person originating each of the problems solved, even to having him observe the actual solution on the computer. Often he will have a "feel" for the problem which will be invaluable in checking out the computer and evaluating the final results.

New Developments in Analog Computers

There are several recent or eminent developments in analog computer equipment and in operating techniques which promise to greatly aid and possibly even revolutionize analog computer operation. Most of these involve digital techniques of one type or another.

One of the major present-day problems with analog computer operation in the process industries is the difficulty of adequately representing a true time delay. The development of a suitable and reasonably priced magnetic tape or drum mechanism for this purpose would be a major boon to the field. Such devices are now under development.

Analog computers are especially designed for the solution of ordinary differential equations and do this extremely well. Digital computers on the other hand are very fast and accurate in the solution of algebraic equations but relatively slow with large systems of differential equations. In addition, analogs have only rudimentary logic capabilities, while extremely complex logic operations are carried out directly on digital machines. There is thus a very fruitful potential in the joint use of these machines for the solution of large process development-type problems which entail all three types of mathematical operation, solution of differential equations, solution of algebraic equations, and logical selection from several possible paths of action. Devices for connecting the two computers together during operation are in use by several of the defense system contractors, such as Space Technology Laboratories, Convair Astronautics, and International Business Machines. Models of these are also under development for use by the process industries.

Another area where aid is needed in analog computation is in the simulation of distributed parameter systems and processes. Adequate mathematical representation of these systems requires the use of partial differential equations or extremely large sets of simultaneous ordinary differential equations. Thus, their solution on analog equipment requires a very large machine. However, the use of a modified form of the data storage drum mentioned above for true time delay simulation offers an aid in the solution of this type of problem. If preliminary results can be stored during the solution of a problem of this type on the analog computer, it can be solved on a much smaller machine than required above by the use of a repetitive trial and error procedure which can be readily programmed. Again these devices are under active development by the computer manufacturers. Thus, digital devices promise to have a major effect on analog computer operation in the process industries.

Digital Computer Installations

One should not leave the discussion of computers, particularly after presenting details of analog computer sizes and the personnel required, without presenting similar data concerning digital computer installations.

Digital computers, because they are available in only a few specific models, do not present as difficult a choice in determining the best size of installation for a specific purpose as do analog computers, since one need not break them down to specific components. The best rule here is to procure the biggest and fastest machine that one can finance and staff. Just as in the case of analogs, the company invariably underestimates the applications that will be made of the computer once it has been installed.

Computer installations of the type necessary for calculations, such as those described in this paper, can be divided into two categories, depending on the size computer installed.

These are first, the medium sized computers of which the Royal McBee LGP-30 is considered the minimum size. These progress through the Bendix G-15, and the IBM-650, to the Burroughs-Electrodata 205. The second group, large sized computers, starts with the Burroughs-Electrodata 220 and progresses through the IBM 704, 709, and Remington Rand Univac 1103A, to the RCA 501, and the recently announced IBM 7090.

Table 5 presents the author's opinions as to the personnel required to adequately man a digital computer of either size. The ranges in numbers of personnel recommended are to allow for the variations in computer size within each group.

TABLE 5

PERSONNEL REQUIREMENTS FOR TYPICAL PROCESSING INDUSTRY DIGITAL COMPUTER INSTALLATIONS

Size of Computer Involved / Type of Personnel Considered	Medium Size Royal McBee LGP-30 Bendix G-15 IBM 650 Burroughs Datatron-205	Large Size Burroughs Datatron 220 IBM 704 Remington Rand Univac 1103A IBM 709 Remington Rand Univac 1105 IBM 7090 RCA 501
Statistical Specialists 1. B.S. Ch.E. with M.S. in Statistics or 2. Ph.D. Ch.E. with Statistics Minor	1–2	2–3
Chemical Engineering Design Specialists M.S. or Ph.D. Ch.E. with Applied Mathematics Minor	2–3	4–8
Linear Programming and Operations Research Specialists 1. M.S. or Ph.D. Ch.E. with Applied Mathematics Minor 2. M.S. or Ph.D. Mathematicians with B.S. in Ch.E.	0–2	3–8

THE IMPACT OF COMPUTER CONTROL AND A DISCUSSION OF ITS PROPER PLACE IN THE CHEMICAL INDUSTRY

Present Status

Digital computer process control is, as everyone knows, one of the most discussed, evaluated, and predicted subjects in the industry today. Therefore it deserves a special mention and evaluation here. Nearly every meeting of any one of the various societies has its full share of such papers — most of them of a speculative nature. Despite this, surprisingly little has yet been published or presented concerning the true performances of these machines in chemical plants. In addition, because of digital computer control, the past two and a half years has been a period of some of the greatest duplication of effort on the part of the computer manufacturers and of the processing companies in our history. Each of the approximately 16 computer manufacturers who build these machines and the 20 processing companies who have purchased them has — by means of both internal and inter-industry study projects — sought out for itself where the economic returns from these new devices may lie. Proprietary consideration, necessary on both sides to protect any and all economic advantages uncovered, has prevented and still does prevent a complete and free disclosure of the results of these tests. Only in very recent months have articles devoted to specific digital computer installations begun to appear[7,8,9] and even these must be somewhat less than full discussions of the topic, for the same reason.

There is, of course, no remedy possible or even desired to such a situation since our economic system demands it. It is mentioned here only because of the drain it has made upon the very small pool of trained manpower available for all process control and process dynamics work.

In this discussion no attempt will be made to compare the specifications and characteristics of the various models since this has been admirably handled by Freilich[10] for all but the very newest of the machines.

Much of the available information concerning process control computers and their applications can be summarized as in Table 6. Since these machines have been used exclusively for supervisory control functions, their place in chemical process control can be diagrammed as shown in Figure 1. Along with the job of maintaining an economic balance of the plant's operation, there are several additional tasks to which they may readily be applied without hindering the performance of their primary function of optimization. These are listed in Table 7.

It is possible now to develop some basis for economic and technical justifications which can be put forward for the use of process control computers as steady state economic optimizers in chemical processing plants and petroleum refineries.

Where are Computers Justifiable— Economic Considerations

If one can make an assumption of generality concerning some conclusions that have been drawn concerning the applicability of process control computers, one can readily diagram the relationship of digital process control computer installed cost to the process plant total investment and the required return on total investment before taxes which is attributable directly to the work of the digital control computer.

The resulting general statements are:

(1) A return on total plant investment of at least 0.5% per annum is probably possible on any process due entirely to the monitoring and long term economic optimizing abilities of the computer alone.

(2) If a plant systems study shows that a return of greater than about 6% per annum is possible, serious engineering study should be given to the possibilities of removing process bottlenecks or improving process work in the plant. After this, the plant should be restudied to determine the remaining return on investment which can still be credited to the computer. If such returns are possible the plant was obviously not designed originally for optimum compatibility of its constituent units.

TABLE 6

SUMMARY OF AVAILABLE INFORMATION CONCERNING PROCESS CONTROL DIGITAL COMPUTERS

(1) All installations to date have exercised *supervisory control* of the process only, either on-line or off-line. That is, they have been used to adjust the set points of conventional instruments either directly from the computer or through manual intervention.

(2) All computers so far have been used for *steady-state* analyses of the process' performance, mainly analyses of the economic returns possible from the process. Thus these computers have not been concerned with the stability of the process control itself or with process start-ups or shut-downs.

(3) Being mainly solid state and derived from tested weapons system or large commercial computers, the process control computers are showing as a rule a truly remarkable reliability and dependability.

(4) Study is showing that the earlier machines contained too small a memory capacity to be truly satisfactory process control computers. Thus the more recent models have provision for large and quite flexible memories. Also several of the older models are being redesigned or modified to have this feature added.

TABLE 7

TASKS FOR WHICH DIGITAL COMPUTER CONTROL MAY BE REQUIRED PROVIDED ECONOMIC JUSTIFICATION IS POSSIBLE

(1) Modification of plant mathematical models on a regular basis to account for such effects as rapid catalyst deterioration, tar buildup, heat exchanger, condenser, or column fouling and others of a similar nature. These coefficients in the plant economic control model must change significantly over periods of as short as a few or even one day to preclude the use of off-line computers for such tasks.

(2) Where the plant mathematical model is too complex, i.e., the plant interactions are too complex, or their kinetics are too detailed, etc., for special analog type computers to be designed for the task.

(3) Where the process or kinetic model is incomplete in that statistical analysis must be regularly made to determine and upgrade kinetic and other mathematical model coefficients and terms.

(4) Data logging, data monitoring and data processing and evaluation. Such tasks are subsidiary to the digital computers main task but may add justification for its use.

(5) Statistical analysis of plant operating data where these must be carried out on a regular repetitive basis.

(6) Regulation of cyclic operations where variable time periods within the cycle are necessary. Batch operations employing catalysts of varying activities are of this type.

(7) Emergency procedures such as partial plant shutdowns.

While the actual limits used here may vary from company to company depending upon accounting and management practices, a relationship such as suggested above appears to hold throughout our industry. With it in mind, Figure 2 outlines the allowable computer size versus plant investment if only the computers monitoring ability is to be capitalized on and none of its special control abilities as listed in Table 7. Lines are shown for one, two and three year payouts after taxes.

Figure 3 details the range of allowable computer installed costs versus plant total investment between the limits of 0.5 and 6% return, with the locations of intermediate return rates indicated. This figure is for a three year payout. Finally Figure 4 lays out in regions of percent return versus plant overall investment the areas where computers are readily justified, where they must be justified by specific studies, where further plant studies for removing bottlenecks should be made, and where computers can not be justified at all because plant investment is too low. Figure 4 shows what is probably the

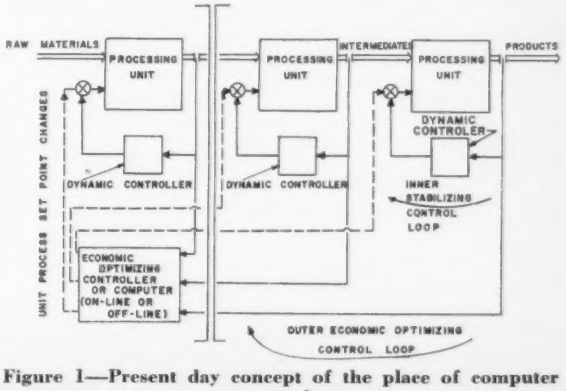

Figure 1—Present day concept of the place of computer control.

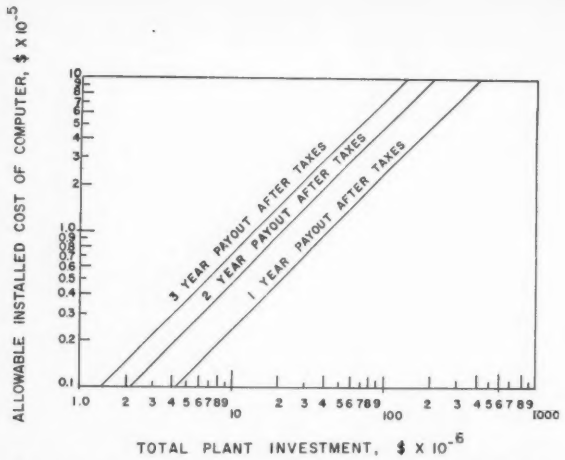
ALLOWABLE INSTALLED COST OF COMPUTER, $ X 10^-5
3 YEAR PAYOUT AFTER TAXES
2 YEAR PAYOUT AFTER TAXES
1 YEAR PAYOUT AFTER TAXES
TOTAL PLANT INVESTMENT, $ X 10^-6

Figure 2—Allowable total cost of computer installation to capitalize on the computers monitoring ability alone (assuming 0.5% return on original investment due to monitoring ability of computer).

present day standard installation, that is, one costing about $300,000 complete and requiring a two year payout after taxes.

The most obvious points brought out by these graphs are first, the extreme dependence upon plant size or better plant total investment, and second, the inverse effect of computer installed cost. From this one can immediately conclude two things; that computer control will always be more important to the petroleum refineries than to chemical plants and that computer control will be much easier to justify on new plants. The first is true because of the generally much larger size of the refineries. Also within the chemical companies, petro-chemical installations will be the most susceptible, again because they are usually larger. New plants are more susceptible to computer control than old because here one is not faced with a tremendous outlay of capital for instrumentation just to make the computer and plant compatible. If properly planned ahead of time, the instrumentation for a new plant to allow computer control should be little more expensive than that planned to operate without it. Thus in contrast to the older plant (where the capital investment includes both computer and instrumentation), the required investment in the new plant includes only the computer and a small amount of associated hardware, and may be only one-third to one-half that of the former.

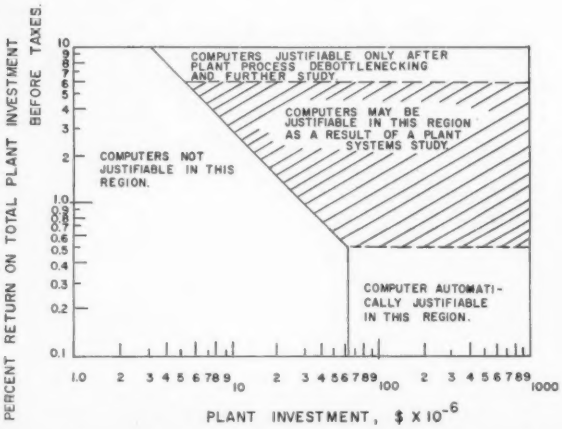
PERCENT RETURN ON TOTAL PLANT INVESTMENT BEFORE TAXES
COMPUTERS JUSTIFIABLE ONLY AFTER PLANT PROCESS DEBOTTLENECKING AND FURTHER STUDY
COMPUTERS MAY BE JUSTIFIABLE IN THIS REGION AS A RESULT OF A PLANT SYSTEMS STUDY
COMPUTERS NOT JUSTIFIABLE IN THIS REGION.
COMPUTER AUTOMATICALLY JUSTIFIABLE IN THIS REGION.
PLANT INVESTMENT, $ X 10^-6

Figure 4 — Relaionship of computer justification, plant investment, and possible increased return on investment. Basis: 2 year payout of a computer with a $300,000 installed cost (the present day standard case).

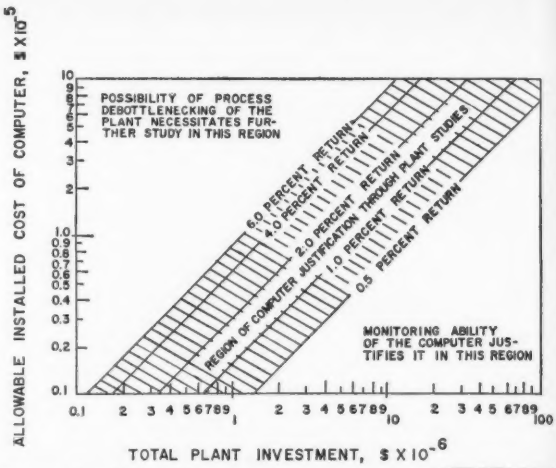
ALLOWABLE INSTALLED COST OF COMPUTER, $ X 10^-5
POSSIBILITY OF PROCESS DEBOTTLENECKING OF THE PLANT NECESSITATES FURTHER STUDY IN THIS REGION
6.0 PERCENT RETURN
4.0 PERCENT RETURN
2.0 PERCENT RETURN
1.0 PERCENT RETURN
0.5 PERCENT RETURN
REGION OF COMPUTER JUSTIFICATION THROUGH PLANT STUDIES
MONITORING ABILITY OF THE COMPUTER JUSTIFIES IT IN THIS REGION
TOTAL PLANT INVESTMENT, $ X 10^-6

Figure 3—Allowable computer costs versus required increased returns on total plant investment before taxes (assuming a three year payout of the computer).

There are also several other factors which should be kept in mind while establishing the economic justification for computer control. These are listed in Table 8.

Where are Computers Justified— Technical Considerations

Considered along with the economic justification of digital computer control and directly related to it is the equally important question of technical justification, i.e., is the computer really necessary for the task assigned to it or will a simpler, cheaper control method accomplish the same results. Table 7 has already listed several tasks which the digital computer can perform and for which it may be necessary. Some other considerations which should be kept in mind are listed in Table 9.

This is also the place to emphasize the necessity for making a thorough plant systems study and for developing a mathematical model of the plant which is as complete and as exact as possible[1]. This is necessary both to permit the proper programming of the machine and also to thoroughly document the claimed economic justification for its use.

It has often been remarked by systems people that there has never been a thorough plant study which has not paid for itself in new knowledge concerning the process and its operation whether a computer was actually purchased or not. While only about one-fourth to one-fifth of the chemical plant studies to date have uncovered potentially profitable digital computer applications[11] their uncovering of new plant knowledge has made them a very worthwhile endeavor for the systems groups.

TABLE 8

ADDITIONAL ECONOMIC FACTORS IN JUSTIFYING DIGITAL COMPUTER CONTROL

(1) One of the primary findings of most systems studies of existing processes is the great gains which can be made from the installation of analytical instrumentation alone. Since such instrumentation is usually necessary to allow digital computer control to even be applied, economic gains really attributable specifically to the more modern instrumentation are often credited to the computer. Great effort should therefore be made to separate those gains due mainly to the greater process knowledge available from analysis instrumentation from that which is due strictly to the computers use of this information.

(2) Similarly one should be careful that the computer installation is not credited with gains attributable only to the specific new knowledge and resulting adjustment of plant operating methods which frequently occurs as a result of a complete plant systems study and which would be applied whether the computer had been purchased or not.

(3) For cases where some of the coefficients of the plant mathematical model are unknown or variable and it is contemplated that the computer will be necessary to compute them, consideration should be given to the situation which will exist once the computer has determined these data or established a correlation for it. Could the plant be converted to some simpler control system at that time? If so, serious consideration should be given to a temporary installation of the computer using one of the several rental systems available rather than an outright purchase of the machine.

TABLE 9

SOME TECHNICAL CRITERIA FOR JUSTIFYING COMPUTER CONTROL

The computations which the computer is to carry out must be of such complexity that no simpler device could perform them sufficiently well to capture all or most of the contemplated returns. That is, the following possibilities must be considered and discarded as impractical for the reasons named:

(1) Nomographs — Solution of simple algebraic equations can often be carried out by means of nomographs or tables. Thus a certain definite level of complexity is necessary to justify the computer.

(2) Analog Computers — Systems of differential equations or of algebraic equations expressed in differential form are rapidly solved on analog computers. For the type of control tasks contemplated today this way will be much cheaper than the corresponding digital machines. However if the optimizing routine includes the adjustment of several of the coefficients of the plant mathematical model, analogs will be impractical and the digital machine will be necessary.

(3) Off-Line Digital Computers — If the computations carried out by the control computer must be repeated at intervals of less than about one hour, off-line computation would be impractical, otherwise it must be considered a definite possibility and a factor in the justification of the on-line, in-plant machine.

It has been mentioned by some in taking a quick survey of the field of computer control that the chances of justifying a computer are inversely proportional to one's degree of knowledge of the process and its kinetics. While this is of course an exaggeration it is nevertheless true that the necessity for making a statistical analysis as part of the computer's task in optimizing the process greatly increases the possibility of a justification for its use.

If off-line analog or digital computation can uncover — by means of theoretical considerations — the kinetic or mass transfer relationship which is the basis for the required statistical evaluation, then a simpler control system is often entirely sufficient.

The Place of Analog Computers in Process Control

Present day process controllers can be considered as essentially one input and one output systems. Therefore one can only control a multi-variable system with conventional equipment through the use of multiple controllers in a cascade arrangement. However, special analog computers can now be designed to carry out these and even more complex control functions in one "black box". Two of these — one designed to correct for the effect of ambient conditions on the operation of a fin-fan cooler used as a condenser on a distillation column[12], and the other designed to make an overall heat balance about a polymerization reactor[13] — have already been described in the literature. The former is being manufactured by several instrument and computer companies. The author's investigations of processes have to date revealed many potential applications for such specialized controllers, particularly in the control of chemical reactors and in the modification, interpretation, and presentation of plant data. Also in contrast to the larger digital computer installations (which because of their complexity and size are usually one of a kind projects), the analog computer-controller designs are often directly transferrable from one process to the next. Because of the press of their other duties, most of the systems and control groups have not had the time, manpower or the facilities to develop these items themselves. It is therefore hoped that the instrument and computer companies will eventually take a more active interest in this presently somewhat neglected field. It is this author's feeling that this can be a very active sales field in the near future once study has shown the best form which these devices should take for maximum flexibility of application from one process to another.

Dynamic or Real-Time Control by Digital Computer

So far digital computer control has only been applied to static or *steady-state* control of chemical processes. What about its use for controlling processes which are subject to rapidly changing operating conditions such as cyclic or batch reactors or tubular reactors with variable feed conditions? The reader should particularly note that the examples considered in this question have all been reactor situations. As will be brought out later, only reactors appear to have the non-monotonic or exponentially monotonic behavior which could possibly necessitate in-line dynamic control. All other processing operations appear to exhibit an overdamped monotonic response which can be adequately handled by conventional instrumentation with the possible aid of supervisory optimizers. Note that reactor, as used here, is the general term which includes the reforming and cracking, etc., operations of the petroleum refinery as well as the various reactors and furnaces in the chemical plant.

In an attempt to evaluate the above question, a generalized chemical processing problem has been formulated and presented to the computer manufacturers for their use[14]. Study of this model has revealed that dynamic control of such situations with the inclusion of an economic optimization feature will be an extremely complex calculation even for relatively simple cases[15,16,17]. Thus present day process control computers are probably much too small (i.e., too little storage) and too slow in their computing speed to be used for this purpose.

At the same time it must be kept in mind that this is the same area for which several possible analog computer controllers have been postulated. Thus there is the possibility that an analog computer controller added to the reactor's internal control loop may make the reaction process perfectly amenable to overall supervisory digital computer control of an economic optimizing type, if the digital computer is used to reset some of the potentially variable control functions of the analog computer controller. Because of its dynamic control ability, the analog computer controller may readily handle the reaction process while the digital computer calculates the next group of optimum settings at its leisure.

It is, of course, also possible that continued research into dynamic optimization procedures and in kinetics and reactor dynamics will reveal an economic justification for a larger and more capable digital computer for these specific process control duties. In this case one of the several new solid-state scientific machines may serve admirably and preclude the necessity for the development of a larger special control computer.

WHAT THE CHEMICAL ENGINEER MUST DO

Because of the sudden breaking of the field of computer analysis and its rapid development of the frontiers of science combined with the chemical engineer's previous devotion to the steady-state aspects of process plant design and plant technology, he has found himself ill prepared to capitalize on computers and their capabilities. This combined with a difference in industrial emphasis has resulted in a decided difference in the degree of application of computers in our branch of engineering compared to aeronautical, electrical, and mechanical engineering.

To make the best use of computers, the chemical engineer must have a broad knowledge of basic chemistry, physics, and properties of materials. He must be thoroughly grounded in mathematics with a good facility in one or preferably more of the following: operational mathematics, numerical analysis, and statistics. In addition, he must be able to think in terms of dynamic behavior of chemical processes: of reaction kinetics, of fluid dynamics, and of mass and heat transfer.

These needs are resulting in a rapid revamping of the chemical engineering curricula to provide a much more fundamental program with more emphasis on mathematics, chemistry, physics, and control system response. To aid the engineer who is already in industry, the technical journals have published many tutorial series of articles and bibliographies[18] on the new aspects of chemical engineering. In addition, the engineering societies are taking an active hand in supplying such information. Examples of these activities are the Summer Conferences on Control Theory for Chemical Engineering Teachers and the Special Lecture Series of the American Institute of Chemical Engineers.

In addition, several of the computer manufacturers such as Electronic Associates Inc., and the International Business Machines Corporation (IBM) conduct periodic short courses in computer programming and computer application to process

industry problems. Also it is the practice of practically all computer manufacturers to train a certain number of the customer's personnel to operate and maintain each new computer purchased. Thus there is every opportunity for the chemical engineer who so desires, whether still a student or already in the field, to acquire the necessary knowledge and experience to take his place in the rapidly growing field of computer usage in our industry.

WHAT ABOUT THE FUTURE?

Approximately three years ago this author made a prediction that the year 1968 would see the following in the use of computers in the process industries:

(1) 75 of the 100 largest process companies in the United States would be engaged in simulation studies with analog computers or advanced digital computers.

(2) All large chemical and petroleum companies would have large scale digital equipment devoted to scientific and engineering work. Many of them will have several of these machines.

(3) If instrumentation development keeps pace, 150 or more large scale machines will be devoted to repeated plant optimization studies. Many will be connected as overall plant supervision machines.

(4) Industry will be actively engaged in "economic automation" or the maximum of automatic control which will show an economic payout.

With the ten-year period only a quarter over these predictions appear, if anything, conservative and we are well on the way to fulfilling all of them. This is particularly true of the last two since instrumentation developments have also been quite spectacular in the last two or three years and promise to continue.

References

(1) Williams, T. J., "Systems Engineering for the Process Industries—Its Application, and Its Future Potential", Fourth E. P. Schoch Lectures, U. of Texas, Austin, Tex., October 16-17, 1959, currently being published in serial form by Chem. Eng.

(2) Machine Computations Committee, Am. Inst. Chem. Eng., "Computer Procedures for Estimating Physical Properties", September 1960.

(3) Petersen, T. I., Chem. Eng. Progr. Symposium Ser., **56**, No. 31, 111-120 (1960).

(4) Computer Systems Inc., Form 80-105-003, Monmouth Junction, N.J., 1960.

(5) Greenstadt, J., Bard, J., and Morse, B., Ind. Eng. Chem., **50**, 1644-1647 (1958).

(6) Rosenbrock, H. H., Brit. Chem. Eng., **3**, 364-367, 432-435, 491-494 (1958).

(7) Eisenhardt, R. D., and Williams, T. J., Contr. Eng., **7**, No. 11, 103-114 (November 1960).

(8) Madigan, J. M., Chem. Eng. Progr., **56**, No. 5, 63-67 (May 1960).

(9) Parsons, J. R., Tolin, E. D., and Andrews, A. J., Contr. Eng., **7**, No. 9, 150-153 (September 1960).

(10) Freilich, Arthur, ISA Journal, **6**, No. 7, 47-65 (July 1959).

(11) Hall, C. R., Chem. Eng. Progr., **56**, No. 2, 62-66, (February 1960).

(12) Lupfer, D. E., and Berger, D. E., ISA Journal, **6**, No. 6, 34-39 (June 1959).

(13) Tolin, E. D., and Fluegel, D. A., ISA Journal, **6**, No. 10, 32-38 (October 1959).

(14) Williams, T. J., and Otto, R. E., Am. Inst. Elec. Eng. Paper CP-60-119, Winter General Meeting, Am. Inst. Elec. Eng. February, 1960.

(15) Beecher, A. E., and Gould, L. A., Am. Inst. Elec. Eng., Paper CP-60-980, Joint Automatic Control Conference, Cambridge, Mass., September 1960.

(16) Boydston, R. E., Am. Inst. Elec. Eng., Paper CP-60-979, Joint Automatic Control Conference, Cambridge, Mass., September 1960.

(17) Kipiniak, W., and Gould, L. A., Am. Inst. Elec. Eng., Paper CP-60-981, Joint Automatic Control Conference, Cambridge, Mass., September 1960.

(18) Williams, T. J., Chem. Eng., **68**, No. 1, 103-110, January 9, 1961.

★ ★ ★

Rail Transportation of Hydrogen Chloride Anhydrous[1]

C. H. DRURY[2]

A railway tank car has been built for Canadian General Transit Co. Limited and is operating in the leased service of Dow Chemical of Canada Limited for the shipment of hydrogen chloride anhydrous shipped at minus 50°F. in single shipments of about 89,000 lb.

Necessary safety devices and a liquid CO_2 refrigeration system are included which will maintain the car at a safe pressure level for an extended period subject to the supply of liquid CO_2.

Commodity

The principal detailed physical data of hydrogen chloride anhydrous are shown in Figure 1 together with its vapor pressure-temperature curve. In addition, this commodity has a tremendous affinity for water and, because of its dehydrating effect, is dangerous to living tissue.

As a dry gas it is essentially inert and does not attack the commonly-used structural metals under temperature and pressure conditions normally used. In the presence of moisture it becomes highly reactive which calls for special design where contact with water vapor is possible, valve stems, open connections, etc.

Economic Considerations

In the past, the cost of transporting aqueous hydrochloric acid solution combined with the fact that no means, other than pipe line, was available to transport the anhydrous material economically forced many users of HCl to locate plants adjacent to producers of HCl.

Because unit costs of shipment normally vary inversely to the size of the shipment it was decided to investigate methods of shipping substantial weights of hydrogen chloride anhydrous in single shipments by rail and in order to obtain economic weights it was obviously essential to ship in liquid form.

Design Considerations

Examination of the HCl temperature vapor pressure curve clearly indicates at 90°F. a vapor pressure of 795 p.s.i. gauge and at about minus 45°F. a vapor pressure of 100 p.s.i. gauge. By comparison, anhydrous ammonia at 90°F. has a vapor pressure of 166 p.s.i. gauge. With such characteristics it is evident that a low temperature technique of handling was essential. If the commodity can be held at that temperature the problem of an economic railway shipping container is relatively simple. Experience on low temperature rail shipments of liquid carbon dioxide was available and it appeared that some adaptation of this container would be satisfactory.

The railway tank cars approved for handling HCl anhydrous are constructed of steel to Specification A-300, Class 1, ASTM A212, Grade B, suitable for service to minus 50°F. and are specially and carefully insulated with 10" Styrofoam, the whole enclosed in a steel jacket, the entire design requirements coming under Container Specification ICC-105A-600W. (Hydraulically tested to 600 p.s.i. with safety valve settings at 450 p.s.i.).

In order to ensure no liquid will be discharged through the safety valve the ICC limits the allowable filling density (ratio of the weight of commodity in pounds to the water capacity of the container in pounds) for HCl to 85%. (ICC Special Permit No. 2308; BTC Special Permit No. 467). Using this factor and a net cubic capacity of about 10,500 Imperial gallons, approximately 89,000 pounds of hydrogen chloride can be carried.

Heat Balances

In order to establish how long the car would remain safely in an ambient temperature of 90°F., on the assumption that the lading was shipped at minus 50°F., a simple heat balance was done which indicated a time lapse of minimum 30 days before the vapor pressure of the hydrogen chloride would reach the discharge pressure setting of the safety valve at 450 p.s.i., equivalent to a temperature of approximately 47°F.

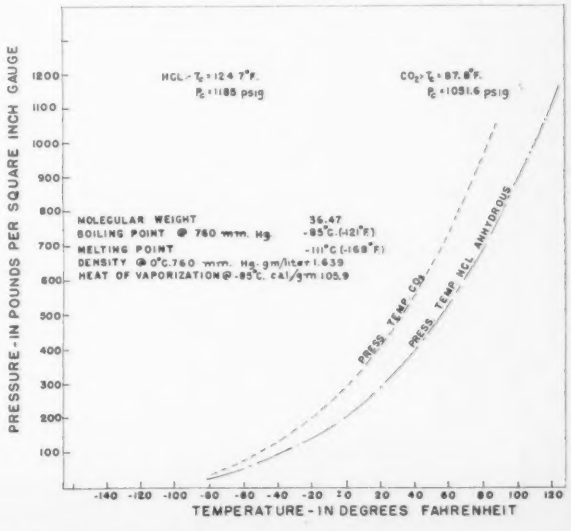

Figure 1—Properties of hydrogen chloride, anhydrous.

[1]*Manuscript received April 12; accepted July 12, 1961.*
[2]*President and Managing Director, Canadian General Transit Co. Limited, Montreal, Que.*

Safety

Although 30 days would seem reasonably adequate protection it was decided that under extreme conditions this time might be exceeded and therefore it was desirable to provide additional protection by refrigeration which could maintain the lading at a suitable temperature for an additional period.

A number of systems, including mechanical refrigeration, were considered with the greatest weight being given to reliability and simplicity of service. After full consideration, it was decided to employ the principle of self-refrigeration, where carbon dioxide would be discharged in the case of emergency or long periods of transit, and the latent heat of vaporization required, extracted from the lading through the medium of heat exchange. This was achieved by locating two liquid CO_2 containers, approximately 330 Imperial gallons each, inside the main tank shell. The use of two containers was decided upon, firstly, to supply adequate heat exchange area and, secondly, two separate systems to ensure one system always being in operation.

The location of the tanks was arranged so that the liquid interface in the CO_2 tanks and the liquid interface of the lading were on similar levels. The internal CO_2 containers were designed to withstand an external pressure in excess of 495 p.s.i., the flow rating pressure of the safety valve on the main tank, which resulted in considerable over-design for the internal pressure. These tanks were hydrostatically tested to 600 p.s.i. prior to installation and, of course, are made of the same low temperature material as the main tank.

Refrigeration

The vapor pressure curves of liquid CO_2 and HCl anhydrous bear a close relationship which makes CO_2 an ideal refrigerant in this case. The liquid CO_2 tanks are supplied with pressure regulators which are set to discharge at 300 p.s.i. equivalent to carbon dioxide at about minus 2°F. By loading the commodity at minus 50°F. about 10 days will elapse in an ambient temperature of 90°F. before the discharge temperature of the CO_2 is reached. There is sufficient carbon dioxide available to maintain approximately 0°F. in this car for an additional 7 days and there is adequate time available in the next 20 days before the pressure in the tank would approach the safety valve setting during which the carbon dioxide containers can be recharged by pumping liquid CO_2 from tank truck or tank car at a pressure of about 275 p.s.i. gauge.

In the event of leakage of HCl safety valve or angle valves, the Type "C" emergency kits available for chlorine tank cars can be used without modification to control leakage. (see Chlorine Institute Inc., "Types and Location of Chlorine Emergency Kits in North America", First Issue April 1959).

Construction Details

Fittings for hydrogen chloride are basically the same as fittings used on chlorine cars plus a thermometer well and two level telltales. Fittings include:

(1) Crosby safety valve with frangible disc, set at 450 p.s.i.
(2) Two 1-in. angle valves for liquid control, on the longitudinal centre line, with excess flow valves, and 1¼-in. pipes extending to a sump in the bottom of the tank. Pipes are screwed to permit maintenance of the excess flow valves, as for chlorine cars.
(3) Two 1-in. angle valves for vapor control on the transverse centre line.
(4) Thermometer well to check lading temperature. Closure is an approved fitting that permits testing for leaks without complete removal.
(5) Two ⅜-in. angle valves of stainless steel with pipes extending into the tank to indicate liquid level at −20°F. and −50°F.

Fittings for carbon dioxide, pressure regulator and safety valve, are the same as those used on carbon dioxide tank cars on the theory that the heat flow will be relatively the same as a carbon dioxide car and they will be capable of handling the same volume. These include the following:

(1) Safety valve set at 375 p.s.i.
(2) Pressure regulator set at 300 p.s.i. (equivalent to carbon dioxide at −2°F.)
(3) One 1-in. angle valve, same as above, for liquid control, with 1-in. pipe to bottom of container.
(4) One 1-in. angle valve, same as above, with 1-in. pipe extending 1¾-in. into container to control vapor and also act as a fixed length dip tube gauging device for loading of carbon dioxide to 95% of volume of container and nozzle.
(5) Thermometer well to check carbon dioxide temperature.

Tank car shipments were commenced several months ago and are now being made on a routine basis in cars owned by Canadian General Transit Co. Limited. The temperature well and liquid level indicators allow the contents as loaded to be checked for level and temperature prior to shipment and in the case of incorrect loading, adjusted through the liquid lines.

Basically simple, the tank car meets the full requirements of safety, it is reliable and it provides a container of reasonable size and reasonable net weight to ship an economical quantity of hydrogen chloride anhydrous by rail.

While a limited number of cars have been put into service in the United States, Dow is the first and so far only Canadian shipper of HCl anhydrous by tank car.

★ ★ ★